Aalto University
School of Engineering
Department of Engineering Design and Production

Hao Wang

Friction Stir Welding of Aluminium Alloy AA5754 to Steel DX54:

Lap Joints with Conventional and New Solution

Thesis submitted as a partial fulfilment of the requirements for the degree of Master of Science in Technology.
Espoo, October 27, 2015

Supervisor: Prof. Pedro Vilaça
Advisors: Tatiana Minav Ph.D.

Aalto University
School of Engineering
Department of Engineering Design and Production

ABSTRACT OF
MASTER'S THESIS

Author:	Hao Wang		
Title:	Friction Stir Welding of Aluminium Alloy AA5754 to Steel DX54: Lap Joints with Conventional and New Solution		
Date:	October 27, 2015	**Pages:**	100
Major:	Mechanical Engineering	**Code:**	IA3027
Supervisor:	Professor Pedro Vilaça		
Advisors:	Tatiana Minav Ph.D.		

The demand for joining of aluminum to steel is increasing in the automotive industry. There are solutions based on Friction Stir Welding (FSW) implemented to join these two dissimilar metals but these have not yet resulted in a reliable joint for the automotive industrial applications. The main reason is the brittle intermetallic compounds (IMCs) that are prone to form in the weld region. The objective of this thesis was to develop and test an innovative overlap joint concept, which may improve the quality of the FSW between aluminum alloy AA5754-H22 (2 mm) and steel DX54 (1.5 mm) for automotive applications.

The innovative overlap joint concept consists of an interface with a wave shape produced on the steel side. The protrusion part of the shape will be directly processed by the tip of the probe with the intention of improving the mechanical resistance of the joint due to localized heat generation, extensive chemically active surfaces and extra mechanical interlocking. The innovative overlap joint concept was tested with three different travel speeds and axial forces. The welds were evaluated by visual inspection, microstructure observation and mechanical tests. Conventional overlap joints concept were produced to enable the evaluation of the efficiency of the innovative concept. Furthermore, multi-pass welds, with 2 and 3 passes, for both overlap joint concepts were conducted to verify the improvement of microstructure and mechanical performance.

With a single-pass weld the conventional overlap joint concept presented higher strength than the innovative concept. The main mechanisms governing this result were the formation of IMCs and higher reduction of effective thickness in the aluminium alloy sheet for the innovative lap joint concept. The multi-pass welds with 2 passes have shown the best tensile shear strength for both overlap joint concepts, about 50 % efficiency in relation to the aluminium alloy base material. One issue affecting the results is the fact that the method applied to produce the pre-weld deformation in the steel sheet, at the contact interface, did not yield the originally planned geometric shape for the innovative overlap joint concept.

Keywords:	Friction stir welding, Dissimilar joints, Aluminium alloy, Steel, Lap joint, Intermetallic compounds
Language:	English

Acknowledgements

This thesis is a development project driven by Professor Pedro Vilaça at the Laboratory of Engineering Materials at Aalto University School of Engineering.

I would like to thank Professor Pedro Vilaça for his support and the opportunity for this interesting work. I am grateful for my instructor, Tatiana Minav, for their assistance and supports. I am also thankful for all the support that I have had during this thesis from Gonçalo Sorger, Topi Taavitsainen, Jari Hellgren, Kim Widell, Teemu Sarikka and Laura Tiainen. This project is a great experience and learning process for me. I would like to thank all the participating coworkers for making my work as fluent as possible.

Lastly, I am grateful to my parent for their encouragement which helped me complete this project.

Many Thanks.

Espoo, October 27, 2015

Hao Wang

Abbreviations and Acronyms

AHSS	Advanced High Strength Steels
CP	Complex Phase
DP	Dual Phase
EDX	Energy Dispersive X-Ray
FSW	Friction Stir Welding
FW	Friction Welding
GTAW	Gas Tungsten Arc Welding
HAZ	Heat Affected Zone
HFSW	Hybrid Friction Stir Welding
IMCs	Intermetallic Compounds
MART	Martensitic
OM	Optical Microscopy
PCBN	Polycrystalline Cubic Boron Nitride
SEM	Scanning Electron Microscopy
TMAZ	Thermomechanically Affected Zone
TWB	Tailored Welded Blanks
USMW	Ultrasonic Metallic Welding
UTS	Ultimate Tensile Strength
YS	Yield Strength

Contents

List of Tables

List of Figures

Chapter 1

Introduction

1.1 Welding aluminium to steel

Currently, energy saving and minimizing environmental impact are important challenges for automotive industries. One efficient solution for these challenges is to reduce vehicle weight, because low vehicle weigh results in the reduction of fuel consumption. Some automobile manufacturers are using thinner steel sheets for car body structure resulting in a maximum reduction of 30% vehicle weight. But further weight reduction is hardly achievable with exclusive dependence on this method [1]. Therefore, an alternative material is needed to replace steel. Aluminium alloys is one of this alternative materials. With good heat transfer, high strength, good formability and weight saving, aluminium alloy are already utilized for aerospace structures, ship building and also automotive application [2]. A number of automotive companies have already succeeded in manufacturing aluminium cars [3]. However, some issues exist in these cars, e.g., aluminium alloys have inferior strength compared to steel, as a result, the safety of the cars are lower, and aluminium alloys are more expensive than steel. Consequently, for achieving high safety and a cost-effective product, the combination of steel and aluminium alloys become the most promising method for automotive industries, which has resulted in increased research interest. Nevertheless, joining of aluminium alloys to steel is challenging due to the differences of physical and chemical properties: their melting points are incompatible and they have different thermal conductivity and coefficient of thermal expansion [4]. Furthermore, the low solubility of iron in aluminium promotes the formation of brittle intermetallic compounds (IMCs) in the weld zone [5]. Although the combination of these two dissimilar materials is desirable, it is extremely hard to obtain a reliable joint by using fusion welding processes.

The solid-state welding methods, such as friction welding (FW) and ultrasonic metallic welding (USMW), are introduced in this study. These methods join dissimilar material without reaching their melting point, which means heat generated from these methods produces peak temperatures lower than that of fusion welding processes. Thereby reducing the formation of brittle IMCs. However, these processes have some disadvantages. For example, FW requires that at least one material to be welded have a circular cross section. The USMW has a drawback that it is viable solely for thin plates [6]. Contrary to the solid-state welding methods, laser welding method uses YAG laser beam to heat a steel plate, resulting in heat conduction from the steel plate to an aluminium alloy plate that leads to melting of an aluminium alloy faying surface thereby joining the two materials together. Nevertheless, like other fusion welding methods, the laser welding method presents difficulties in that brittle IMCs are still formed and it is difficult to control the heat input and the melting amount of the aluminium alloy by laser irradiation [7]. In addition, laser equipment is quite expensive.

Some experimental results have been reported on friction stir welding (FSW), a process patented by The Welding Institute[8]. This method is widely employed in industries for joining of aluminium to steel. Because the process is a solid-state welding method, with correct selection of welding parameters, dissimilar materials can be welded without reaching melting point. As a result, the formation of IMCs could be reduced significantly [1]. Moreover, it can weld a wide range of material thicknesses. Based on these merits, FSW as a promising technique has been investigated in several studies. For example, Xun et al. [1] investigated the effects of process parameters on the joint microstructure evolution of butt welded 1.5mm AA6061-T651 to TRIP780/800 steel. The result shows that the joint exhibited 85% of ultimate tensile strength of aluminium base alloy. Tests reveal that a fracture occurs in the heat affected zone (HAZ) of aluminium alloy. The reason is dissolution and over aging of fine precipitates form inside aluminium alloy as a result of surplus friction heat conduction from steel faying surface. Rodrigo et al. [9]. investigated the characterization of the microstructure formation of 1.5mm AA6181-T4 and HC340LA steel sheet by FSW of overlap joints. Their research shows the maximum force of the friction stir welded joints obtained in shear test amounts to 73% of the forces obtained for respective welds of the AA6181-T4 base material. A fracture occurs on the retreating side of the AA6181-T4 stir zone where the steel fragments are present. The result shows that conventional FSW cannot achieve desirable weld quality.

Other authors present modification of FSW techniques to improve weld strength. For example, Han Sur et al. [10] utilized gas tungsten arc welding (GTAW) assisted hybrid friction stir welding (HFSW) of 3 mm thick AA6061-

T6 aluminium alloy and STS304 stainless steel to evaluate the potential for this process to join dissimilar materials. A solid joint was successfully achieved without defects in welds. The maximum tensile strengths obtained at the weld were 93% of the aluminium alloy base metal tensile strength for HFSW and 78% for general FSW. Figure 1.1 shows the difference of tensile strength between FSW and HFSW. This result shows HFSW substantially increase weld strength. However, the additional equipments are expensive. Moreover, a weak weld generates if welding parameters are not controlled precisely. Although these innovative FSW methods are able to create high strength weld, the cost of production may stay at relative high level.

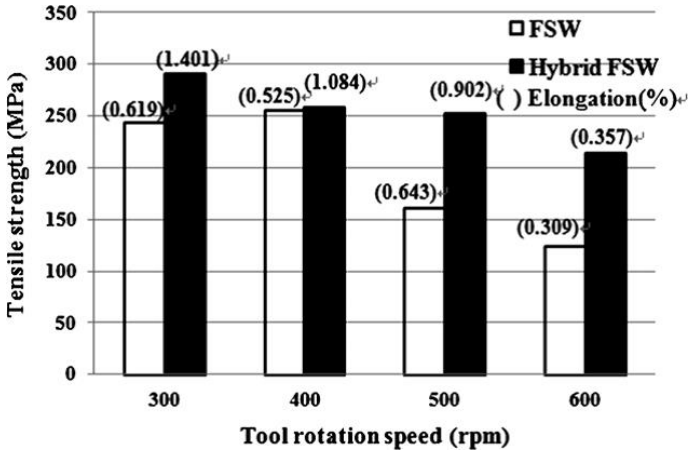

Figure 1.1: The comparison of tensile strength between HFSW and FSW at different tool rotation speeds [10].

1.2 Methodology and objectives

In the present investigation, an innovative overlap (or simply 'lap') joint concept was developed and tested for welding 2mm thick aluminium alloy (AA5754-H22) to 1.5mm thick steel (DX54). The innovation is to form a special geometry at the joining interface by modifying the original planar shape of the steel side. The objective of this modification is to promote a higher direct interaction between the probe of the FSW tool and the steel surface leading to an increased localized interfacial diffusion with additional mechanical interlocking of two welded materials. This new joint design is easily produced in automotive industry by utilizing the deep drawing technique, which is one of the most widely used sheet metal forming processes

in automotive industry for the manufacturing of car body parts. The analysis on how the new weld interface affect weld strength will be investigated and compared with FSW of conventional lap joint concept. This is will be done by using tensile shear test, peel test, microhardness measurement, optical microscopy (OM) and scanning electron microscopy (SEM) with energy dispersive X-Ray (EDX) analysis to indicate the different metallurgical properties and mechanical behaviours. Furthermore, multi-pass welding with 2 and 3 passes of both innovative and conventional lap joints will be evaluated.

1.3 Structure of the thesis

Chapter 2 introduces the literature review, addressing current methods for joining aluminium alloy to steel. This part concentrates on the advantages and disadvantages of different types of joining methods. First, the available joining technologies are introduced. Second, the recommendations for welding material, tool design and FSW parameters are explained. Third, two already existing FSW methods are presented.

Chapter 3 concentrates on experimental plan, which consists of base material properties, equipments description, parameters selection and test conditions. Also, the development of joint concept will be shown in this chapter.

In Chapter 4, both conventional and innovative lap joint configurations are analyzed by utilizing the results of tensile shear test, peel test, hardness profile, OM , and SEM with EDX. The innovative concept is evaluated by comparing the results of the conventional lap joint and innovative lap joint configurations. In addition, multi-pass welding for both lap joint configurations are evaluated by tensile shear test and optical microscopic observation which contributed to further development.

Finally, Chapter 5 establishes the main findings of the experiments, and also introduces discussions for further development of the investigation.

Chapter 2

Literature review

2.1 Introduction

When people talk about the joining of dissimilar material in automotive industry, the first picture that comes into mind is several mechanical ways of assembling : screwing, riveting or clinching [7]. However, there are many welding methods were successfully utilized, such as laser welding, ultrasonic welding and FSW. In this section, the working principles of these previous mentioned methods are presented. Moreover, the characterization of the conventional FSW method is presented which consists of base material selection and its application, tool design and FSW parameters establishment. Based on the conventional FSW method, new solutions are introduced to give a perspective of current technical development. In the end, the advantages and disadvantages of the presented technologies are compared and discussed.

2.2 Technological solutions for dissimilar joints between aluminium alloy and steel

2.2.1 Mechanical joining based solutions

Mechanical jointing methods, such as clinching and riveting, are established in many car body manufacturing companies for joining dissimilar materials [11, 12]. These methods are very easy to use and do not require complicated processes or expensive equipment.

Figure 2.1 (a) shows the procedure of clinching. This process starts with the punch and forms the clinch joint in the die. In this process, the local defects in the joint is easily created because of relatively high forming grade

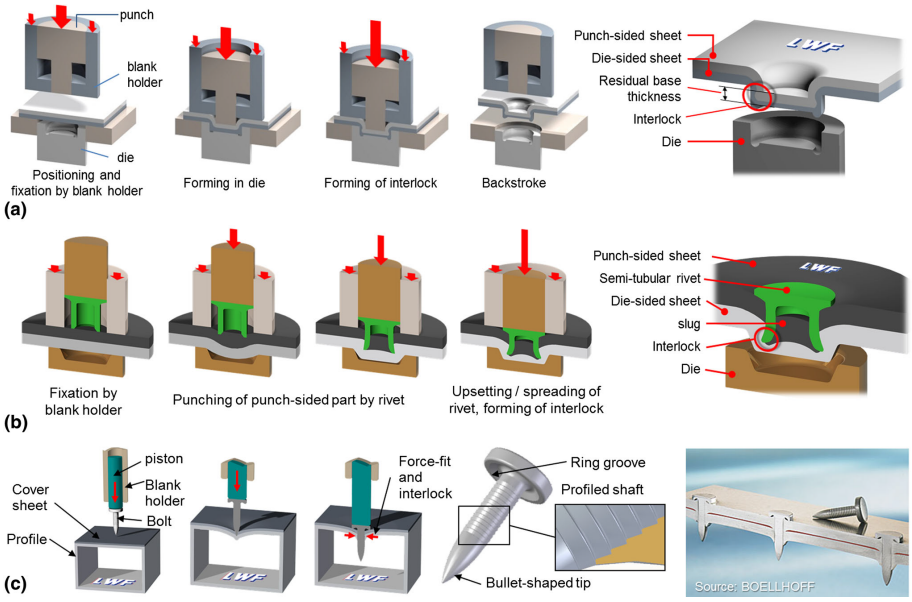

Figure 2.1: Illustration of selected mechanical joining processes for automotive applications. (a) clinching with static die (b) self-pierce riveting (c) high-speed bolt joining [16].

[13, 14]. Figure 2.1 (b) shows the procedure of self-pierce riveting method which is similar to clinching but with the use of a semi tubular rivet. This rivet needs to drive through the top sheet and spread the rivet skirt in order to create the interlock with a suitable die. Mori et al. [15] investigated that riveting of an 5000 series aluminium alloy to a steel with a tensile strength of 980 MPa. The results show that the rivet skirt is severely deformed and compressed, even with an optimized die. The reason is that the high tensile strength of the joining material results in the the deformation of the rivet when piercing the overlapped materials. Comparing to clinching and riveting, high-speed bolt joining is a new mechanical joining method for car body manufacturing. As Figure 2.1 (c) shows, the profiled shaft with bullet-shaped tip is punched into the workpieces at speed 20 and 40 m/s using the piston. Only a small deformation forms at punching area because of large mass inertia. Additionally, the generated local friction heat between the bolt and workpieces can improve the flow properties which can soften high strength material. Nonetheless, the tensile strength of the bolt cannot be increased greatly. This is because the high strength bolt can lead to cracks in materials during the joining process, which results in poor quality under fatigue loads.

Since joint quality is always one of the most important consideration in automotive industrial application, the specific drawbacks of above mentioned spot joints can be avoided with the help of adhesive bonding. The combination of spot joint and adhesive bonding is called hybrid joining which can increase joint strength significantly. In addition, the adhesive layer isolates joint interface which can reduce corrosion effects result from the difference of dissimilar materials' electrochemical potential.

2.2.2 Laser welding

M.J Torkaman et al. [7] investigated the laser welding of low carbon steel St14 with 0.8mm thickness to aluminium alloy AA5754 with 2mm thickness in keyhole welding mode. Steel sheet was placed on aluminium alloy sheet in an overlap configuration. Figure 2.2 presents a schematic illustration of the welding set up. The laser source is a pulsed Nd:YAG laser with a maximum mean power of 400 W. The high intensity heat from laser beam heat the steel sheet. And then, the heat converts solid aluminium alloy to liquid aluminium alloy by heat conduction. Finally, the liquid aluminium alloy sheet and solid steel sheet form a sound bonding because of metallurgical reactions.

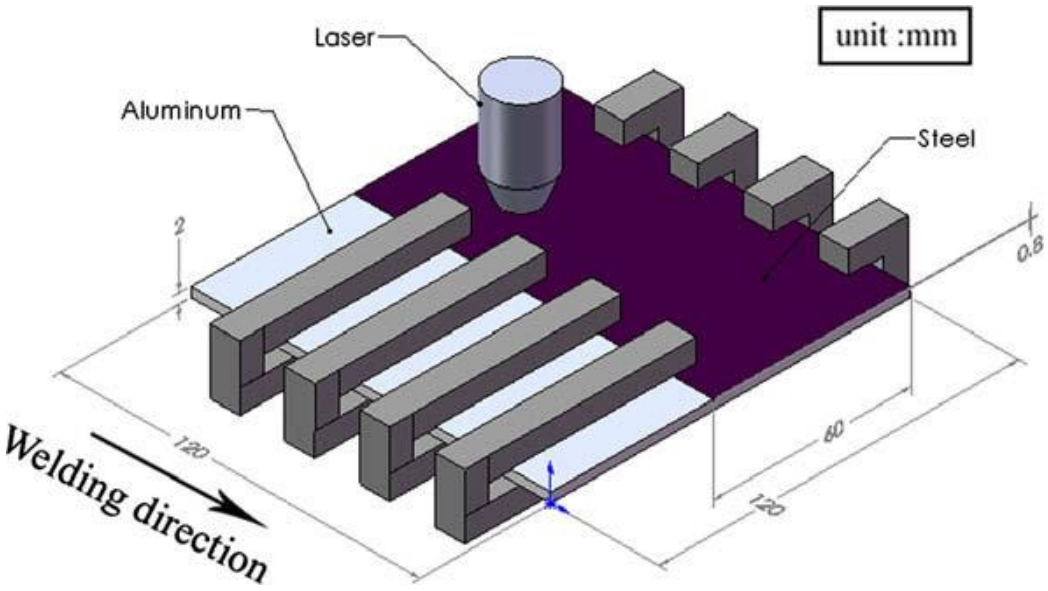

Figure 2.2: Schematic illustration of the steel/aluminium welding set up [7].

The advantages of laser welding are to minimize the size of IMCs layer as a result of a concentrated energy input of the laser beam, high cooling

rates and short process time [7]. More importantly, laser welding parameters can be optimized to cover a wider range of dissimilar metal combinations than other welding techniques. However, the laser welding method presents some disadvantages because some brittle IMCs are still formed and it is hard to control the localized heat input and the melting of the aluminium alloy caused by laser irradiation; therefore, the weld quality is not stable. In addition, laser equipment is extremely expensive.

2.2.3 Ultrasonic welding

Farid [17] reported ultrasonic spot welding of aluminium alloy AA6111 to steel DC04 with 1 mm thickness. A flat serrated sonotrode tip located on the top of aluminium alloy sheet, a dome shaped serrated sonotrode tip is located on the bottom of steel sheet as shown in Figure 2.3 (b) and (c). Subsequently, the linear oscillations are applied to the weld components by sonotrode tips which are connected to transducers (Figure 2.3 (a)). Transducer coverts electrical energy into mechanical vibration. And then the weld is formed, which is due to the destruction of oxides and the formation of atomic bonding because of severe plastic deformation [18]. The final result shows that a maximum 2.7 kN of strength was obtained in the joint.

Ultrasonic spot and friction stir spot welding are two solid state processes that can substitute resistance spot welding, and use only 10% of the energy of resistance spot welding [19]. Furthermore, the reduction of IMCs contributes to a solid weld formation, because the heat input is low. In comparison to friction stir welding, ultrasonic spot welding has not undesirable aspects, such as the keyhole, and reduction of the top sheet thickness [20], and also the duration of welding is less than a second especially for difficult dissimilar material joining such as aluminium to steel [17]. Reversely, high rate plastic deformation in ultrasonic spot welding results in the formation of IMCs thereby deteriorating mechanical performance. Moreover, ultrasonic welding also has the drawback that it is viable only to thin plate [6].

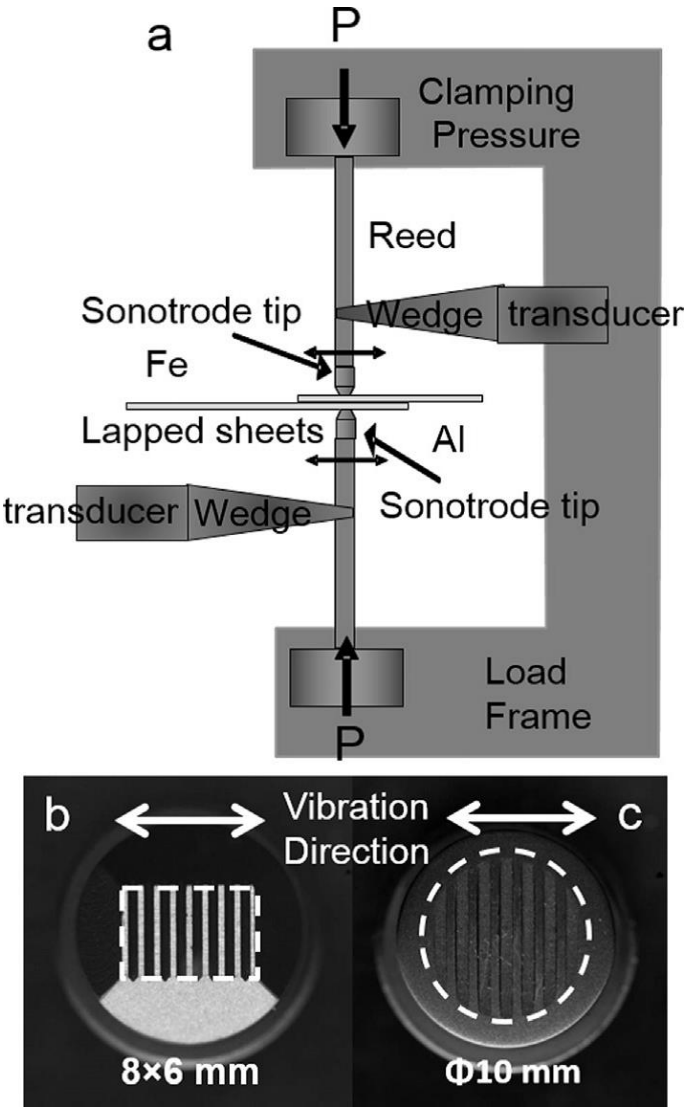

Figure 2.3: (a) schematic demonstration of ultrasonic spot welding, (b) flat serrated sonotrode tip touching aluminium and (c) domed shaped serrated bottom sonotrode tip touching steel [17].

2.2.4 Friction stir spot welding

Watanabe et al. [21] investigated that friction stir spot welding of aluminium alloy to mild steel. As Figure 2.4 shows, the welding begins with a rotating probe plunging into aluminium sheet. The friction heat generated between tool and workpieces facilitates the penetration of the probe. Furthermore,

the heat softens the materials into a plastic state. The axial force from the shoulder keeps these metals in intimate contact to facilitate the bonding. In the end, the tool is retracted, a round dent is made on the stirred spot. The results show that the thickness of IMCs is related to dwell time. This is because if the heated probe stays in the weld area for longer time more diffusion time can be obtained.

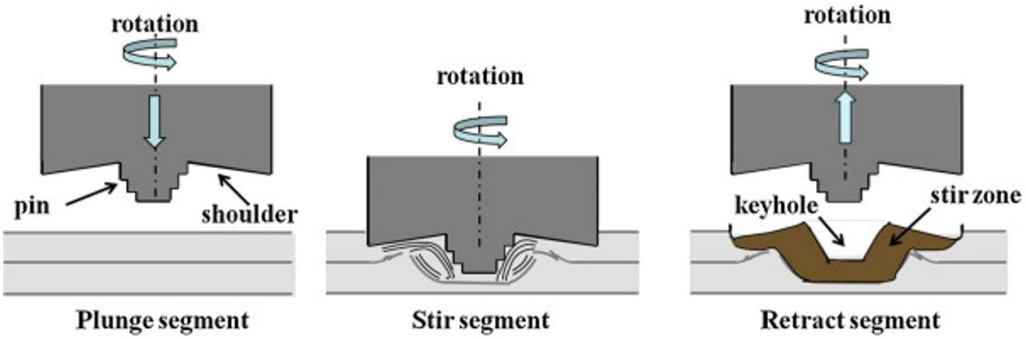

Figure 2.4: Schematic illustration of friction stir spot welding [22].

Bozzi et al. [23] investigated that friction stir spot welding of an aluminium alloy AA6016 to a high strength steel. The results show that different IMCs were formed because of the variation of probe penetration and rotation velocity. Similar results were also obtained by Qiu et al. [24] where an aluminium alloy AA5052 and a mild steel were bonded by this method. As in ultrasonic spot welding method, the welding machine and control system for the friction stir spot welding is simple and easy to use in mass production. Moreover, Mazda reported that friction stir spot welding had over 90 % energy saving when compared to resistance spot welding of aluminium alloys [25].

2.2.5 Friction stir welding

Figure 2.5 shows the schematic of the friction stir welding process in overlap configuration. The FSW tool is rotated and the probe is plunged into the materials, until the shoulder is in close contact with the aluminium alloy sheet. Subsequently, the probe moves forward and mixes the softened materials by plastic deformation resulting in joining both materials in a solid state [26].

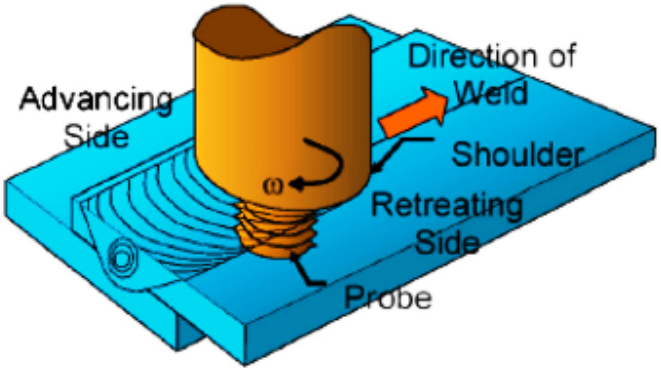

Figure 2.5: Schematic of the process: friction stir overlap welding process[26].

The advantages of FSW is that no gas shielding is needed during the welding process. Similar to friction stir spot welding, FSW is also a high energy efficiency process. Additionally, a low distortion and shrinkage weld can be easily achieved. However, an undesirable keyhole is left by the tool probe at the end of welding. The reduction of the top sheet thickness caused by the penetration of the shoulder into aluminum alloy sheet may influence the strength of the weld.

2.3 Friction stir welding characterization of joining dissimilar materials

2.3.1 Dissimilar base materials and its application

From all the referenced literature, various materials were employed for the investigations. However, most authors did not explain why they were employing these materials. Leitao et al. [26] studied two series of aluminium alloy which are very popular in automotive industry. 5000 series aluminium alloys, such as AA5182 aluminium alloy, are characterized by its high content on magnesium. Due to its excellent formability, especially during deep drawing with a high amount of stretch forming, this material is suited for complicated critical inner panel applications. 6000 series aluminium alloys, such as AA6016 aluminium alloy, are supplied as a solution alloy heat-treated and naturally aged to a stable condition (T4). This aluminium alloy that presents stable formability, is usually used for car skin sheet applications and for vehicle's inner panel applications. Consequently, a limited range of aluminium alloys, such as the Al-Mg non-heat treatable 5000 series and Al-Mg-Si heat

treatable 6000 series, are suited for automotive application [17]. On the other hand, almost all the studies selected mild steel, which has a relatively low yield strength, for investigation. However, some literature [1, 9, 27, 28] have reported FSW of aluminium alloy to advanced high strength steels (AHSS), which is more suitable in lightweight vehicle structures. AHSS consists of four subcategories, i.e. dual phase (DP) steel, transformation induced plasticity (TRIP) steel, complex phase (CP) steel and martensitic (MART) steel [2].

2.3.2 Tools

According to previous investigations [29–32], the joint quality is sensitive to friction stir welding tool. If steel is not sufficiently mixed with melted aluminium alloy, the welds can easily generate porosity. Furthermore, high welding force demand for stirring steel tool accelerates tool wear. There are two general solutions for overcoming the problems. The first one is to design FSW tools with particular geometries made from high strength materials, such as tungsten carbide, tungsten-rhenium, Si3N4 and polycrystalline cubic boron nitride (PCBN). In Ref. [1] investigation, tungsten carbide with 10% cobalt content was selected for its good wear resistance and much lower cost compared with PCBN. The second one is that the rotating probe is plunged into the aluminium without deeply penetrating the steel; consequently, the rotating probe performs minimal wear. For the second solution, tool can be made from relative low strength material, such as high-speed tool steel SKH57 [6]. However, the low penetration may cause insufficient removal of the oxide film on the surface of steel, which may result in a low weld quality [1, 6, 33].

Tool geometries should be as simple as possible, to reduce manufacturing cost, and sufficient stirring effect is required to producing solid welds [29]. For example, probes with columnar shape are suitable to welding low melting temperature metals such as steel whose deformation resistance is relatively low. Unlike the columnar probe, a trapezoidal probe with more complex profiled was introduced in Ref. [30]. Trapezoidal probe can create more heat input and better material flow compared to columnar tool. Moreover, the complex profiled tools (triangular, trapezoidal and tapered cylindrical tool, see Figure 2.6) can also reduce the vibration of machine at the plunging phase [30]. However, the surface area of the probe is difficult to control. If the surface area is large, there are tunnel defects due to surplus heat input. If the surface area is small, there are piping defect because of insufficient heat input. In addition, probes with thread can facilitate the three dimensional material flow. Lin et al. [31] mentioned that clock-wise rotating probe with

left-handed threads forces the material flow from upper sheet to lower sheet which can be beneficial to weld quality.

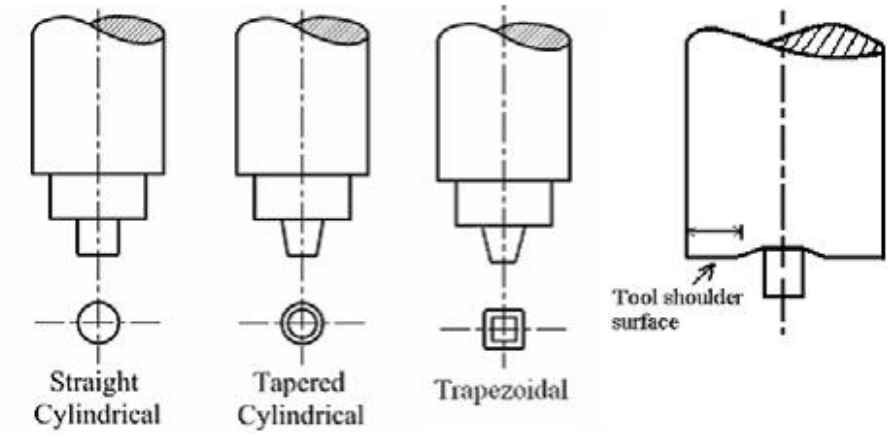

Figure 2.6: Different FSW tool geometries used in the experiment [30].

2.3.3 FSW parameters

The effects of various FSW parameters, such as tool travel speed and plunge depth, on the formation of IMCs, void formation and tensile shear strength of joints were investigated widely in literature [1, 5, 6, 32, 33]. In this section, individual studies will be summarized with needed details according to their comparative importance in the literature.

2.3.3.1 Effects of travel speed and rotation speed

According to [1, 5], when travel speed is too low or rotation is too high, thick IMCs are formed in the weld zone resulting in very poor strength of joints. Reversely, when travel speed is too high or the rotation is too low, the joint strength decreased due to insufficient heat input. The insufficient eat input can also lead to the probe wore out in a short time. Consequently, an optimum range of travel speed and rotation speed relation is needed to make a sound joint [1, 5, 6, 33].

2.3.3.2 Effects of plunge depth

Authors [5] showed that plunge depth has a pronounced effect on dissimilar FSW of aluminium and steel. A decrease of 0.1 mm in plunge depth decreased the strength of the weld noticeably. If the plunge depth is too large, the

tunnel defect is eliminated while IMCs form in the weld nugget and the joint strength decreased. Contrarily, if the plunge depth is too low, the tunnel defect forms in weld region.

2.3.3.3 Effects of tool tilt angle

According to [32], increasing the tool tilt angle can eliminate the tunnel due to increased heat input and downward forging force. However, it might cause the formation of thick IMCs thereby decreasing the tensile strength. Typically tilt angle ranging from 2 degree to 4 degree is recommended (in some cases, such as welding pure titanium, the tool tilt angle is 1 degree).

2.4 Current development of FSW

In order to improve the weld strength, a redesigned FSW method is required. Innovative FSW methods obtained a higher tensile strength weld. Two innovative methods GTAW assisted weld and electrically assisted weld are depicted in this section.

2.4.1 GTAW assisted FSW

GTAW assisted HFSW improved the weld strength of 3 mm aluminium alloy AA6061-T6 to stainless steel STS304 by preheating the stainless surface using GTAW. For inhibiting the formation of surface oxidation during welding, 7 L/min of shielding gas (argon) was applied [10]. As shown in Figure 2.7, the aluminium alloy plate is placed on the retreating side and stainless steel plate on the advancing side. The GTAW nozzle is placed at the stainless steel side 2 mm away from the weld center.

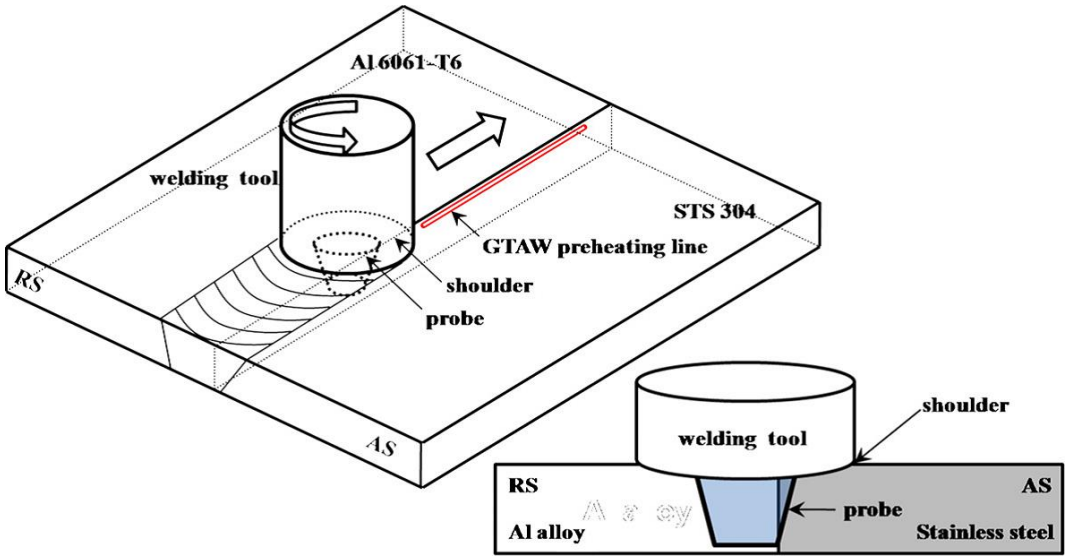

Figure 2.7: Schematic illustration of HFSW process [10].

The weld was successfully achieved without defects at the rotation speed of 300 rpm. The maximum tensile strength of the HFSW joint achieved at the weld were 93% of the aluminium alloy base metal compared to 78% for conventional FSW joint [10]. This result indicates that the improved material plastic flow and also annealing effect by GTAW preheating process result in improved ductility and increased weld strength. Furthermore, the duration of the tool was improved due to decreased axial force between the tool and heated material. Nevertheless, this method may not be desirable in automotive industry. Because, firstly, both GTAW equipment and shielding gases are costly. Secondly, an arc gives off light radiation which may causes vision injury.

2.4.2 Electrically assisted FSW

Figure 2.8 shows a schematic diagram of the electrically assisted FSW for joining 1.4 mm thick AA6061 to TRIP780 steel [27]. Two copper brushes are placed on the top surface of the parent material, serving as the anode and cathode respectively. The copper brushes are mounted to the spindle holder and travel together with the FSW tool. In case of height fluctuations due to workpiece surface roughness, two electrodes are connected to compressive springs. Furthermore, the steel and aluminium alloy workpieces are electrically isolated from backing plate, in order to achieve a maximum current density.

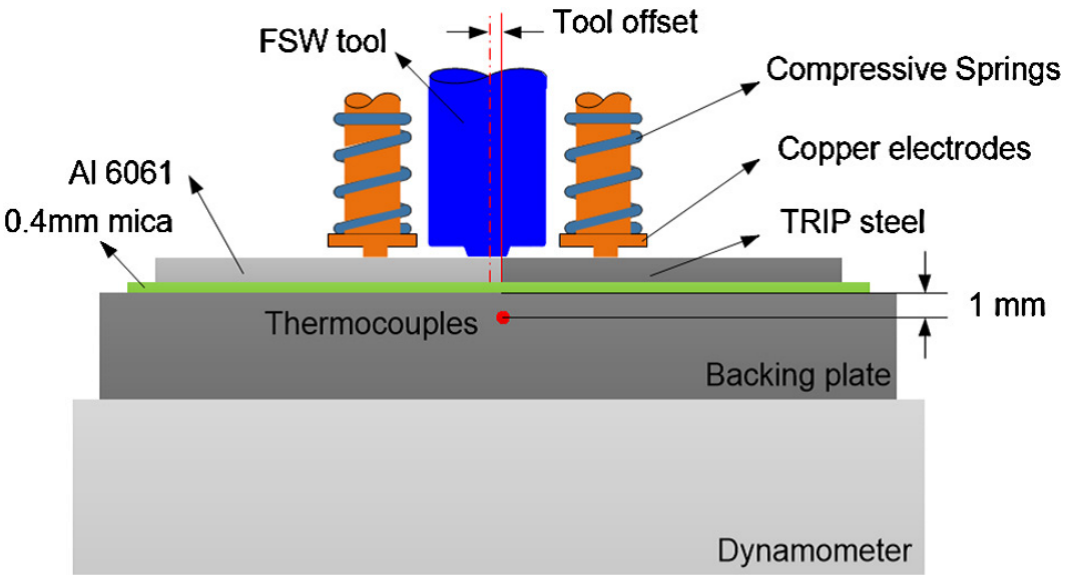

Figure 2.8: Schematic illustration of the experimental configuration for the electrically assisted FSW process [27].

Additionally, electrical current is always concentrated on the vicinity of electrodes. Consequently, to make an intimate contact between electrodes and stirring zone is necessary. An efficient configuration is, therefore, presented and shown in Figure 2.9, where the electrode on steel side is positioned at the front of the tool so that it can sweep through the whole workpiece surface and stay close to the stirring zone. The locations of the electrodes and relevant temperature distribution are shown in Figure 2.10, where A—A cross section is same as the tool axis plane. The temperature on the steel side has been substantially increased while that in aluminium side slightly changed. Applying high density current during welding can soften parent materials. This phenomenon is called electro-plastic effect. Thus axial welding force can be reduced with application of current and the phenomenon is more notable under a low rotating speed and a small tool offset into steel side. Moreover, the formation of a very thin IMCs layer at the interface is considered to be favourable for joint quality. As for GTAW assisted FSW, the electrically assisted FSW can only be applied on butt joint configuration and the equipment is costly and very difficult to be assembled.

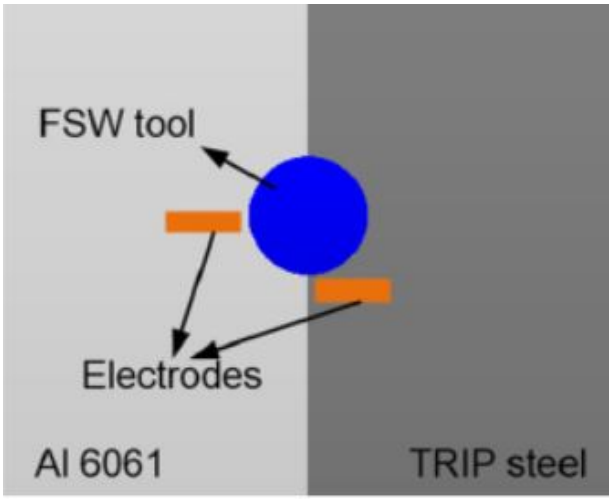

Figure 2.9: Schematic illustration of the experimental configuration for the electrically assisted FSW process [27].

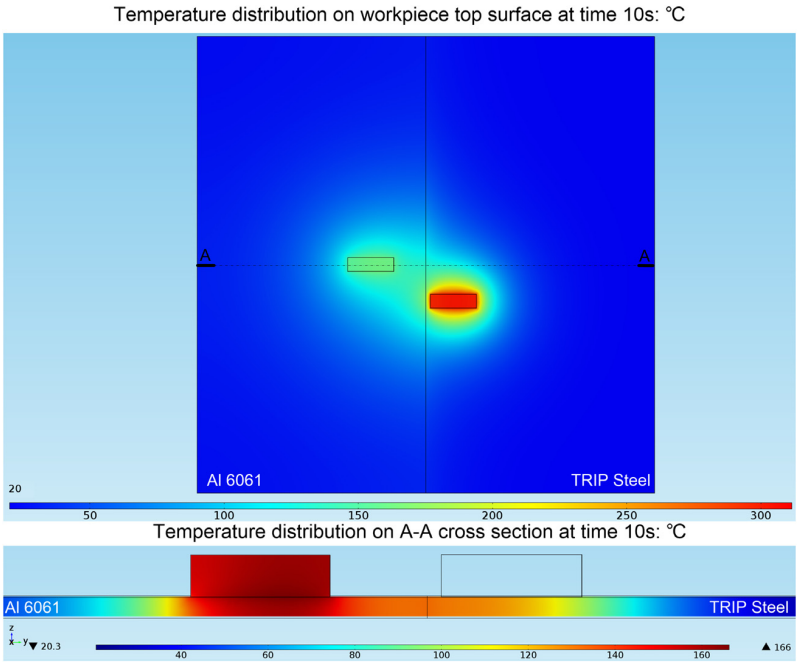

Figure 2.10: Temperature distribution at 10 s for the asymmetric electrodes configuration [27].

2.5 Summary

Mechanical joining methods are broadly used in automotive industrial applications. These methods have the advantages of energy saving and cost efficiency. However, the tensile strength of the joints is limited by discontinuous joining mechanism. Thus high productivity welding methods are gradually replacing the conventional mechanical joining methods. These welding methods can be divided into two main categories, fusion welding and solid state welding. Fusion welding, such as laser welding, generates IMCs and weld shrinkage due to inhomogeneous and varied heat input. The solid state welding methods, such as ultrasonic welding and friction stir welding, can produce a reasonable high strength weld. However, there are also some drawbacks of the solid state welding methods, such as the keyhole left on the end of welds. Although all the above mentioned methods can provide sound mechanical or metallurgical joints, it is very difficult to say which technique is the best for automotive industry because each technique has its own unique advantages. More importantly, the joining is also dependent on maintaining issues, operation costs, cycle time and reliability which are merely a few of the many considerations that must be well thought of. So that a more efficient vehicle joining technique can be adopted [34]. The purpose of the literature review was to give an overview of the recent works on joining dissimilar materials. A large amount of parent materials, tools and welding parameters were investigated which is a great step toward the better joint.

Chapter 3

Experimental plan and conditions

3.1 Introduction

In the present investigation, lap joint configurations were tested for welding aluminium alloy to steel, including two different concepts and different numbers of welding passes. One innovative lap joint design was developed and implemented. This chapter starts by introducing the experimental plan which consists of single pass weld joints, including both conventional and innovative concepts, and multi-pass weld joints. Next, the base material selection is described addressing the dimensions, mechanical properties and chemical composition. The FSW conditions are presented namely the FSW tool, clamping system and a roller to support the innovative lap joint design. The welding parameters implemented in this investigation of the conventional and innovative joint concepts are established. After the welding, all the joints were visually inspected and prepared for microstructure observation, mechanical resistance and microhardness analysis. The used experimental test methods and conditions are presented in this chapter.

3.2 Experimental plan

3.2.1 Overall welding plan

An innovative single pass lap joint was developed and compared with the conventional single pass lap joint. Subsequently, multi-pass welding for these two types of lap joints was conducted to verify the effect on microstructure and mechanical performance. Two lap joint configurations were adopted for this experiment. The schematics of these two configurations are shown in Table 3.1 where arrows stand for parent materials. The left side schematic shows

	Lap Joint Configuration			
	Symmetric lap joint configuration		Asymmetric lap joint configuration *Only for peel test	
Conventional Lap Joint Concept 	Yes	Yes	Yes	No
Innovative Lap Joint Concept 	Yes	Yes	Yes	No
	Single Pass	Multi Pass (2 and 3 passes)	Single Pass	Multi Pass (2 and 3 passes)
	Type of Weld Pass			

Table 3.1: Summary of FSW tests: lap joint configurations of single pass weld joint and multi-pass weld joint for both conventional and innovative lap joint concepts.

that two arrows are symmetrical to the center axis of the tool; therefore, it is named symmetric lap joint configuration. Likewise, the right side schematic is named asymmetric lap joint configuration. For single pass weld joints (both conventional single lap joint and innovative single lap joint), three different sets of welding parameters were employed on these two configurations. After the welding process, 6 joints (3 conventional lap joints and 3 innovative lap joints) in symmetric lap joint configuration were visually inspected and then cut into specimens for optical microscopic observation and tensile shear test. The arrangement of specimens shown in Figure 3.1. Similarly, 6 joints in asymmetric lap joint configuration were cut into specimens for peel test, as shown in Figure 3.2. Two joints, one from conventional symmetric lap joint configuration and another from innovative lap joint configuration, with good mechanical performance were selected for further investigations, including microhardness tests and SEM tests in combination with EDX analysis. Next, two welding parameters which produced the joints with the best mechanical performance in the preceding single pass joint tests were used to conventional multi-pass lap joint and innovative multi-pass lap joint. Table 3.1 shows that only symmetric lap joint configuration was applied for multi-pass welding. During the multi-pass welding process, after the first weld was made, the sheets were turned 180 degree for the second pass and were turned back to the original position for third pass. The third pass was only carried out until half of the weld length. Therefore, 3 pass weld on one half and 2 passes on the other. After welding process, these joints were visually in-

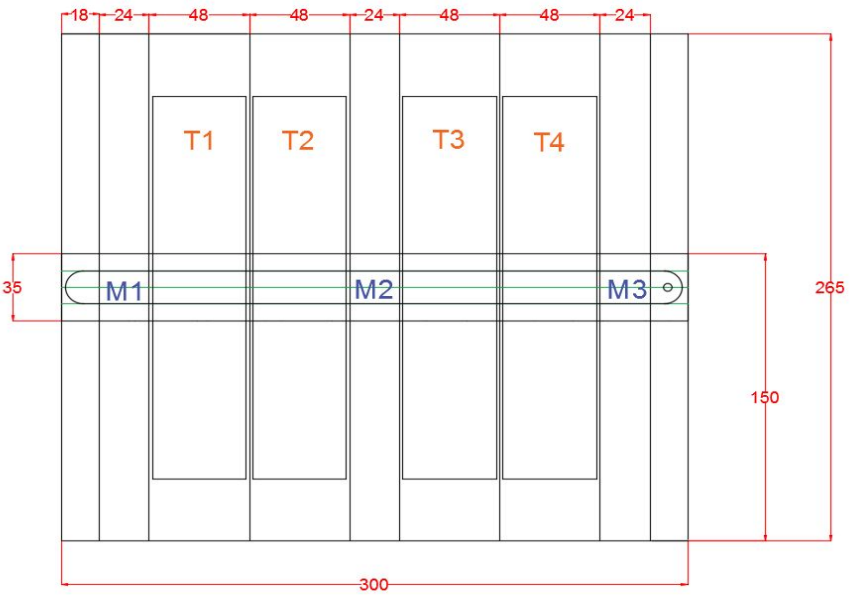

Figure 3.1: The arrangement of specimens for tensile shear test, metallurgical analysis and microhardness test. T stands for specimens for tensile shear test, M stands for specimens for metallurgical analysis and microhardness test.

spected and then cut into specimens for optical microscopic observation and tensile shear test. The arrangement of specimens shown in Figure 3.3.

3.2.2 Conventional lap joint concept

Figure 3.4 and Figure 3.5 show that symmetric and asymmetric lap joint configurations with conventional joint interface. At the beginning of FSW welding process, a rotating probe penetrated into the dissimilar materials. Heat input results in the aluminium alloy into plastic state. The planar steel surface was mechanically stirred by the probe and becomes activated. When the probe started shifting, the aluminium alloy was transferred by the rotating probe and bonded to the activated steel surface, thereby, forming a metallic bonding on the weld interface.

3.2.3 Innovative lap joint concept

The concept of the innovative lap joint is to create localized interfacial diffusion and to utilize additional interlocking mechanism to form a sound joint. Different from the two conventional lap joint configurations, the weld in-

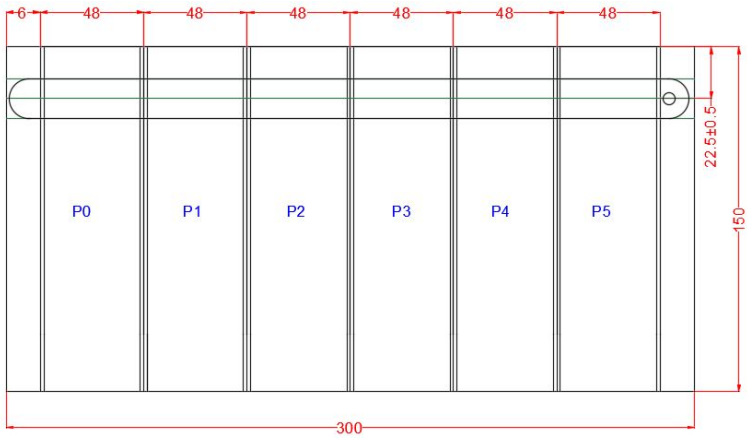

Figure 3.2: The arrangement of specimens for peel test. P stands for specimens for peel test.

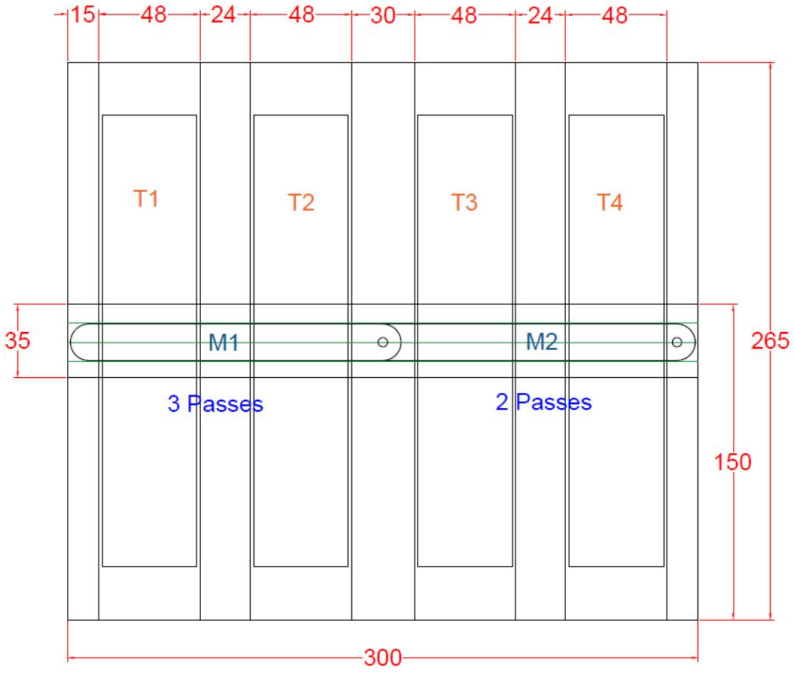

Figure 3.3: The arrangement of specimens for the multi-pass welds. T stands for specimens for tensile shear test, M stands for specimens for optical microscopic observation.

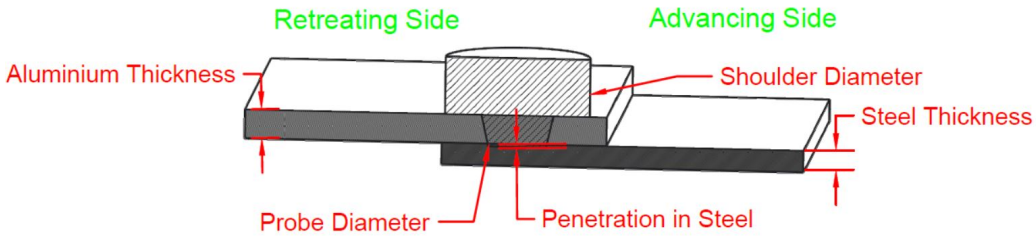

Figure 3.4: Symmetric lap joint configuration with conventional joint interface.

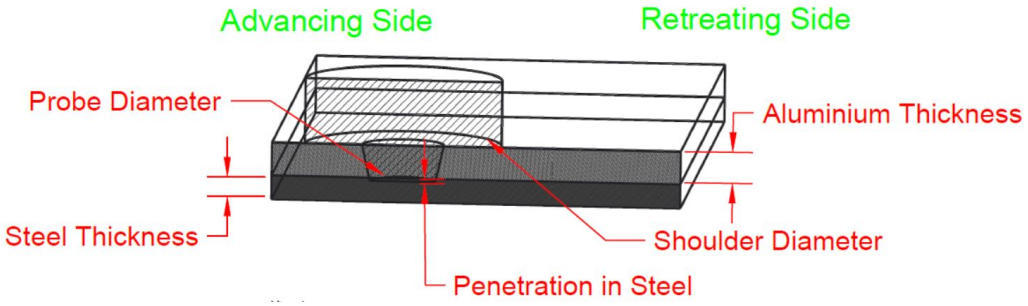

Figure 3.5: Asymmetric lap joint configuration with conventional joint interface.

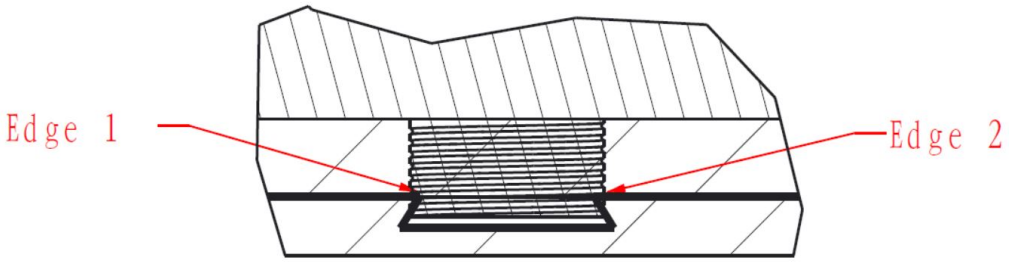

Figure 3.6: Initial lap joint concept.

terfaces of the innovative lap joint configurations have a specific geometry. Figure 3.6 illustrates the initial lap joint concept. A trapezoidal groove is machined along the welding line of the steel sheet. When the welding starts, an enormous pressure, that comes from the cylindrical and threaded probe, acts on two upper edges (Edge 1 and Edge 2) of the groove resulting in plastic deformation. As a result, two new chemically active surfaces are created and exposed to aluminium alloy flow thereby facilitating localized interfacial diffusion and atomic bonding. In addition, the generated heat from plastic deformation can also accelerate interfacial diffusion of these two localized chemically active surfaces. Furthermore, the aluminium alloy will flow into the groove. After solidification, the aluminium alloy sheet and steel sheet are mechanically locked together. However, the trapezoidal groove is difficult to manufacture in the laboratory of Aalto university. Consequently, the innovative lap joint concept was further developed using the same design concept but a different joint geometry. As the Figure 3.7 shown, the wave shape geometry on the surface of steel sheet produced by a roller. The conical probe will destroy the centre convex and two edges (Edge 3 and Edge 4) thereby forming chemically active surfaces. Similar to the initial lap joint design, the aluminium alloy will flow into the grooves resulting in a mechanical interlocking.

3.3 Selected base materials

Aluminium alloy AA5754-H22 and steel DX54 have excellent formability which are suited for complicated automotive inner panel applications [5, 6, 17, 26, 33]. Thus these metals were used as the test materials for all experiments. The test sheets of both materials have a length of 300 mm and

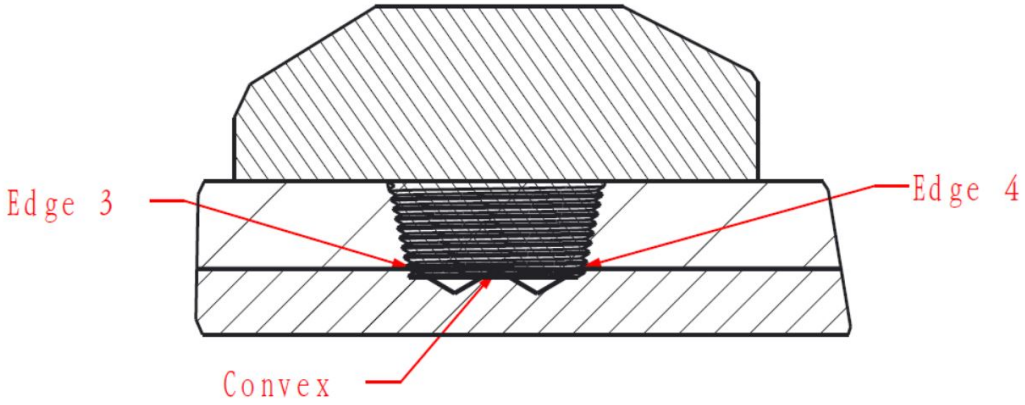

Figure 3.7: Final lap joint concept.

	Chemical composition							
AA 5754	%Si	%Fe	%Cu	%Mn	%Mg	%Cr	%Zn	%Ti
	0.40	0.40	0.10	0.50	2.6-3.6	0.30	0.20	0.15
DX 54	%C	%Si	%Mn	%P	%S	%Ti		
	0.12	0.50	0.60	0.10	0.045	0.30		

Table 3.2: Chemical composition of the AA5754-H22 aluminium alloy and DX54 steel [35].

a width of 150 mm. The thickness of aluminium alloy sheets is 2 mm and the thickness of steel sheets is 1.5 mm. It is worth noting that the welding direction was always along the rolling direction of the test materials, which is consistent with the length of test materials. Moreover, the zinc coating from galvanized steel sheets was removed before experiments using a grinder. The chemical composition of these metals is listed in Table 3.2, the mechanical properties are listed in Table 3.3.

3.4 FSW experimental conditions

3.4.1 FSW tool and other equipments

Throughout the process, it is clear that a FSW tool and a clamping system were needed for the experiments. Furthermore, a roller with unique geometry was also required to be manufactured for making the wave shape on the joining interface of steel. In this part, the materials and critical dimensions

	Mechanical properties			
	YS (MPa)	UTS (MPa)	Hardness (HV 0.2)	Elongation (%)
AA 5754	191.89	257.40	68	14.8
DX 54	165.49	287.17	109	52.4

Table 3.3: Mechanical properties of the AA5754-H22 aluminium alloy and DX54 steel. YS stands for yield strength, UTS stands for ultimate tensile strength.

of FSW tool and roller are introduced. The configurations of clamping system are also described.

3.4.1.1 FSW tools

The FSW tool (Figure 3.8) was composed of a shank (Figure 3.9), a shoulder (Figure 3.10), and a probe (Figure 3.11). The shoulder with a 17 mm diameter and 3.6° concavity of smooth surface was used for the experiments. Two groups of holes were located on the shoulder surface. These holes were used for fixing the shoulder into the shank using two bolts. Prior to fixing, the shoulder can be rotated to a specific position thereby changing the length of the immovable probe. The length of the probe can be adjusted as required. In this investigation, the probe length was always 2.7 mm. The biggest diameter of the conical probe is 5 mm and the smallest diameter of the probe is 4 mm. Moreover, the conical probes has left-handed threads with 1.5 mm pitch and 1 mm depth. The orientation of the threads should always be the opposite of the FSW machine's rotating direction. This generates a vertical downward material flow. Both the shoulder and the probe were made of H13 steel, same as cited literature [28, 36]. The engineering drawings of the shoulder and the probe are illustrated in Appendix A.

3.4.1.2 Clamping system

To carry out the FSW process, a stationary and flat clamping system was necessary. Ref [9, 37] suggest that steel should be always kept on the bottom for lap joint configurations. Moreover, the advancing side was located near the closest sheet edge. Figure 3.12 demonstrates the schematic of symmetric lap joint clamping configuration where two shims were employed for clamping the welding materials. According to ISO 14273 standard, the width of overlap part should be 35 mm in order to proceed with the tensile shear test. Figure 3.13 demonstrates the schematic of asymmetric lap joint clamping configuration. Based on ISO 14270 standard, the distance from the centre

Figure 3.8: FSW tool.

Figure 3.9: Shank.

Figure 3.10: Shoulder.

Figure 3.11: Probe.

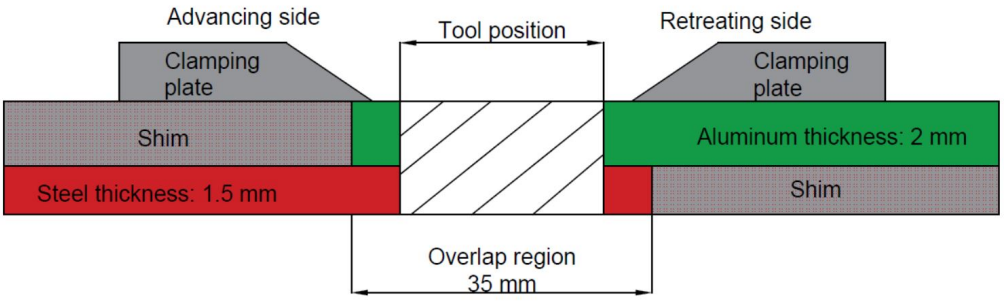

Figure 3.12: Schematic of symmetric lap joint clamping configuration.

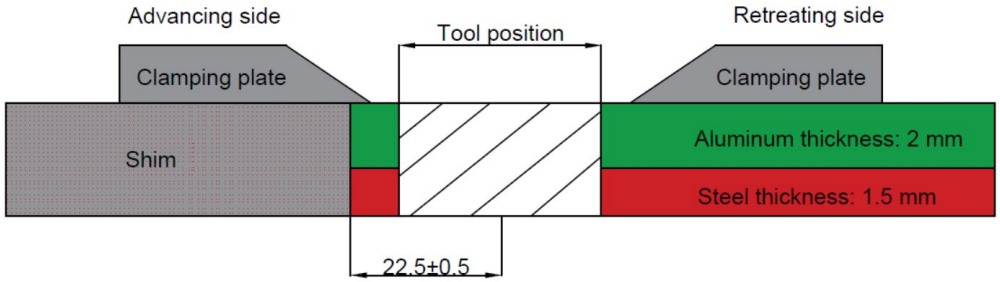

Figure 3.13: Schematic of asymmetric lap joint clamping configuration.

line of nugget to the closest edge should be 22.5 ± 0.5 mm for peel test. As per these two clamping configurations, the sheets were clamped on a flat support plate which was fixed on a horizontal backing table for welding.

3.4.1.3 Roller

The concept of innovative lap joint requires a wave shape on the joining interface of steel. This special joint geometry is readily obtained by using deep drawing technique, which is one of the most widely used sheet metal forming processes in the automotive industry. Nevertheless, the deep drawing machine is not available at the Engineering Materials laboratory of Aalto university. Thus a roller with specific geometry was employed in forming the particular joint geometry. The roller, made from a prehardened mould steel (Uddeholm Impax Supreme), was machined at the laboratory. Figure 3.14 shows the engineering drawing of the roller. Furthermore, an HK 2524.2RS drawn cup needle roller bearing was required for assembling the roller to the

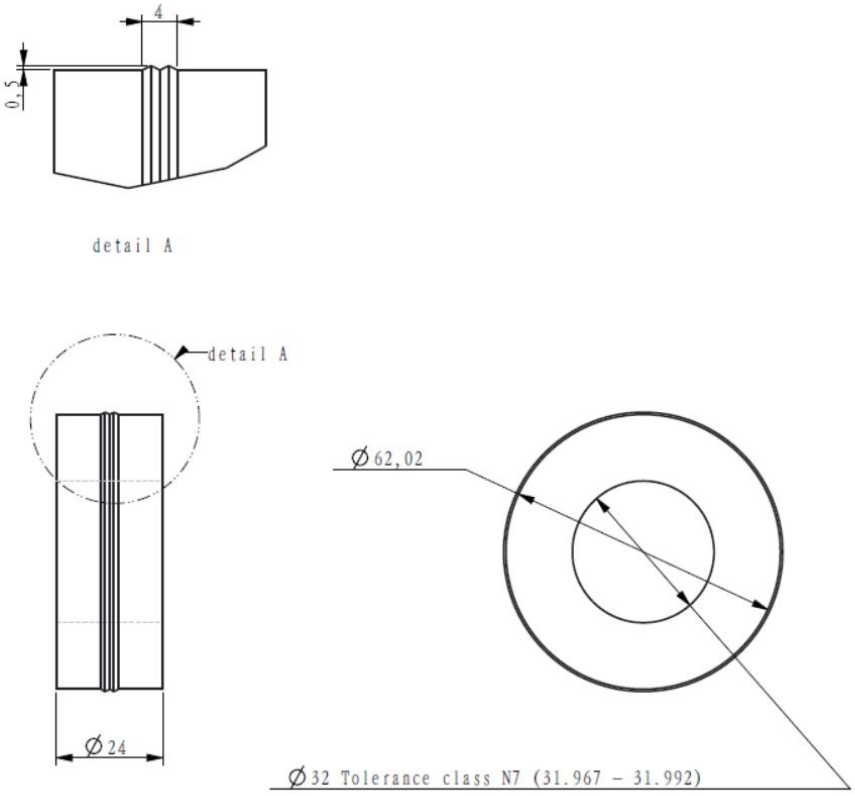

Figure 3.14: The engineering drawing of the roller.

FSW machine. After the roller was fixed in the machine and then rolled over the surface of the steel under 15 kN load, a wave shape was formed due to plastic deformation.

3.4.2 Parameters

The experiments were operated with the ESAB FSW machine (Figure 3.15) at Engineering Materials laboratory in Aalto university. Before the welding process, the base materials were fixed on a horizontal clamping system, and then the FSW machine was tilted 2° with respect to the vertical axis of the surface of the sheets. During the welding process, a FSW tool (Figure 3.8) which was fixed in the tilted FSW machine was plunged into the materials at a speed of 0.1 mm/s to the specified depth (-2.5 mm). Subsequently, the tool kept rotating and moving along the weld line until it reached a preset position. The main welding parameters for both convention lap joints (weld

Travel Speed (mm/min)	Axial Force (kN)	Rotation Speed (rpm)	Probe Depth (mm)	Innovative interface (Yes/No)	Weld No.
100	3.5	800	2.7	No	1
200	7.5	800	2.7	No	2
400	12	800	2.7	No	3
100	3.5	800	2.7	Yes	1'
200	7.5	800	2.7	Yes	2'
400	12	800	2.7	Yes	3'

Table 3.4: Welding parameters for the conventional and the innovative friction stir lap joints.

1, 2 and 3) and innovative lap joints (weld 1', 2' and 3'), are listed in Table 3.4.2.

3.5 Test methods and conditions

3.5.1 Superficial inspection

Visual inspection is the most simplest and quickest way to inspect surface features,which are visible to the eyes, such as excess flash, voids and surface defects. These features are directly affected by welding parameters such as travel speed, axial force and penetration depth. Consequently, all joints were visually inspected to ensure high surface quality of joints under chosen welding parameters.

3.5.2 Microstructural analysis

OM observation and SEM in combination with EDX analysis are two common methods used for friction stirred lap joint microstructure analysis. In this study, both methods were carried out on the weld cross sections perpendicular to the weld line. OM with different ranges of magnification was used for initial observation and examination of different regions of the weld. Then SEM equipped with EDX was employed to confirm the OM observations and obtain a more detailed investigation.

The specimens for OM were sectioned by saw and then cutting wheel. With the saw, surface damage of the specimen was severe. This damage can be reduced considerably by using the cutting wheel. A 2000 rpm rotation speed and 0.3 mm/s feed rate were used for slicing the specimen. And then, specimens were hot mounted with a hot mounting press in bakelite powder.

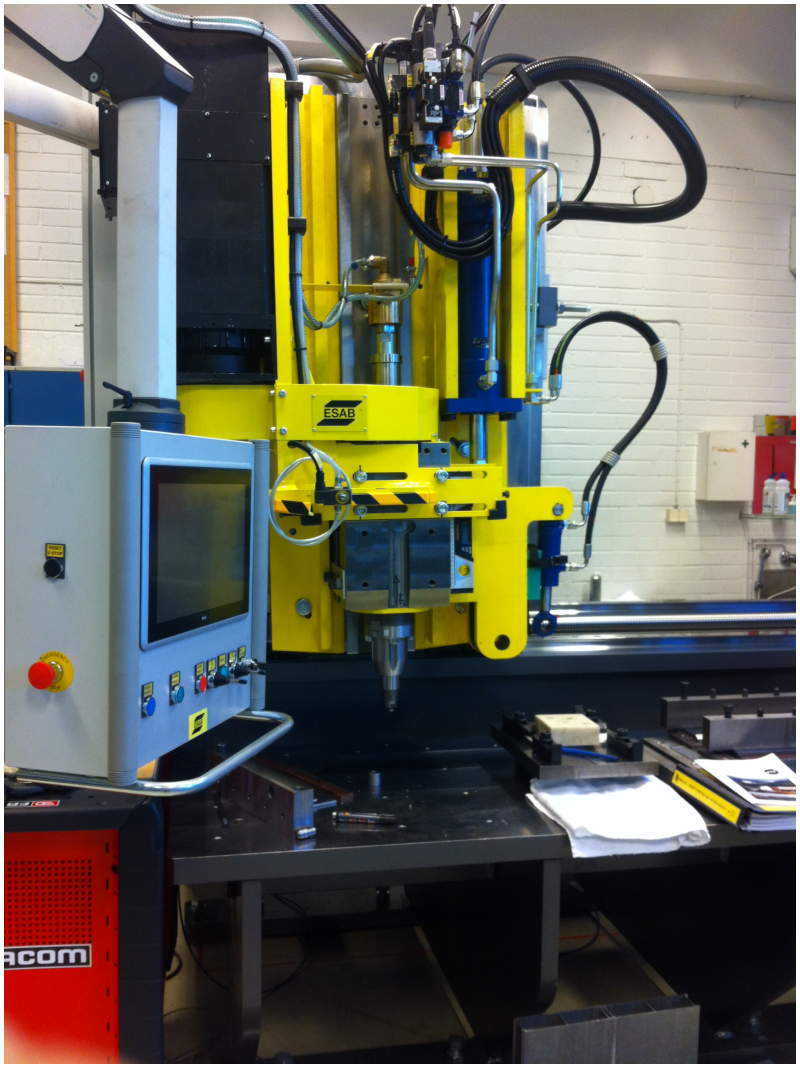

Figure 3.15: FSW machine.

Mounted samples were then progressively rough ground with 180, 320, 800, 1200, 2000 grit abrasive paper. The final polishing was done with 3 and 1 micron diamond suspension on polishing wheels. Before etching, Nikon EPIPHOT 200 machine with 2.5X magnification was used to take macrographs of polished samples. This machine can detect cross section defects, like macroscopic cracks, voids and so on. Subsequently, 3 % Nital solution was used to etch the steel. 1 % hydrogen fluoride reagent was used to etch the aluminium alloy. After etching, microstructural details, such as interlayer mixing and grain boundaries, were revealed under the OM.

SEM coupled with EDX was employed to obtain the microstructure and elemental composition of the specimens. The modeling process for EDX analysis was similar to the process for OM specimens. Except that the specimens for EDX were needed to be polished to a finer grit (0.5 micron). Compared to OM observation, EDX analysis could display data in a variety of ways:

- Detect one or more spots of the weld region and generate spectra which can identify element composition.
- Display the distribution and intensity of already defined elements over the detected areas.

3.5.3 Microhardness tests

The microhardness gradient of the welds along a cross section can be used to reveal hardness changes. In addition, the measurements can be also used to provide necessary data for quality analysis to assure that the weld meet automotive specification.

In this study, two specimens with the best mechanical performance (one made by conventional FSW and another made by innovative FSW) were sectioned and polished so that the microhardness could be measured using a BUEHLER Vickers microhardness testing machine with a load of 200 g and a holding time of 12 s. The microhardness was measured on the horizontal centerline of each sheet and the vertical centerline of weld zone with 1 mm grid spacing. Microhardness map was placed on the weld zone with 0.5 mm grid spacing. The hardness is reported as HV 0.2 where '0.2' stands for 0.2 kilogram force load.

3.5.4 Mechanical tests

Tensile shear test and peel test have been the primary methods used for evaluating strength of friction stir lap welds in literature [9, 37–40]. These test methods were adopted in this study. These two tests were performed

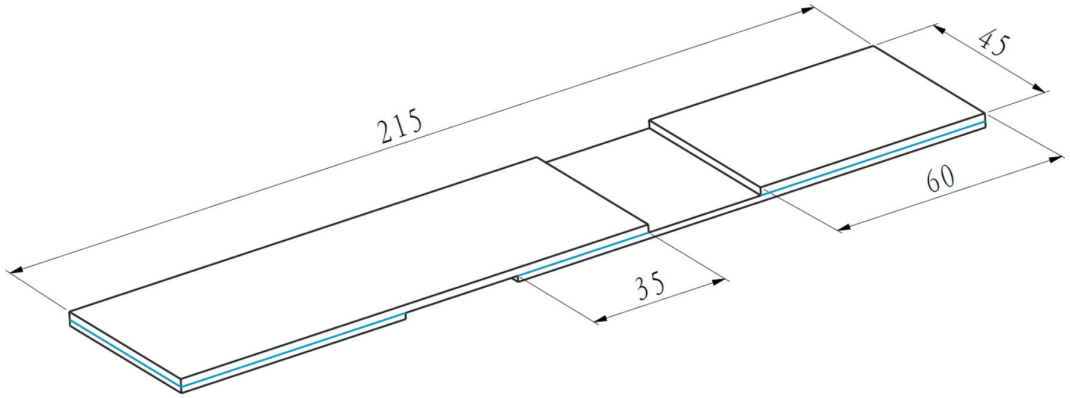

Figure 3.16: Tensile shear specimen. All dimensions are in mm.

for several reasons. Firstly, the results of tests can be used in analyzing the mechanical properties of the joints with different welding parameters. Secondly, the results can be compared between two concepts. Finally, it also can be regarded as reference standard for future studies to predict the mechanical properties of joints under various forms of loading.

Tensile shear test was conducted on a MTS 810 Material Test System at room temperature using a constant crosshead displacement rate of 5 mm/min and the maximum load of each weld joint was recorded for the mechanical analysis. The shape of the samples is rectangular and the dimensions of the specimens were 45 mm wide and 215 mm long. The thickness of specimens is consistent with the thickness of base materials. To be noted, the test specimens should be cut perpendicular to the rolling direction. Because rolled sheets have different mechanical properties in the longitudinal and transverse directions, the specimens should align with the longitudinal direction which has the least strength and ductility. Figure 3.16 schematically shows the shape and dimension of the test piece for the tensile shear test together with two shim plates. Four specimens were taken from the same weld and the maximum loads were averaged. The failure load of specimens were then divided by the width of the specimens as σ (N/mm), which is employed in [36, 39]. Furthermore, UTS of the un-welded aluminium alloy has been measured to be 257 MPa, that is, 514 N/mm.

A peel test was used to measure progressive bond strength changes of the joints by means of T-shape specimens using the tension testing machine.

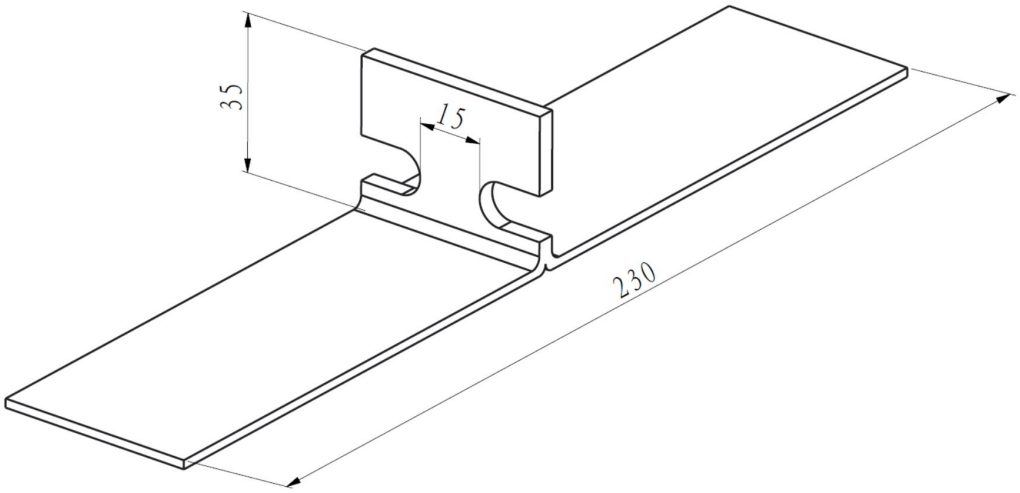

Figure 3.17: Peel test specimen. All dimensions are in mm.

The schematic view of the specimen used for the peel test is shown in Figure 3.17. It is worth noting that the weld was machined to 15 mm. This is because the aluminium alloy sheet was over bended, therefore, fracture was easily happened at the bend part of aluminium alloy sheet. Reducing the length of the weld resulted in the strength of the weld decrease which led to fracture occur on weld zone instead of the bend part of aluminium alloy sheet. During the peel test, the unbonded ends of aluminium alloy and steel were clamped in the test grips and a constant crosshead displacement rate 2 mm/min applied on the ends. Simultaneously, a curve recording of peel strength versus displacement was made. The transition of the curve was used for mechanical analysis.

3.6 Summary

In this study, the aluminium alloy AA5754-H22 and steel DX54 were selected as the test materials. This experiment was divided into two groups, the conventional FSW group (Weld 1, 2 and 3) and the innovative FSW group (Weld 1', 2' and 3'). The difference between the two groups is the wave shape on the interface of steel. The FSW tool used for the experiment contained a shank, a shoulder and a conical probe. The horizontal and stationary clamping system was used to fix the overlap joining configuration. The roller was manufactured specifically for the special weld interface of the

innovative FSW. Three different sets of welding parameters were employed for each group. After the welding process, the welds were visually inspected by naked eye. And then, these test welds were cut and analyzed by OM, tensile shear test and peel test. OM was used for initial observation. After chemically etching by 3 % nital solution and 1 % hydrogen fluoride reagent, microstructure details were investigated under high magnification OM. Tensile shear test was carried out at room temperature using a constant crosshead displacement rate of 5 mm/min. The maximum failure loads were divided by the width of the specimens as σ (N/mm). Furthermore, UTS of the unwelded aluminium alloy was measured to be 514 N/mm. The peel test was conducted on a tension testing machine by means of T-shape specimens. A curve of peel strength versus displacement was recorded to show progressive bond strength changes of the joints. Two welds with the superior mechanical performance were selected from conventional lap welds group and innovative lap welds group for microhardness analysis and EDX analysis. The vickers microhardness values were measured under 200 g load. The microhardness profile was performed on the horizontal centerline of each sheet and the vertical centerline of weld zone with 1 mm grid spacing. The microhardness map was performed on the weld zone with 0.5 mm grid spacing. In later series of experiments, multi-pass test for both lap joint concepts was conducted to verify the improvement of microstructure and mechanical performance by using OM observation and tensile shear test. Finally, reliable results can be obtained to test the innovative concept.

Chapter 4

Analysis of Results

4.1 Introduction

The Figure 4.1 shows the joining interfaces of conventional lap joint and innovative lap joint before the welding process. During the innovative welding process, the center convex and two edges were stirred by the rotating probe which resulted in new chemically active surfaces. Moreover, the aluminium alloy flowed into the grooves which lead to an additional mechanical interlocking. To evaluate the innovative lap joints under different welding parameters, visual inspection, microstructure observation, microhardness test and mechanical tests were used in this study. To serve as comparison criteria, the conventional lap joints were analyzed with the same test methods. Furthermore, multi-pass welds for both FSW methods were carried out with welding parameters that resulted in the best mechanical performance. The completion of second and third overlapping passes increased material flow and eliminated voids. Superficial inspection, OM and tensile shear test were used in order to evaluate the quality of the multi-pass welds.

4.2 Conventional lap joint concept

4.2.1 Superficial inspection

Three sets of parameters were produced for the conventional lap joints. Initially, visual inspection was used to inspect the superficial condition of the welds. Through visual inspection of the top surface of aluminium alloy sheet (Figure 4.2), no defects were found. All the welds demonstrated good surface appearance with regularly spaced arc shaped striations. However, excess flash was visibly formed at the start point of weld 3, as emphasized in Figure

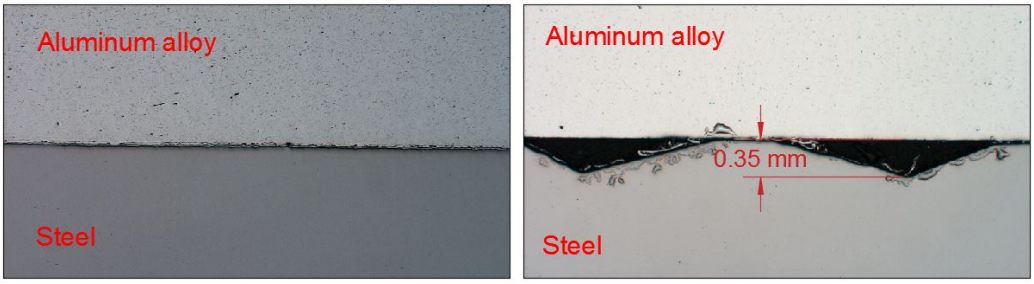

Figure 4.1: The cross section of the joints before welding, the left is conventional lap joint without grooves, the right is innovative lap joint with grooves.

4.2. It can be attributed to excessive penetration in the dwell period. If heat input is too low, the stress flow will be high and the material is not able to flow within the processing zone resulting in voids or tunnels. No joints show any voids or tunnels open up to the top surface layer.

4.2.2 Microstructure analysis

The optical macrographs of the cross section for the three welds are shown in Figure 4.3. The left column shows the optical macrographs of these three welds before chemical etching. The void locations are marked on this figure. From the left column macrographs we can see that the size of void in weld 1 is apparently larger than voids in weld 2 and weld 3. This may result in a weak weld quality.

Corresponding to left column, the right column shows the optical macrographs of these specimens after chemical etching and the optical micrographs in position 1 to 6 of Figure 4.3 are shown in Figure 4.4. Comparing these two columns of macrographs (Figure 4.3), some areas of the steel turned into dark color. These areas are the mixture of aluminium alloy and steel, and the vertical distance of these areas are mainly affected by the axial force of the rotating probe. The axial force of the weld 1 is 3.5 kN which is less than weld 2 (7.5 kN) and weld 3 (12 kN). Figure 4.3 (right column) shows the vertical distance of mixture area in weld 1 (0.04 mm) is evidently less than weld 2 (0.38 mm) and weld 3 (0.45mm). The axial force can provide a downward pressure to facilitate the consolidation of the lap joints. Consequently, the weld 1 performed an insufficient boning than other welds. Furthermore, the axial forging force was not the only factor that affects the quality of the weld in this study. The variation of travel speed also need to be considered.

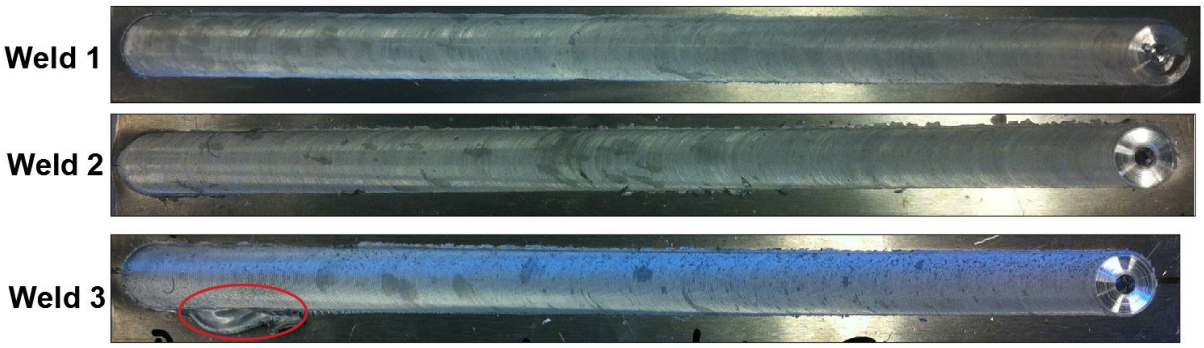

Figure 4.2: Visual inspection of conventional FSW lap joints with three different welding parameters.

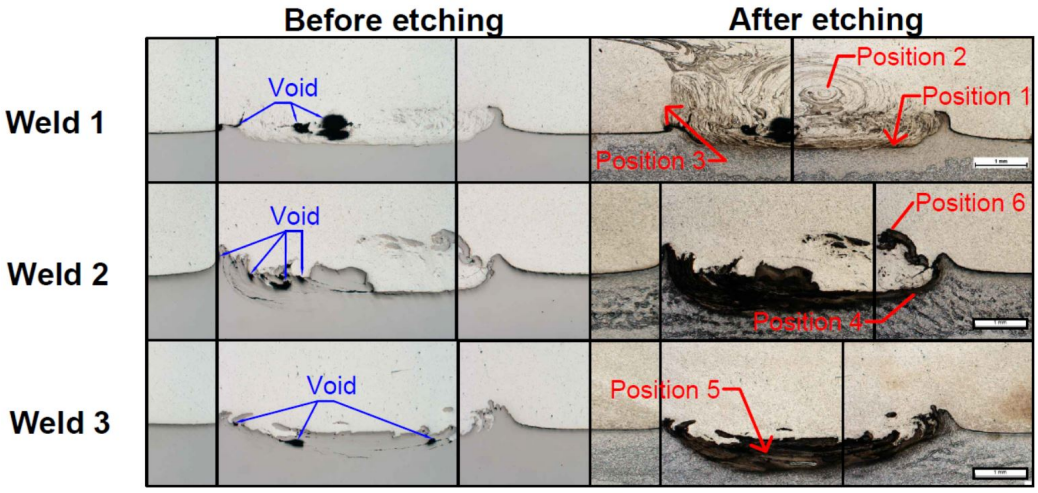

Figure 4.3: Optical macrographs of a weld 1 made using a travel speed of 100 mm/min, a weld 2 made using a travel speed of 200 mm/min, a weld 3 using a travel speed of 400 mm/min.

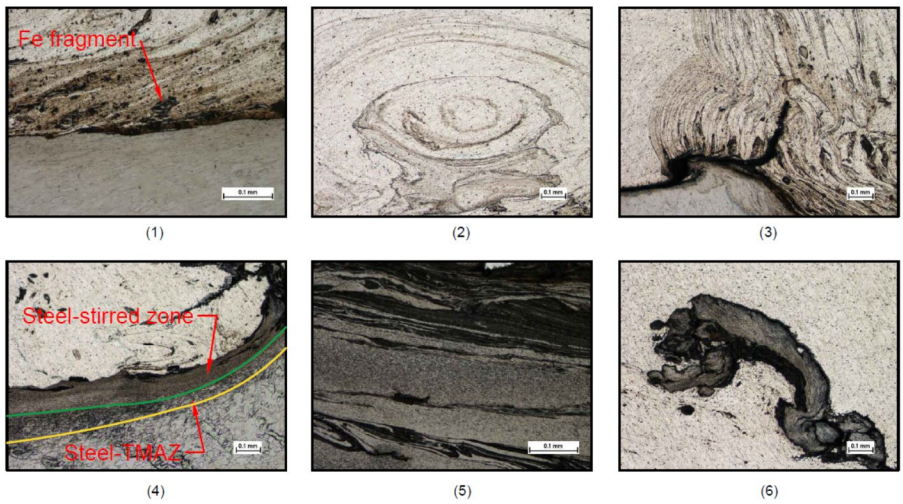

Figure 4.4: Micrographs of the joints shown in Figure 4.29 from position 1 to 6, (1) fine Fe fragments generated in weld 1, (2) swirl-like pattern in weld 1, (3) Al-TMAZ generated in weld 1, (4) steel-stir zone and steel-TMAZ, (5) steel -stir zone of mixture of aluminium alloy and steel : layered structure, (6) a big Fe inclusion existed in the retreating side of weld 2.

According to [37, 40], decreasing the travel speed results in increased heat input. The higher temperature can accelerate the formation of IMCs. In addition, the higher temperature can also soften the steel and promotes material flow around the rotating probe. In weld 1, fine Fe fragments (Figure 4.4 position 1) were sheared and then distributed in the processing zone. A swirl-like pattern (Figure 4.4 position 2) forms on weld 1. However, this pattern does not show on either weld 2 or weld 3. This pattern is the outcome of the thermo-mechanical history and disappears when travel speed increased. The boundary of the aluminium alloy stir zone (Figure 4.4 position 3) in weld 1 is defined as Al-TMAZ. On the contrary, the stir zone and TMAZ of steel on weld 2 and weld 3 are easier to distinguish than that of weld 1. As mentioned before, this is because the axial force of weld 2 and weld 3 are larger than that of weld 1. An example is given in Figure 4.4 position 4 (steel-stir zone and steel-TMAZ). The fine grain size on the steel-stir zone is due to the recrystallization of the steel after experiencing plastic deformation. Additionally, a layered structure is obtained in steel-stir zone of both weld 2 and weld 3, which can offer an additional bonding mechanism [9]. An example is given in Figure 4.4 position 5. Conversely, no layered structure formed in weld 1.

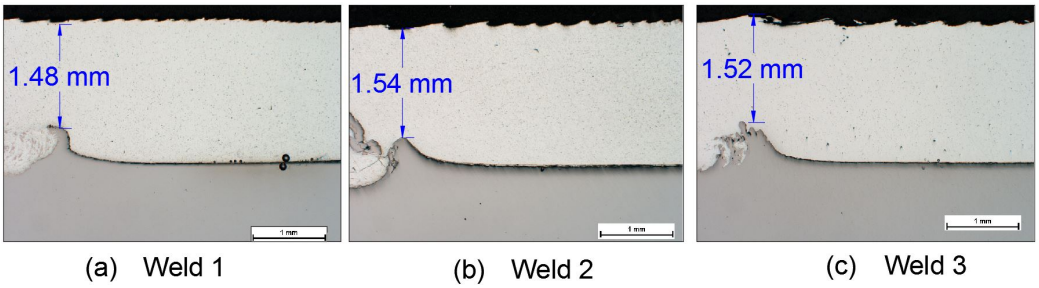

Figure 4.5: The effective thickness of aluminium alloy sheet of weld 1, weld 2 and weld 3.

Cantin et al. [41] described that a threaded probe led to a specific material flow which lifted up the un-welded lap. The lifted un-welded lap is named hook which can reduce the effective thickness of aluminium alloy sheet. Namely, the hook size can affect the mechanical test results considerably as a result of the thickness of the aluminium alloy sheet reduced. Figure 4.5 shows the effective thickness of aluminium alloy sheet on the retreating side for these three welds. The effective thickness of these three aluminium alloy sheets are similar, which means they have similar load bearing capacity. Nevertheless, from the micrograph of cross section of weld 2, a big Fe particle surrounded by fine layers of IMCs was observed on the retreating side, as shown in Figure 4.4 position 6. During the mechanical tests, the particle likely serves as a stress riser which causes crack formation and thus reducing the strength of the weld 2.

The microstructural features of weld 3 were examined further by SEM equipped with EDX. Figure 4.6 shows the scattered voids distributed on the weld region, which is consistent with the previous optical macroscopic observation. As Figure 4.7 shows, a layer with 13.59 μm thickness existed in between aluminium (black) and steel (grey). Figure 4.8 shows that the chemical composition of the un-welded interfacial layer which constituted zinc and aluminium. The content of zinc on the interface resulted from incomplete removal of zinc coating. The result of EDX maps (Figure 4.10) show that the layered structure, which represents mechanical interlocking, is achieved in the steel-stir zone. It is worth noting that the diffusion between aluminium and zinc occurred on the weld zone, which attributes to suppress the melting point of the stirred material so that a better atomic bonding can be obtained [28, 42]. Figure 4.9 shows that a line analysis passing through the centerline of the weld zone. The interlocking zone which consists of steel and IMCs is emphasized on this figure. The distance of interlocking zone

is 200 μm. The aluminium composition of IMCs ranges from 5 % to 45 %. In addition, the nonuniform IMCs layer are present along the entire weld interface between the steel and aluminium alloy. The thickness of IMCs is 1.2 μm to 3.3 μm.

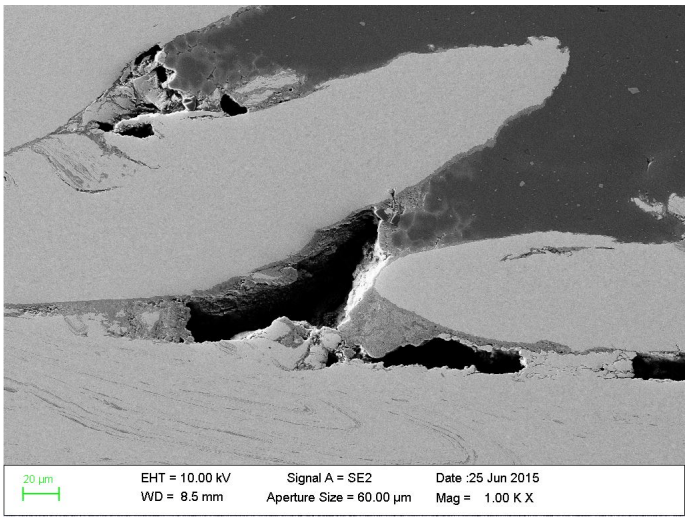

Figure 4.6: Electron microscopic image: voids.

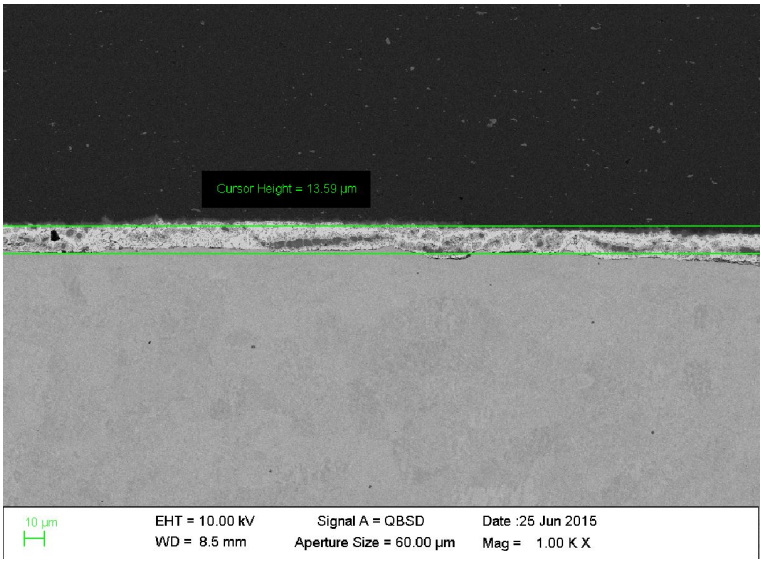

Figure 4.7: Electron microscopic image: layer between aluminium (black) and steel (grey).

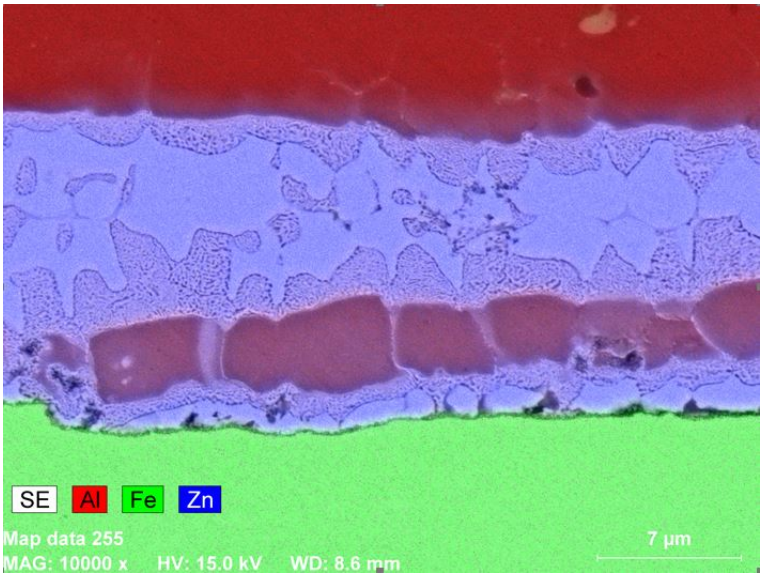

Figure 4.8: Electron microscopic image: EDX map of un-welded layer.

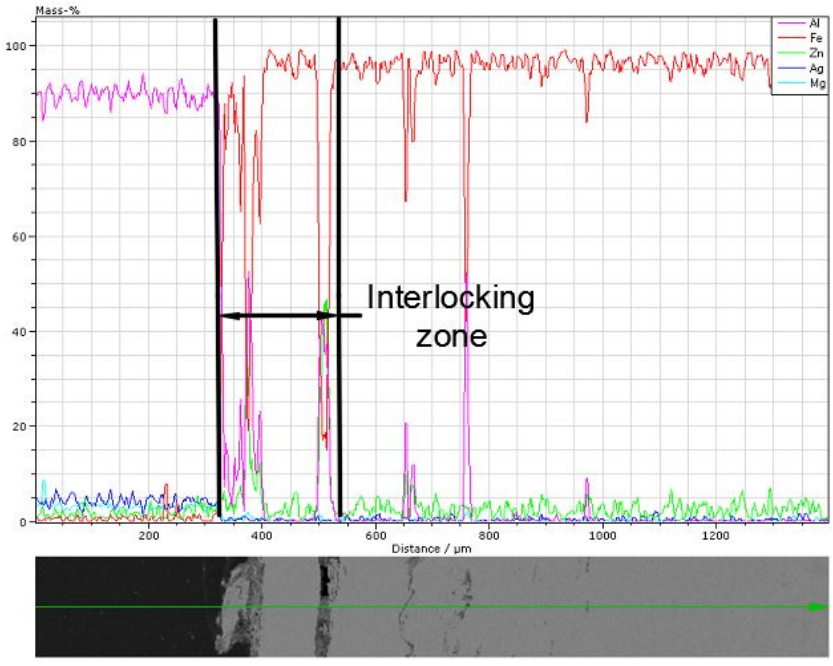

Figure 4.9: Electron image: line analysis pass through the center of weld zone.

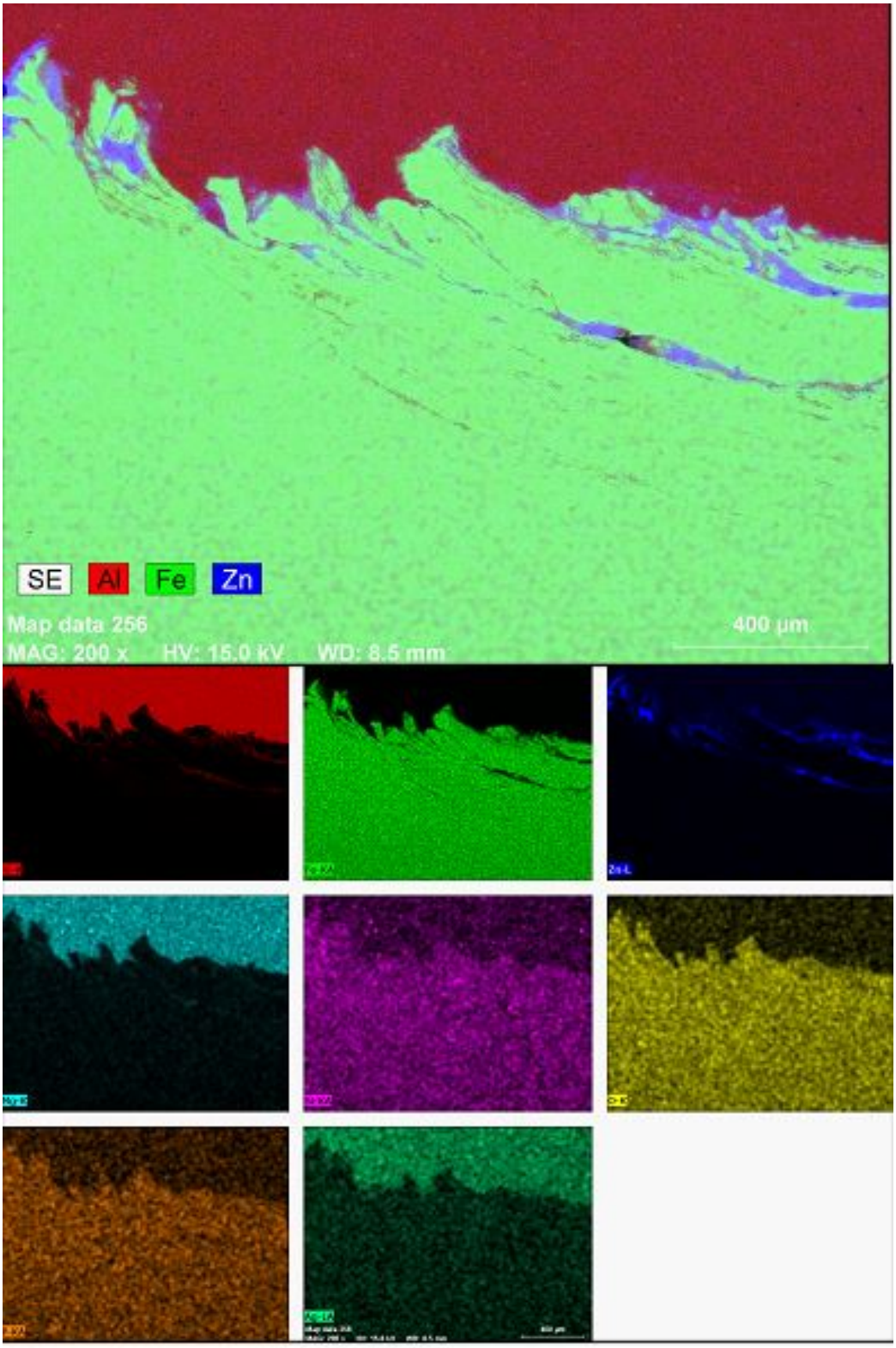

Figure 4.10: Electron image: EDX maps of weld zone.

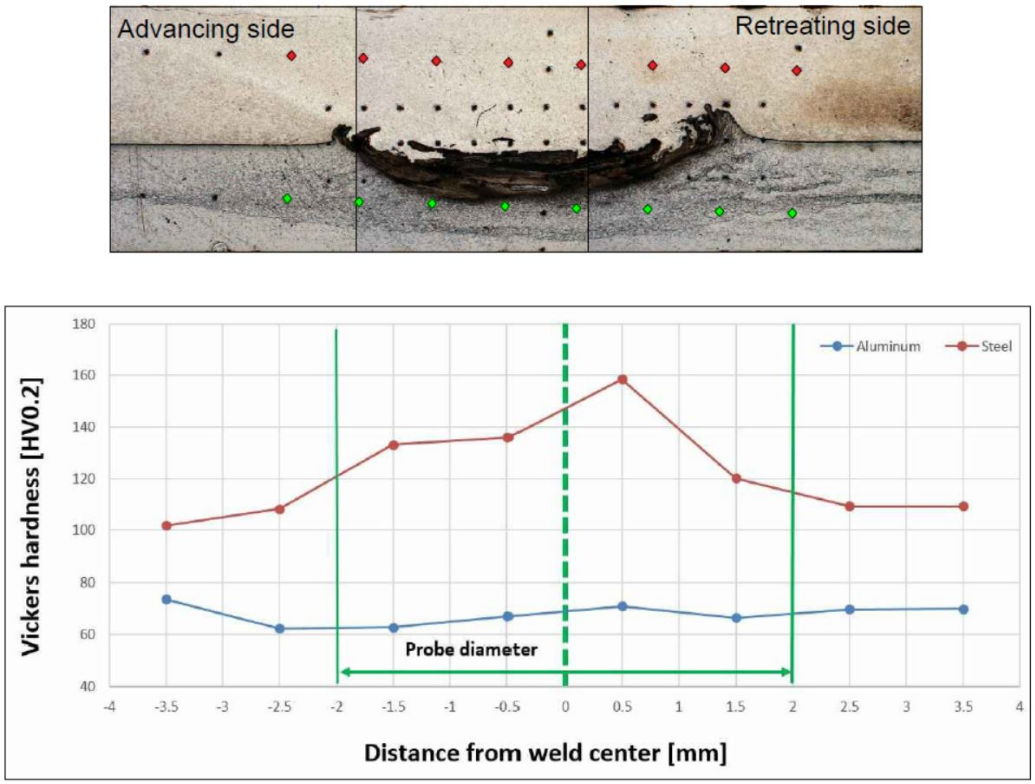

Figure 4.11: Microhardness measurements: horizontally along the aluminium and steel centerline.

4.2.3 Microhardness tests

In the weld 3, the distribution of microhardness along the horizontal centerline of both the aluminium alloy and the steel sheets is shown in Figure 4.11. The microhardness values on the aluminium alloy side are not significantly different in both, base material and stir zone. This is because the aluminium alloy is neither a heat-treatable nor a strain-hardened material. The average microhardness value is 68 HV 0.2. On the steel side, the microhardness values are different on the base material and TMAZ. The average microhardness is 109 HV 0.2 on the steel-base material and 143 HV 0.2 on the steel-TMAZ. The hardness increment in the steel-TMAZ is due to strain hardening result from the plastic deformation by the rotating probe.

The distribution of microhardness along the vertical centerline of the weld zone is shown in Figure 4.12. The microhardness of aluminium alloy in vertical direction is constant. The microhardness of steel is constant at the base material and the value become larger at the stir zone and TMAZ. The

largest microhardness value, which is 184 HV 0.2, located on steel-stir zone. This high microhardness value is due to high microhardness characteristic of the stain hardened steel.

Figure 4.13 shows the microhardness map on the stir zone. From this figure we can see that layered structure yield highest microhardness value, which was 228.3 HV 0.2, as a result of the high microhardenss characteristic of the IMCs.

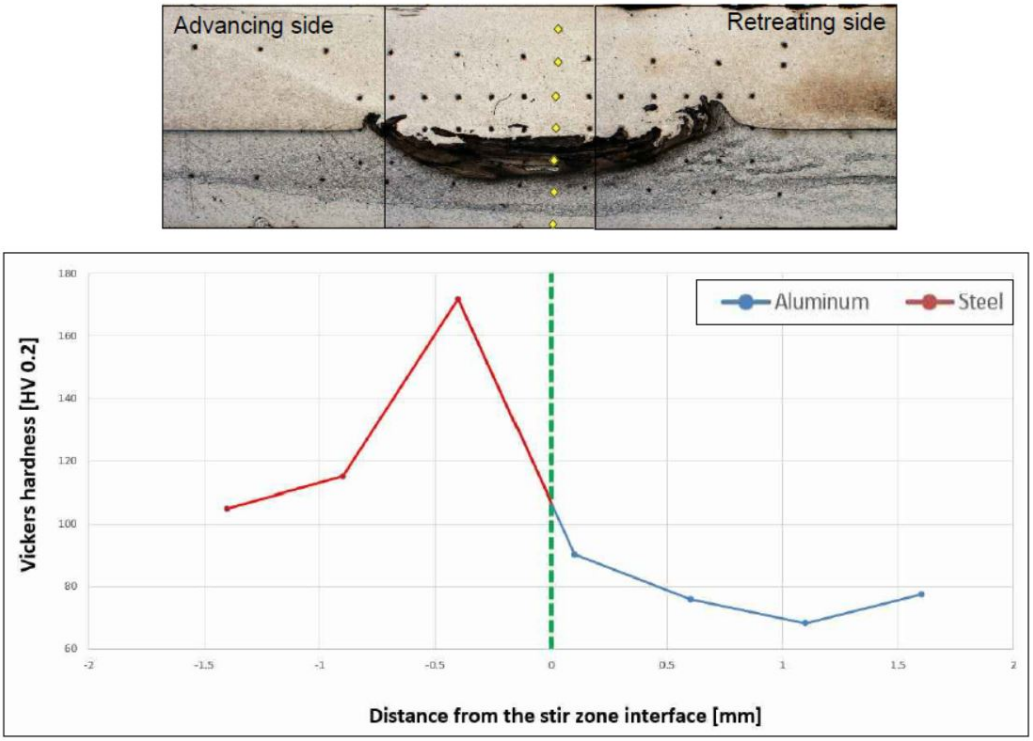

Figure 4.12: Microhardness measurements: vertically across both materials.

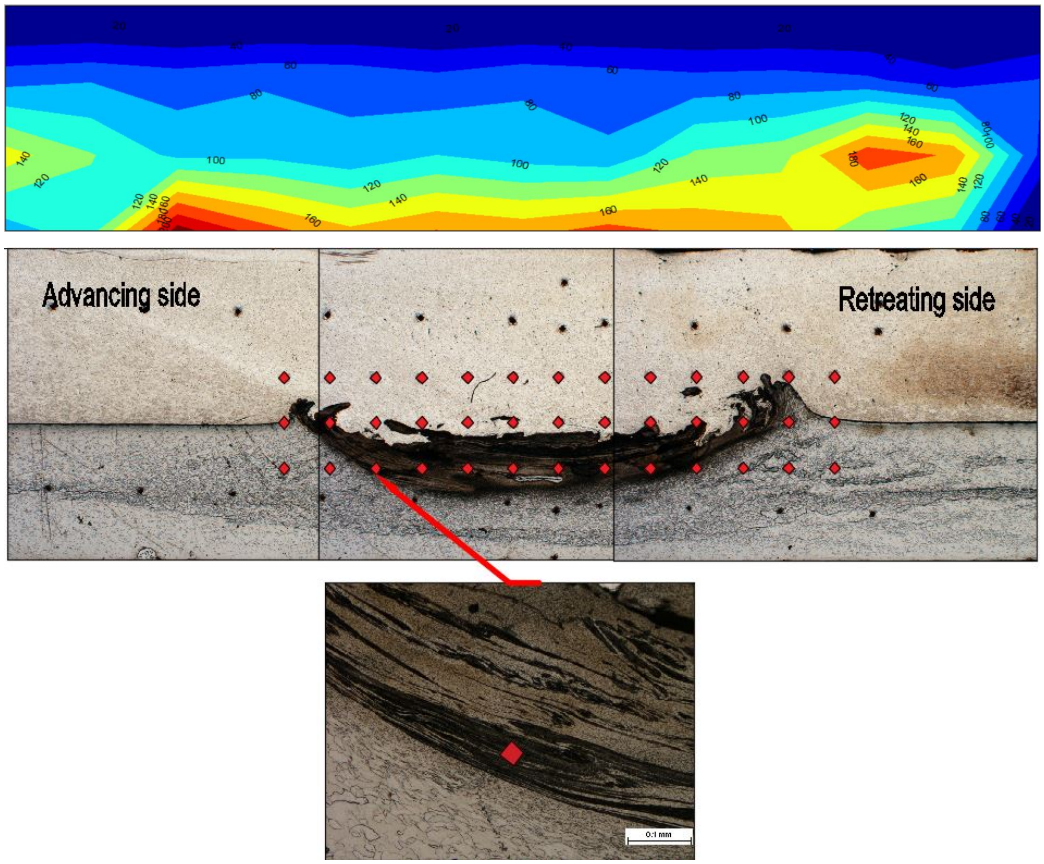

Figure 4.13: Microhardness map on stir zone.

4.2.4 Mechanical tests

The Figure 4.14 shows the tensile shear test results of conventional symmetric lap joints. The weld 3 exhibited the best mechanical behaviour. The average failure load was 249 N/mm, 50 % of the UTS of the un-welded aluminium alloy. The weld 2 gave medium mechanical behaviour. The average failure load was 203 N/mm, 40 % of the UTS of the un-welded aluminium alloy. The failure load of weld 1 was 156 N/mm, which was the worst and 31 % of the UTS of the un-welded aluminium alloy. Moreover, specimens demonstrated two fracture modes. Figure 4.29 mode 1 shows, an example from weld 1 which represents a shear fracture pass throughout the weld interface. Below the mode 1, two examples were selected from the weld 2 (middle) and weld 3 (bottom). As we can see, the overlapping parts of mode 2 specimens were bent significantly. This is because the aluminium alloy and steel were

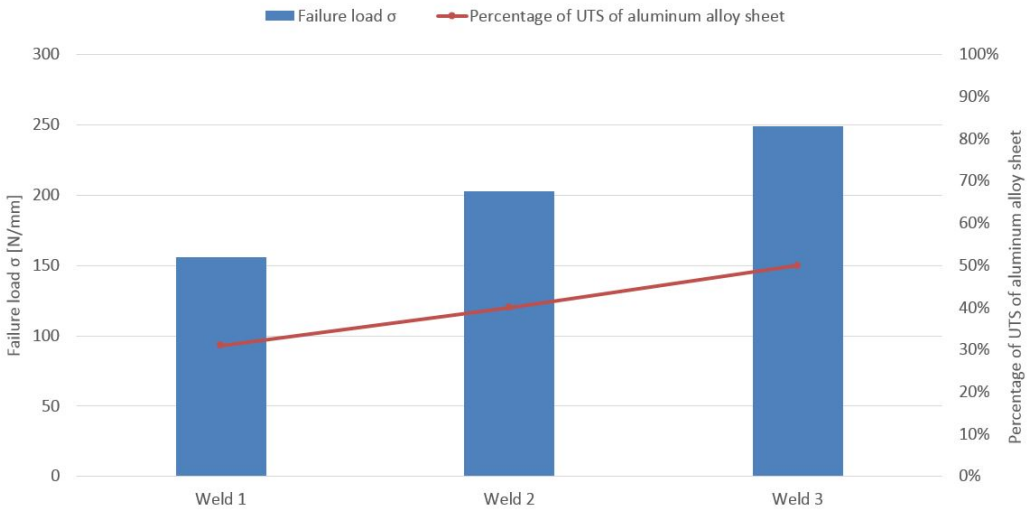

Figure 4.14: The results of tensile shear test of conventional symmetric lap joints.

sufficiently bonded together on the weld zone so that all the loads were forced to concentrate on un-welded part. All fractures of mode 2 specimens initiated from the un-welded interface and then propagate along the hook and ultimately broke at the aluminium sheet. Consequently, the final fractures were similar to normal tensile fractures instead of a tensile shear fracture.

On the other hand, the measured failure loads and fracture modes of the peel test have similar tendencies with the tensile shear test. Figure 4.16 shows the Force-Displacement curves of conventional asymmetric lap joints. As same as the fracture mode 1, weld 1 with asymmetric joint configuration also broke at the weld interface during the peel test. The Figure 4.16 shows that the failure load of the asymmetric weld 1 is 900 N which is the worst result. Based on preceding microstructure analysis, this inferior strength of the weld 1 is due to the low axial forging force. No layer structure formed in steel resulting in poor mechanical interlocking. In addition, thick IMCs were easily formed in the processing zone as a result of high heat input. Furthermore, the Figure 4.16 shows that the bonding strength of weld 1 presents a step shape after reaching the maximum values. This step shape means that a discrete bond was formed along the welding interface. The formation of discrete bond is due to the presence of voids and Fe fragments on the weld interface.

Additionally, the Figure 4.16 contains two other Force-Displacement curves which were selected from asymmetric lap weld 2 and 3. The failure loads of

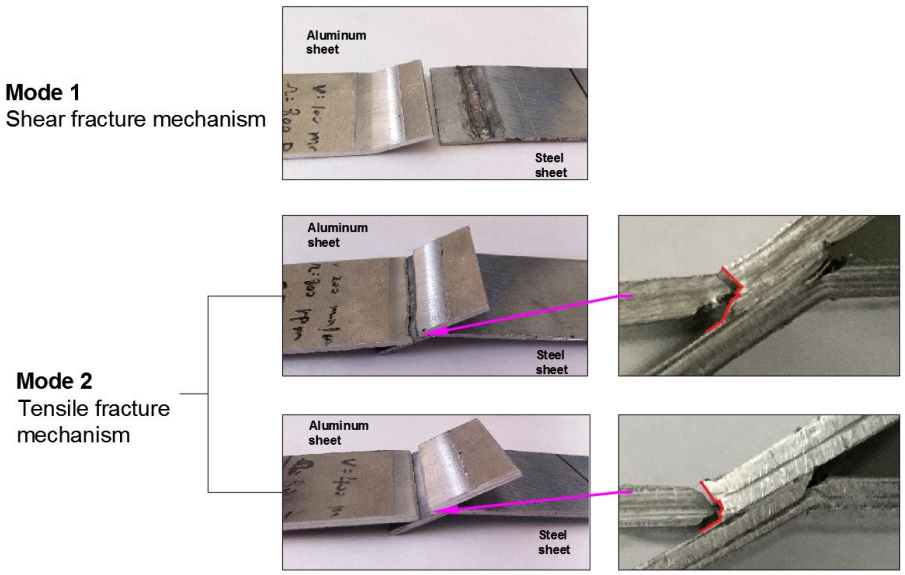

Figure 4.15: Various modes of fracture, Mode 1 throughout nugget fracture, Mode 2 tensile fracture with the crack initiated from the hook.

the weld 2 is 1050 N and the failure loads of the weld 3 is 1310 N. Comparing to the Force-Displacement curve of weld 1, the bonding strength of the weld 2 and the weld 3 drop rapidly after reaching the maximum values rather than form a step shape. This is because the fracture happened on aluminium sheet which is similar to normal tensile fracture. Consequently, the strength of the welds depend on the effective thickness of the aluminium alloy sheet which affected by hook size. As per the previous measurement of the effective thickness of aluminium alloy sheet, the results indicate that the effective thickness of the weld 2 and the weld 3 are basically identical. Therefore, the hook size is not the reason why the strength of the weld 3 is larger than that of the weld 2. Figure 4.29 (mode 2) demonstrates the highlighted fracture paths of symmetric lap joint. It is important to note that fracture path of symmetric lap weld 2 is largely parallel to the overlapped interface in contrast to fracture path of symmetric lap weld 3. This is because of the crack propagated along the Fe particle on the retreating side of the weld 2, which is consistent with previous microstructure analysis. Thus, the existence of the big Fe particle in both symmetric and asymmetric weld 2 may be the reason why the strength of the weld 2 is less than that of the weld 3.

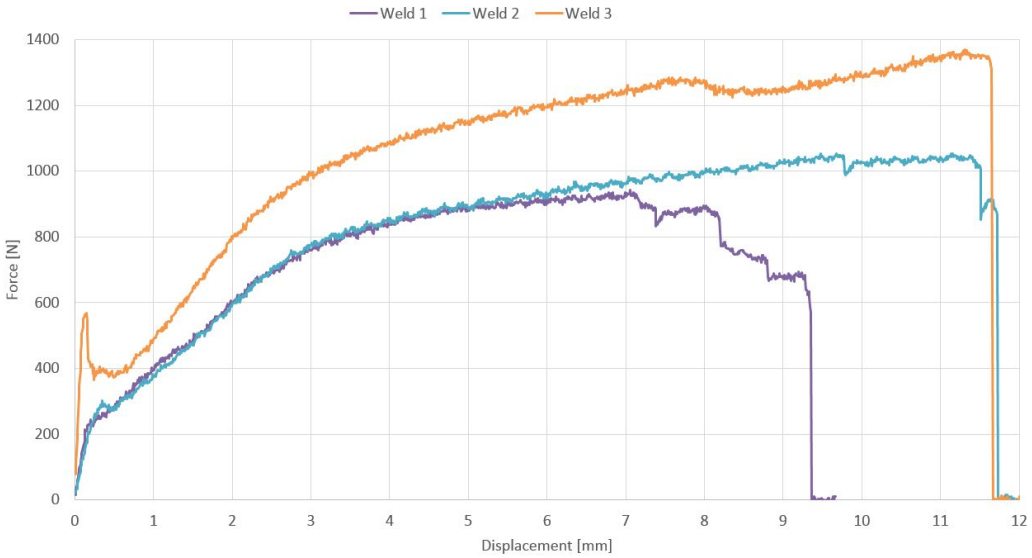

Figure 4.16: Peel test: Force-displacement curves for asymmetric lap weld 1, 2 and 3 .

4.3 Innovative lap joint concept

4.3.1 Superficial inspection

As same as in the conventional lap joints, no voids and channels were detected from innovative lap joints. Nonetheless, a small volume of flash of weld 1', a medium volume of flash of weld 2' and a heavy volume of flash of weld 3' were observed at the beginning of the welds (Figure 4.17). This is because excessive plunge of the shoulder into the aluminium alloy sheet in the dwell period. Additionally, a certain amount aluminium alloy adhered on the shoulder during welding process resulting in the surface defect on the weld 1' which emphasized in Figure 4.17.

4.3.2 Microstructure analysis

The optical macrographs of the three innovative symmetric joints are shown in Figure 4.18. The left column shows the locations and features of the voids. A big void is found in the weld 1' and a number of voids are found in the steel-stir zone of the weld 3'. These void can reduce the strength of the welds. In comparison, the weld 2' has relatively smaller voids. The right column shows the macrographs of these welds after chemical etching. The yellow circle

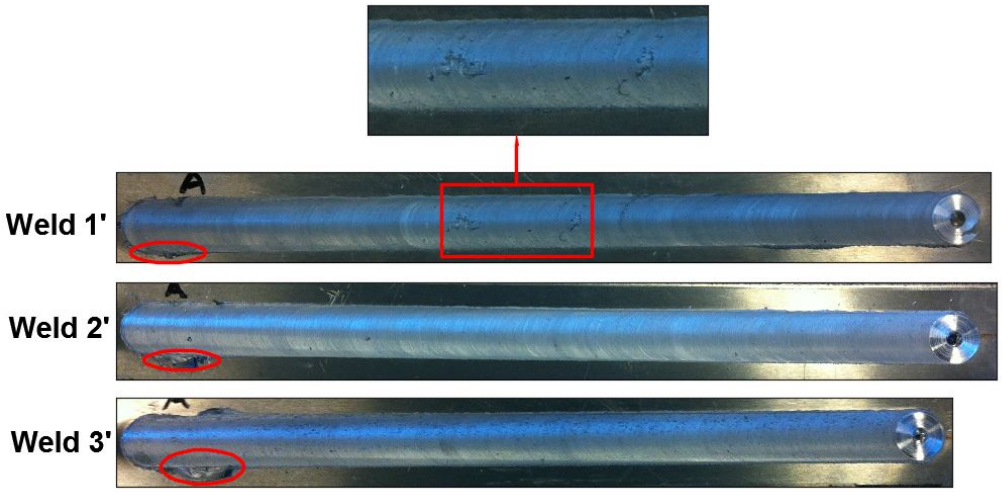

Figure 4.17: Visual inspection of innovative FSW lap joints with three different welding parameters.

highlights the interlocking regions, an evident mechanical interlocking feature formed in weld 3', which may contribute to weld's mechanical performance. However, this feature was not formed in weld 1' and weld 2' as expected.

Comparing the left column of the macrographs Figure 4.18 to the right column of the macropgraphs, the mixture zone caused by axial forging force in weld 1' is low, only 0.05 mm. Thus no distinct steel-stir zone and steel-TMAZ are observed on the weld 1'. On the other hand, the steel-stir zone and steel-TMAZ are easily distinguished in weld 2' and weld 3' because of higher axial forging force. The vertical distance of mixture zone in weld 2' is 0.4 mm and the vertical distance of mixture zone in weld 3' is 0.47 mm. In Figure 4.19 position 1, an example selected from weld 2' displays the steel-stir zone and steel-TMAZ.

Similar to conventional symmetric lap joints, fine Fe fragments and thick IMCs are located on the weld interface of weld 1' as a result of high heat input, as shown in Figure 4.19 position 2. In addition, the swirl-like pattern forms in the weld 1' because of thermo-mechanical history which is analogous to the weld 1. An unclear swirl-like pattern also forms in the weld 2', which is due to the extra heat generated from the plastic deformation of the innovative lap joint. Different from the weld 1', a number of Fe fragments surrounded with IMCs are distributed in the swirl-like pattern in the weld 2'. This is because the rotating probe crushed the center convex of the weld interface led to the shattered Fe fragments distributed into aluminium alloy flow. No swirl-like

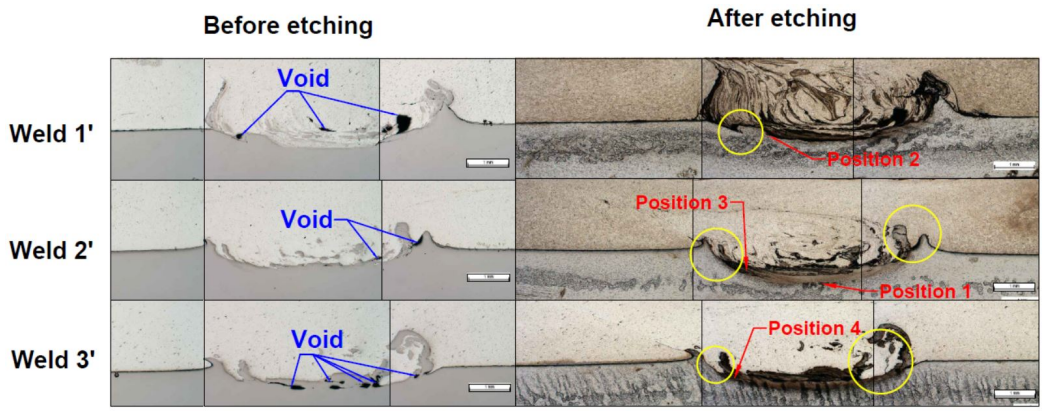

Figure 4.18: Optical macrographs of a weld 1' made using a travel speed of 100 mm/min, a weld 2' made using a travel speed of 200 mm/min, a weld 3' using a travel speed of 400 mm/min.

pattern formed in the weld 3' because of increased travel speed. The presence of Fe fragment and thick IMCs were detrimental to the mechanical resistance of the weld. Figure 4.19 position 3 shows that the layered structure existed in steel-stir zone of weld 2'. Similar layered structure was observed at weld 3' (Figure 4.19 position 4) as well. These layered structures in steel-stir zone and IMCs formed in a weld could provide an additional bonding mechanism thereby increasing the strength of the welds.

Figure 4.20 shows the effective thickness of aluminium alloy sheet. The weld 1' has 1.29 mm effective thickness which is thinner than the weld 2' (1.44 mm). The weld 3' has only 0.9 mm effective thickness. A void was inspected near the hook in the weld 3' which may induce fracture passing through the weld nugget rather than along the hook profile, as emphasized in Figure 4.20.

The weld 2' was examined further using SEM coupled with EDX. Figure 4.21 shows a zinc layer with thickness 10 μm located between aluminium alloy sheet and steel sheet which is similar to conventional symmetric lap joint. As mentioned in optical observation, the layered structure was found in the steel-stir zone of the weld 2'. Figure 4.22 shows the EDX maps of the layered structure. A huge amount of aluminium alloy was blended into steel and then formed IMCs layers. Figure 4.23 shows a line analysis passing through the centerline of the weld region. The distance of the interlocking zone is 175 μm. The aluminium composition of IMCs ranges from 10 % to 23 %. Furthermore, an uniform IMCs layer with thickness 1 μm is presented along

the entire interface of aluminium alloy and steel and the IMCs composition is shown in Figure 4.24. The aluminium composition of IMCs ranges from 20 % to 60 %. Additionally, IMCs with high aluminium composition was also discovered on the hook. Figure 4.25 shows that Fe fragments surrounded with thick IMCs located on the advancing side of the hook. After examination, the chemical composition of the IMCs is shown in Figure 4.25. The average aluminium composition of IMCs is 50 %. Furthermore, several voids are discovered near to the hook. Both IMCs with high Al composition and voids may cause a negative effect on the hook.

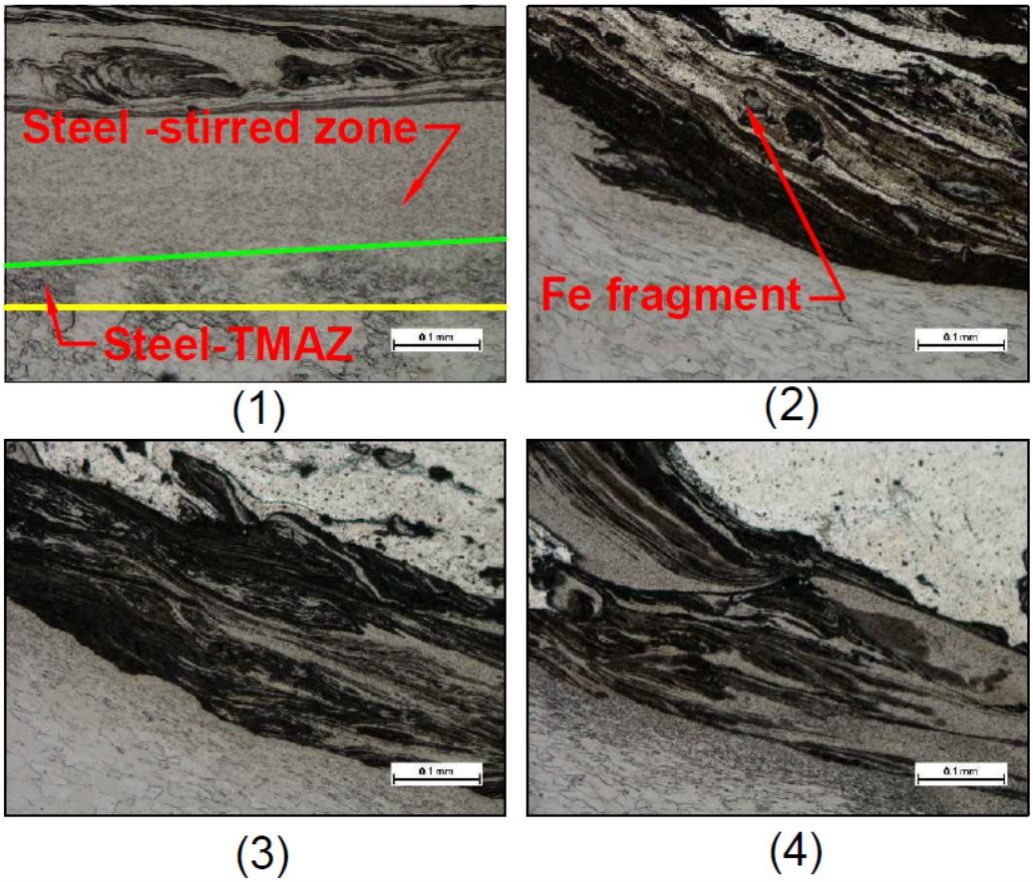

Figure 4.19: Micrographs of the joints shown in Figure 4.18 from position 1 to 4, (1) steel-stirred zone and steel-TMAZ in the weld 2', (2) fine Fe fragments generated in the interface of the weld 1', (3) layered structure on the weld 2', (4) layered structure on the weld 3'.

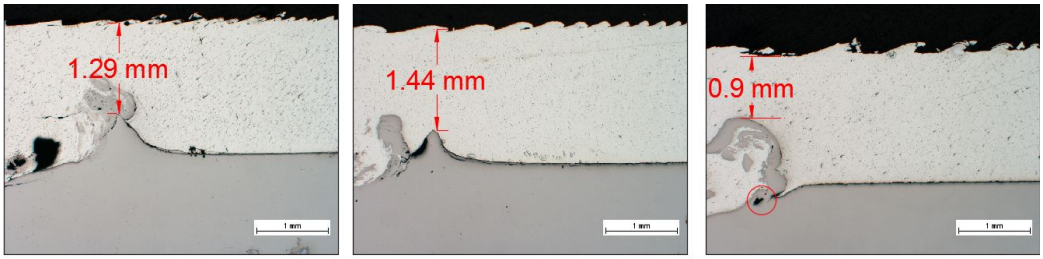

Figure 4.20: The effective thickness of aluminium alloy sheet of weld 1', weld 2' and weld 3'.

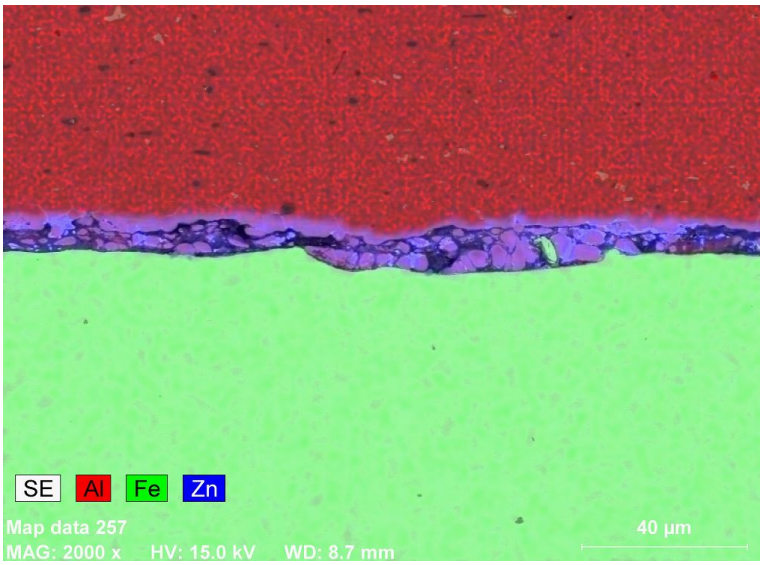

Figure 4.21: Electron microscopic image : EDX map of un-welded interface with zinc layer.

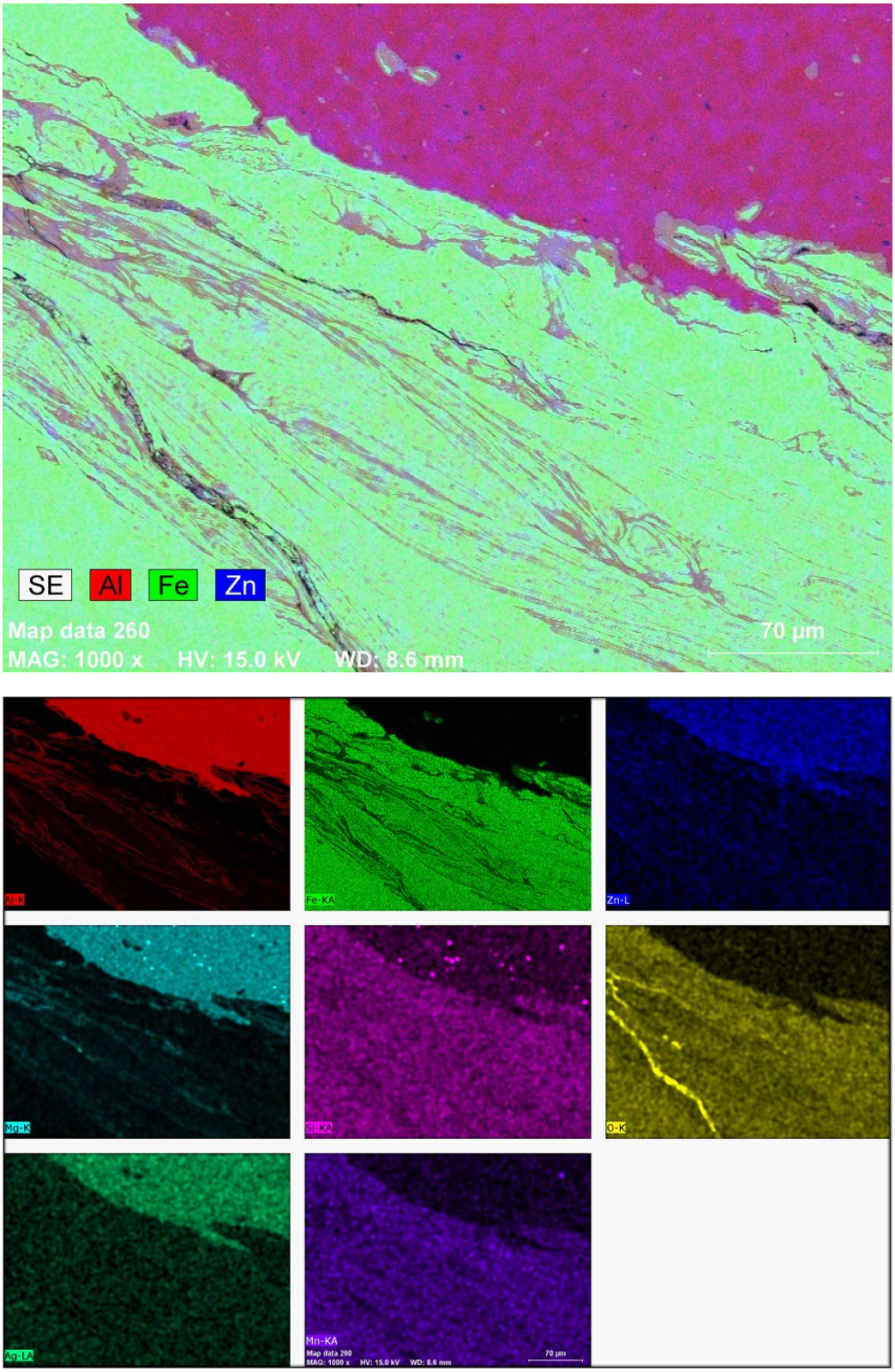

Figure 4.22: Electron microscopic image: EDX maps of layered structure.

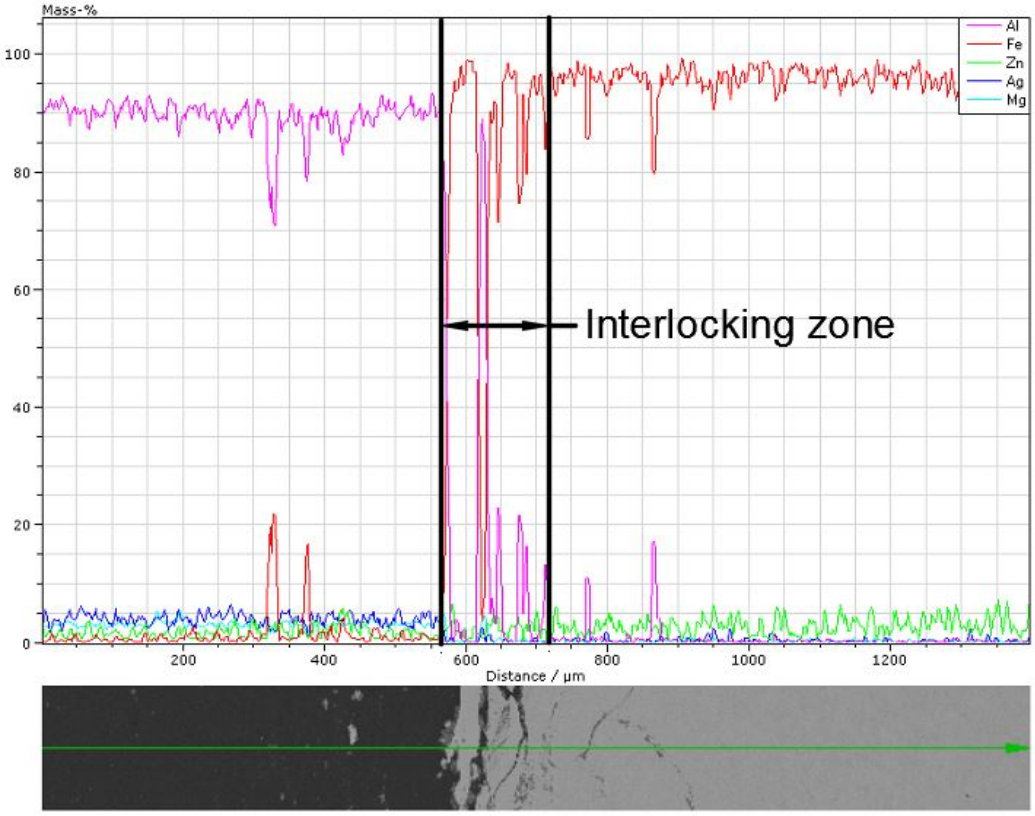

Figure 4.23: Electron microscopic image: line analysis pass through the center of weld 2'.

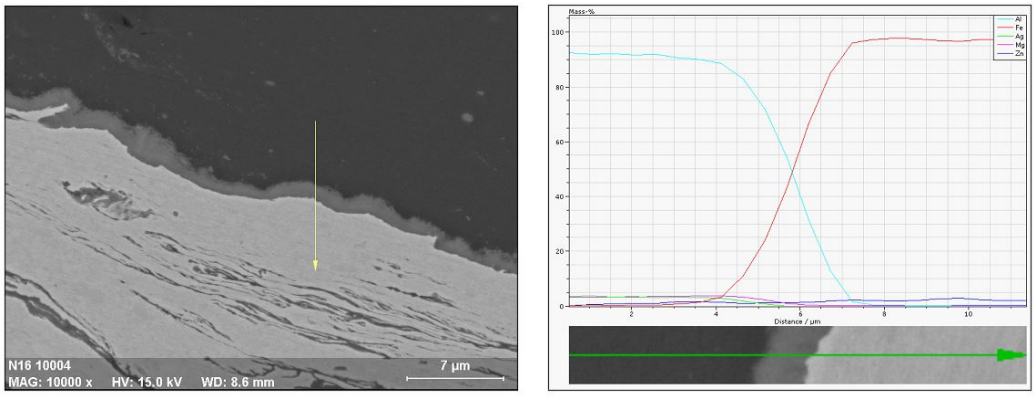

Figure 4.24: Electron microscopic image: line analysis pass through the continuous IMCs layer on the weld interface.

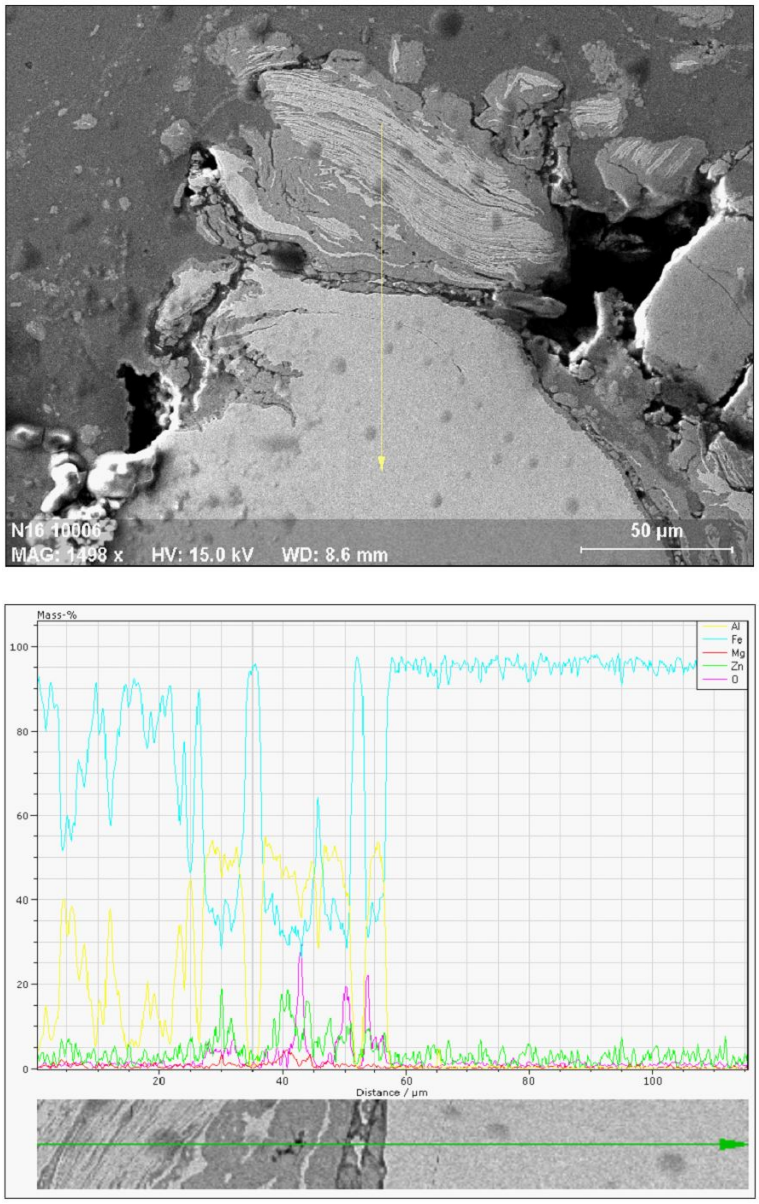

Figure 4.25: Electron microscopic image: hook feature and its chemical composition.

4.3.3 Microhardness tests

Figure 4.26 shows the variation of microhardness values in weld 2' along the horizontal line passing through the center of both materials. The aluminium alloy is neither a heat-treatable nor a stain-hardened material, therefore, the

microhardness curve of aluminium alloy is stable. The average microhardness value is 60 HV 0.2. On the steel side, the microhardness values on steel-stir zone and steel-TMAZ are larger than that on the steel-base material because of strain hardening. The average microhardness value is 107 HV 0.2 on base material, 142 HV 0.2 on steel-TMAZ and 193 HV 0.2 on steel-stir zone.

The microhardness value variation in vertical direction is shown in Figure 4.27. The microhardness values increase significantly from steel-base material to steel-stir zone due to strain hardening effect, and reach the maximum value at a strip of IMCs. The microhardness value of this IMCs is 277 HV 0.2. Subsequently, the hardness goes down to a constant value (73 HV 0.2) on aluminium alloy stir zone.

Figure 4.28 shows the microhardness map on weld zone. In this figure, the microscopic image (magnified area) shows the largest microhardness value, which is 284 HV 0.2, located on the advancing side of weld zone where a huge amount of IMCs are present.

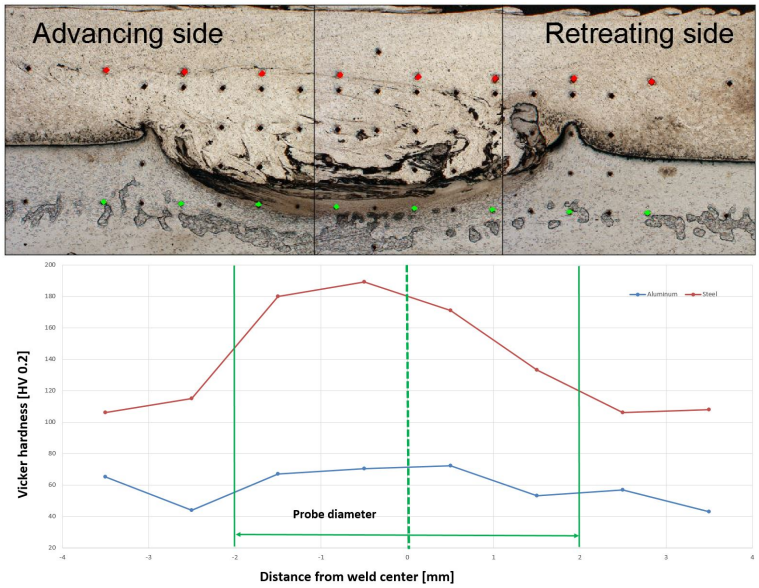

Figure 4.26: Microhardness measurement: horizontally along the aluminium and steel centerline.

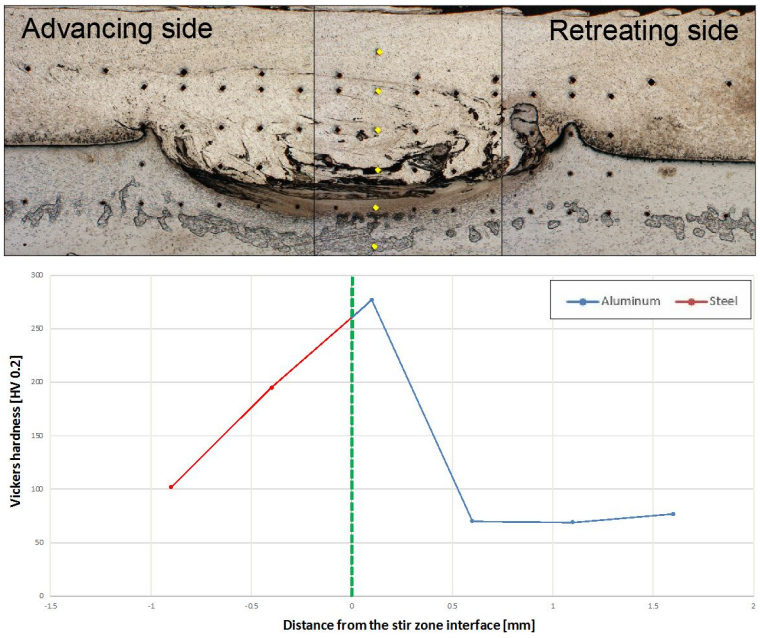

Figure 4.27: Microhardness measurements: vertically across both materials.

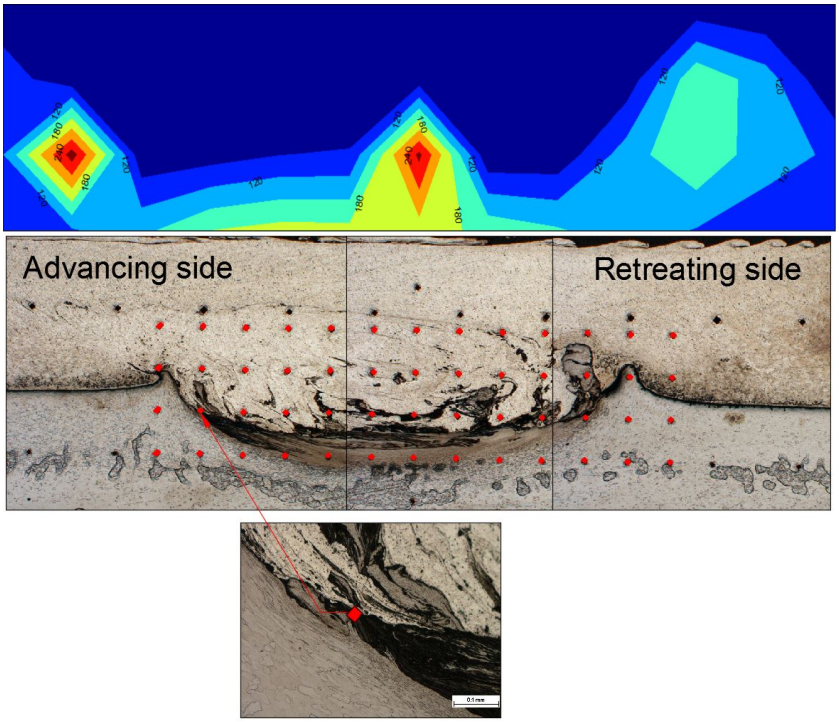

Figure 4.28: Microhardness map on weld zone.

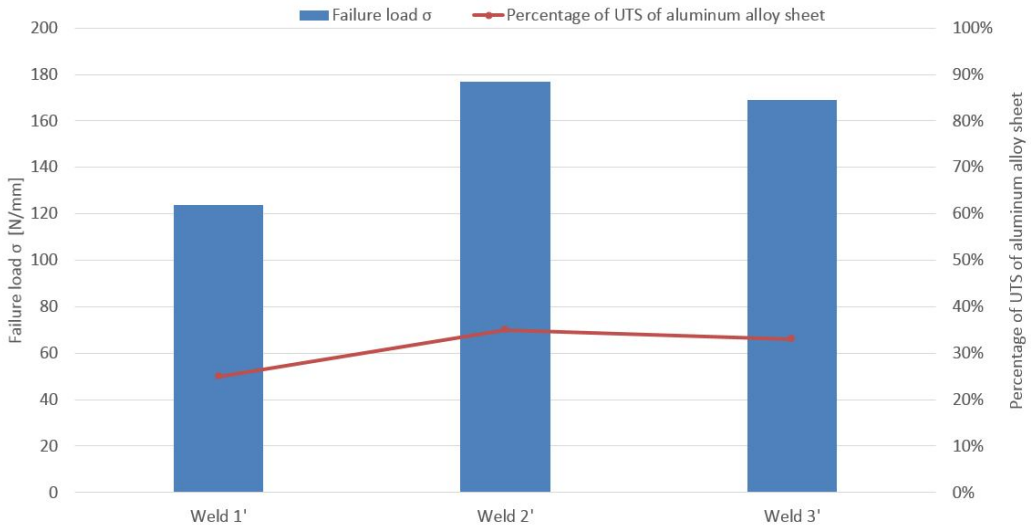

Figure 4.29: The result of tensile shear test of innovative symmetric lap joints.

4.3.4 Mechanical tests

The Figure 4.29 shows the tensile shear test results of innovative symmetric lap joints. The weld 2' exhibited the best tensile shear strength of 177 N/mm which is 35 % of the UTS of unwelded aluminium sheet. The weld 3' exhibited medium tensile shear strength of 169 N/mm which is 33 % of the unwelded aluminium sheet. The failure load of weld 1' was 124 N/mm, which was the worst result, only 25 % of the UTS of the unwelded aluminium sheet. Furthermore, Figure 4.30 shows that two fracture modes of the innovative symmetric lap joints are analogous to that of conventional symmetric lap joints. In the tensile shear test of innovative symmetric lap joints, all specimens from weld 1' and two specimens from weld 3' broke at the weld interface (mode 1). All specimens from weld 2' and two specimens from weld 3' broke at the aluminium alloy sheet. The two specimens from the weld 3' which broke at the weld interface is presumably due to many voids existing in steel-stir zone which is consistent with previous microstructure observation.

For further investigation, Force-Displacement curves of the innovative asymmetric lap joints are shown in Figure 4.31 which display the history of peel strength variation. And then, finding out the reasons that cause the joint failure in terms of the progressive bond strength changes of the

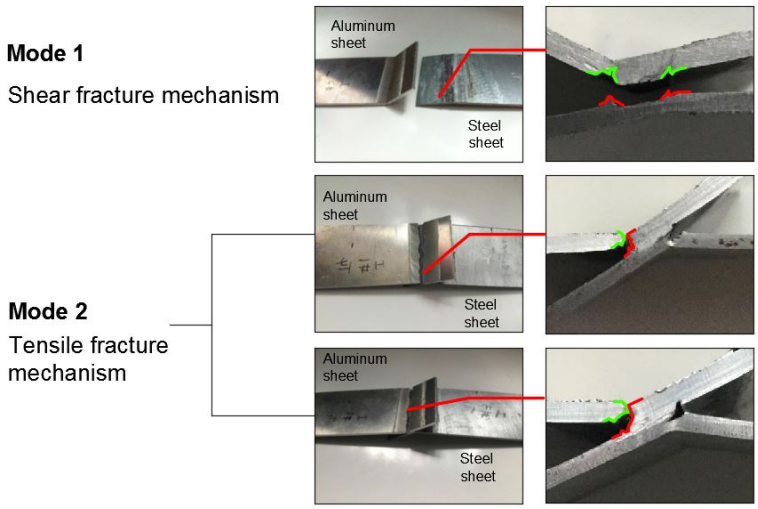

Figure 4.30: Various modes of fracture, Mode 1 shear fracture, Mode 2 tensile fracture with the crack initiated from the hook.

joints. As Figure 4.31 shown, the asymmetric lap weld 1' presents the worst results. The maximum load of the weld 1' is 453 N. In agreement with microstructure analysis, insufficient axial forging force and thick IMCs along the weld interface can be the reasons why weld 1' has the most inferior strength. In addition, the step shape is shown again after reaching maximum load. This is because of the presence of voids and Fe fragments on the weld interface.

Two representative Force-Displacement curves of innovative asymmetric lap weld 2' and 3' are shown in Figure 4.31 as well. The maximum peel test load of the weld 2' is 1150 N and the maximum load of the weld 3' is 1000 N. Comparing to the Force-Displacement of the weld 1', the displacement of the weld 2' and the weld 3' is large than that of weld 1'. And also, no step shape is shown on the weld 2' and weld 3'. This is due to the fracture happening at the aluminium sheet which resembles failure in tensile test. In contrast with the Force-Displacement curves of conventional asymmetric lap weld 2 and 3, the bonding strength of the weld 2' and 3' drop gradually after reaching the maximum loads. This is due to the crack propagating along with larger hooks and ultimately breaking at the thin aluminium alloy sheet. As shown in the fracture modes of tensile shear test (Figure 4.30), the fracture path of weld 2' (middle) is almost perpendicular to the overlapped interface. The fracture path of weld 3' (bottom) is largely parallel to the overlapped interface which is consistent with hook shape. Consequently, the hook feature is the critical

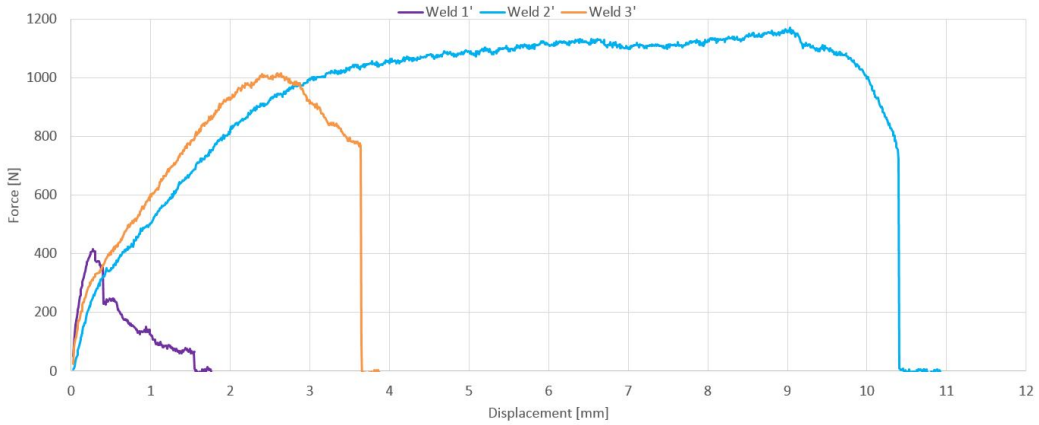

Figure 4.31: Peel test: Force-Displacement curves for asymmetric lap weld 1', 2' and 3'.

factor affecting the strength of the welds. Based on EDX observation, a number of voids and Fe fragments surrounded by thick IMCs were formed near to the hook of weld 2' which resulted in inferior bonding at this region.

In addition, the interlocking feature in the weld 3' does not provide additional mechanical bonding strength. The failure is due to voids and large hook exiting in the weld zone. Furthermore, the fracture did not occur by pure shear. Rather, it was due to the separation of the sheets because of bending and peeling.

4.4 Global analysis

4.4.1 Superficial inspection

Comparing Figure 4.2 and Figure 4.17, no voids and tunnels are found from both groups. For conventional lap joints, the excessive flash is solely found in weld 3. Nonetheless, all the innovative lap joints show various degree of flashes. This is because excessive penetration of the shoulder into the aluminium alloy sheet in the dwell period result from the load bearing capacity of innovative joint interface is lower than the conventional joint interface. Furthermore, the surface defects are found on weld 1'. The formation of this defects are due to aluminium alloy adhered on the shoulder during the welding process resulting in the scratched surface of aluminium alloy sheet.

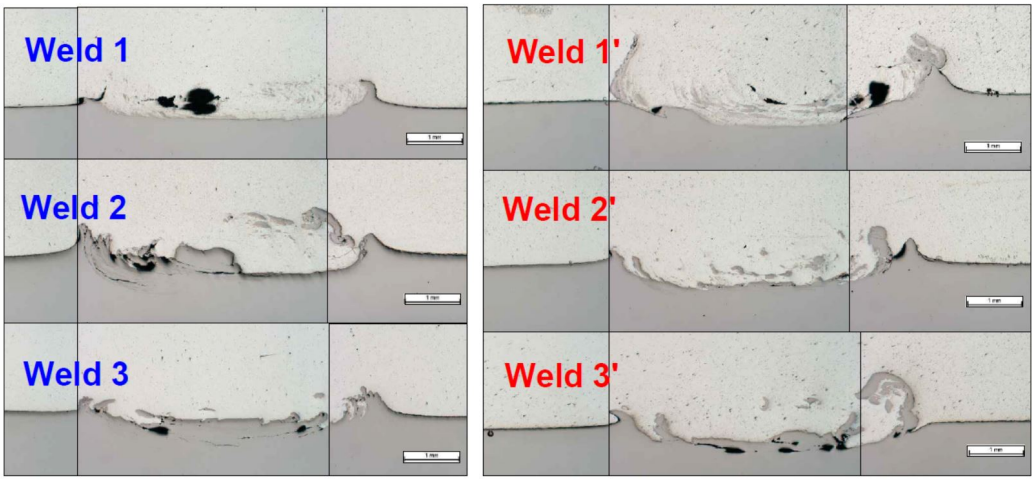

Figure 4.32: Macrographs for both conventional symmetric lap joints and innovative symmetric lap joints before etching.

4.4.2 Microstructure analysis

Figure 4.32 shows the macrographs of these two groups' welds before etching. The relative big voids are found in aluminium alloy sheets of the weld 1 and weld 1'. This is because downward force of the material flow is insufficient which can be improved by increasing axial force or probe thread depth. The relative small voids are found in steel sheets in the weld 2, weld 2', weld 3, weld 3'. It is because the heat input was low and the plastic material flow was not complete during the welding process. These voids on the weld region can reduce the strength of the welds. Comparing these six welds, the weld 2' has the relatively lesser and smaller voids which are helpful to increase the strength of the welds.

The aim of the innovative lap joints is to let the aluminium alloy flow into the grooves and then to form an additional mechanical interlocking after solidification. Nonetheless, this feature was not formed in the weld 1' and the weld 2' as expected. The failure is caused by the inadequate depth of the grooves. An evident mechanical interlocking feature formed in the weld 3' between two outer edges of grooves and inner hooks which may provide additional interlocking force.

Different from the interlocking feature generated by grooves, the rotating probe can stir aluminium alloy into steel and then form a layered structure which consists of IMCs layers and steel layers. This layered structure can offer an additional interlocking mechanism which increases the strength of

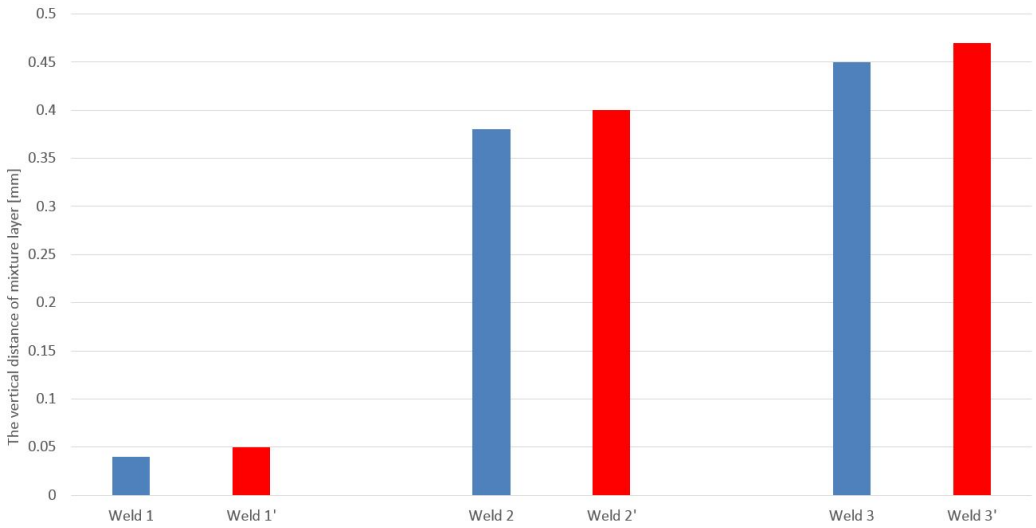

Figure 4.33: The vertical distance of mixture layer for both conventional lap joints and innovative lap joints after welding process .

welds. Figure 4.33 shows that the weld 1 and weld 1' have significantly low mixture layers compared to other welds because the axial forging force of weld 1 and weld 1' are lower than other welds. Consequently, the additional interlocking and the downward forging pressure for weld 1 and weld 1' are considerably less than other welds .

In addition, the low travel speed of the weld 1 and 1' resulted in high heat input. The high temperature softened the steel and the steel was sheared by the rotating probe and distributed in the processing zone which was detrimental to quality of the welds. Moreover, the high temperature can also lead to the formation of thick IMCs which decrease the strength of the welds. Figure 4.34 shows that swirl-like patterns present on the weld 1 and 1'. The pattern is the outcome of the thermo-mechanical history. It is worth noting that a vague swirl-like pattern also present in the weld 2'. However, no swirl-like pattern is discovered in the weld 2. This is because the probe crushed the center convex of the innovative faying surface of the weld 2'. The plastic deformation of the center part of the steel generated extra heat into the weld resulting in the formation of the vague swirl-like pattern. Correspondingly, the extra heat input may thicken the IMCs in weld 1' and weaken the strength of the weld 1'. Furthermore, no swirl-like pattern exists in weld 3 and 3' because of lower heat input.

The hook can reduce the thickness of aluminium sheet which considerably influence the mechanical resistance of the welds. Consequently, the effective

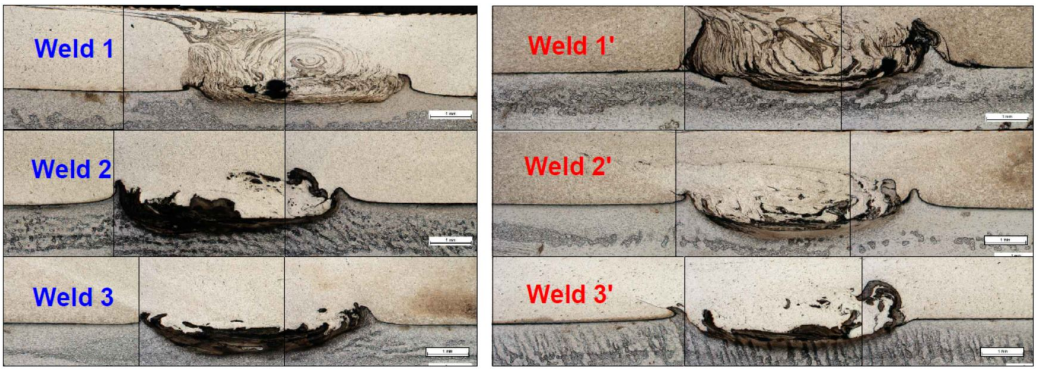

Figure 4.34: Macrographs for both conventional symmetric lap joints and innovative symmetric lap joints after etching.

thickness of the aluminium alloy sheet is considered as a critical factor affecting the mechanical performance of the welds. Figure 4.35 shows the effective thickness of the aluminium alloy sheet of these welds. The effective thickness of conventional symmetric lap joints are similar with each other. However, a big Fe particle was observed on the retreating side of the weld 2 which is detrimental to the strength of the weld. The effective thickness of innovative symmetric joints are less than that of conventional symmetric lap joints. The weld 3' has only 0.9 mm effective thickness. This phenomena was due to the rotating probe stirred two edges of the innovative joint interface resulting in extra plastic deformation. This plastic deformation generated heat that increased the material flow of steel. Consequently, a larger hook formed in the innovative lap joints.

Two welds (weld 3 and weld 2') with the best mechanical performance were selected for EDX analysis. According to the results of line analysis, the distance of the interlocking zone of weld 3 and weld 2' are 200 μm and 175 μm, respectively. But the result does not represent the weld 3 has superior mechanical interlocking than weld 2'. As mentioned before, the interlocking zone is layered structure which consists of IMCs layers and steel layers. The EDX maps of Figure 4.10 and Figure 4.22 shows the intensity of the IMCs layers. The intensity of IMCs layers in weld 2' are denser than the intensity of IMCs layers in weld 3. Furthermore, the interlocking strength also depends on the thickness and chemical composition of IMCs. Haghshenas et al. [28] suggest that the thickness and types of IMCs formed at weld interface are vital to achieve a weld with optimum mechanical performance. The presence of IMCs with high aluminium composition is detrimental to mechanical performance compared to the IMCs with high Fe composition. The EDX test

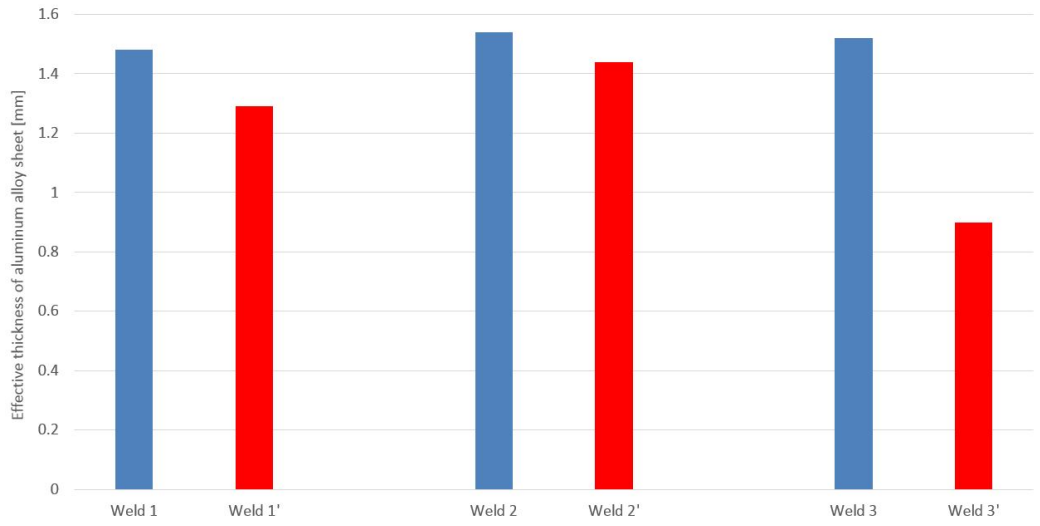

Figure 4.35: Effective thickness of aluminium alloy sheet of both conventional symmetric lap joints and innovative symmetric lap joints.

shows that the aluminium composition of IMCs in weld 3 ranges from 5 % to 45 %. The aluminium composition of IMCs in weld 2' ranges from 10 % to 23 %. By comparison, the IMCs of weld 2' has lower aluminium composition. Moreover, weld 2' has a uniform 1 μm thickness IMCs along the weld interface. Weld 3 has a nonuniform IMCs layer formed on the weld interface, the thickness ranged from 1.2 μm to 3.3 μm. Consequently, the formation of thinner IMCs layer with low aluminium composition in the weld 2' is better than the weld 3.

4.4.3 Microhardness tests

Figure 4.36 shows the comparison of microhardness values between conventional weld 3 and innovative weld 2'. The mcirohardness values on both aluminium-base material and aluminium-stir zone are basically same. The aluminium-TMAZ is difficult to be distinguished on these two welds. But the microhardness on aluminium-TMAZ should be same as the microharndness on aluminium-base material and aluminium-stir zone. This is because the aluminu alloy (AA5754-H23) is neither a heat-treatable nor a strain-hardened material. On the steel side, the microhardness value on steel-stir zone ans steel-TMAZ are larger than that on the steel-base material because of strain hardening. Furthermore, the highest microhardness value of conventional weld 3 is 228 HV 0.2 which located on layered structure of steel and IMCs,

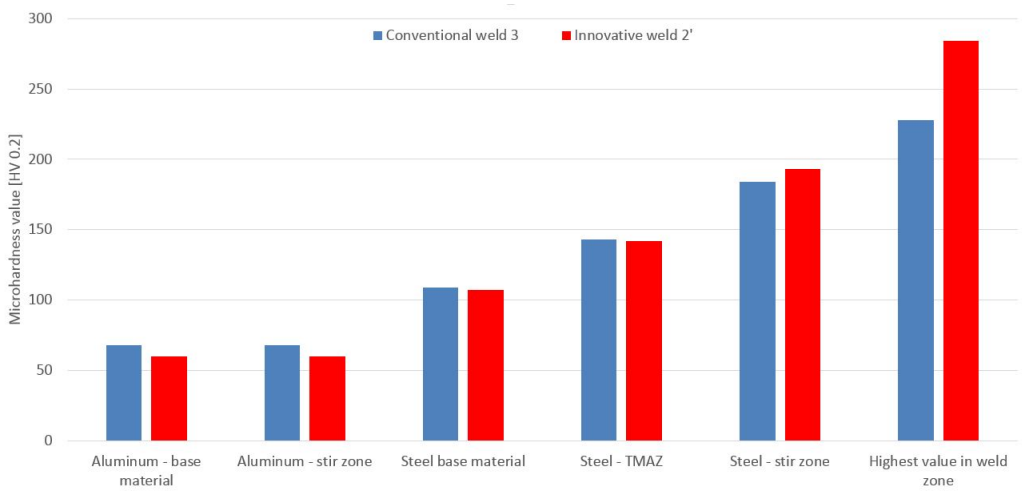

Figure 4.36: The comparison of microhardness between weld 3 and weld 2'.

the highest microhardness value of innovative weld 2' is 284 HV 0.2 which located on IMCs. Comparing the microhardness maps of the weld 3 (4.13) and the weld 2' (4.28), more IMCs with high microhardness value formed in the weld 2' which indicated the heat input in the weld 2' is larger than the weld 3.

4.4.4 Mechanical tests

According to the fracture position, all specimens were divided into two types of fracture modes. Mode 1 was shear fracture throughout the nugget. Mode 2 was tensile fracture which broke at aluminium alloy sheet. All specimens from weld 1 and weld 1' were fracture on the mode 1. This is mainly because of excessive heat input thereby forming thick IMCs and Fe fragments over the weld interface. Figure 4.37 shows the maximum failure loads of tensile shear test, the reason why the weld 1' shows inferior mechanical performance than the weld 1 is due to increased IMCs results from the additional heat input generated by extra plastic deformation of the innovative faying surface. The peel Force-Displacement curves of the weld 1 and 1' showed step shape variation after the peel force reached the maximum load, which is due to crack meet low bonded or unbonded zone during the progressive propagation. Furthermore, two specimens from the weld 3' also fracture on mode 1, this is because of the presence of voids on the steel-stir zone.

The Force-Displacement curves of weld 2, 2', 3 and 3' are similar to

Force-Displacement curves of normal tensile test, that is, the force dropped immediately after reaching the maximum loads. This is because the fracture happened on aluminium alloy sheets (mode 2). The Figure 4.37 shows the maximum failure loads of the tensile shear test, the welds which fractured at the aluminium alloy sheet (mode 2) were mainly dependent on the effective thickness of aluminium alloy sheet which was affected by hook feature and Fe fragments near to the hook. The Figure 4.35 from previous microstructure analysis shows the comparison of the effective thickness of aluminium alloy sheets. The effective thickness of aluminium alloy sheet in innovative FSW group is thinner than that in conventional FSW group. This is due to the rotating probe stirred two edges of the innovative welding interface resulting in extra plastic deformation. This plastic deformation generated local heat on these two edges which accelerated material flow. Consequently, larger hooks formed in innovative welds. The weld 3 displayed the best mechanical behaviour and the effective thickness is 1.52 mm which is similar to weld 2. However, the tensile shear failure load of weld 2 is 203 N/mm which is lower than that of weld 3. This is because a big Fe particle near to the hook served as stress riser thereby reducing the effective thickness. Weld 3' has the minimum effective thickness (0.9 mm), therefore, showing inferior mechanical behaviour. In addition, the interlocking feature was found in innovative weld 3'. However, it does not provide any additional bonding mechanism. The failure was due to the fracture did not occur by pure shear. Rather, it was due to the separation of the sheets because of bending and peeling.

4.5 Multi-pass welds

4.5.1 Superficial inspection

Figure 4.38 shows the superficial conditions of the single pass weld 3 and the multi-pass welds (2 and 3 passes) which were carried out using the same welding parameters as the weld 3. Figure 4.39 shows the superficial conditions of the weld 2' and its multi-pass welds (2 and 3 passes). Through visual inspection of the top surface of aluminium alloy sheet, no defects are found on these welds. Excessive flash is visibly formed at the start point of single pass weld 3 and 2'. It can be attributed to excessive penetration in the dwell period. Different from the flash on the single pass weld 3 and 2', the excessive flash on the conventional lap joint with three passes welding and on the innovative lap joints with two and three passes welding presents not only on the start point but also on the remaining part of the welds. It is due to multi-pass welding can accelerate the material flow so that the shoulder is easier to

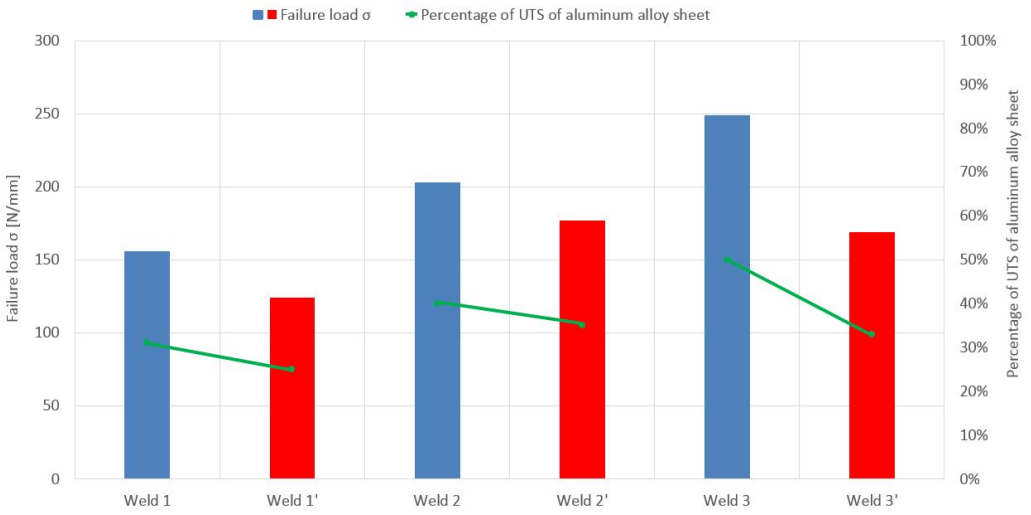

Figure 4.37: The result of tensile shear test for both conventional lap joints and innovative lap joints.

plunge into the aluminium alloy sheet. Comparing the superficial condition between innovative lap joints with multi-pass welding to conventional lap joints with multi-pass welding, it is obvious that the penetration of shoulder in innovative lap joints with multi-pass welding are larger than conventional lap joints with multi-pass welding. This is because the load bearing capacity of innovative lap joint interface is lower than conventional lap joint interface, thus the shoulder has more penetration on the aluminium alloy sheet of the innovative lap joints, which can decrease the effective thickness of aluminium alloy sheet.

4.5.2 Microstructure analysis

Figure 4.40 shows the conventional single pass weld 3 and its multi-pass welds. The left column shows the optical macrographs of these welds before chemical etching. The right column shows the optical macrographs of these welds after chemical etching. Similarly, Figure 4.41 show the optical macrographs of innovative single pass weld 2' and its multi-pass welds. These two figures shows that the voids in multi-pass welds are less than that in single pass welds. This is attributed to the multi-pass welding has more heat input than single pass welding. Consequently, the material is able to sufficiently flow within the processing zone, which is helpful to eliminate voids.

Figure 4.42 shows the vertical distance of the mixture layers. The vertical

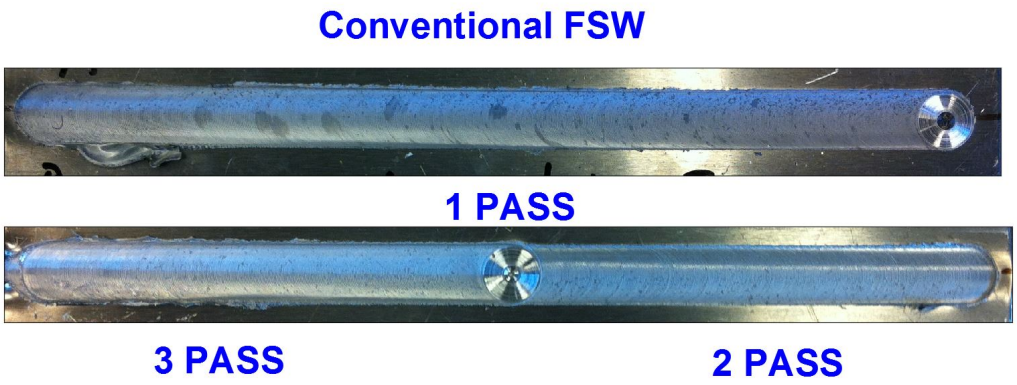

Figure 4.38: Superficial condition of multi-pass welds (2 and 3 passes) which were carried out as same welding parameters as weld 3.

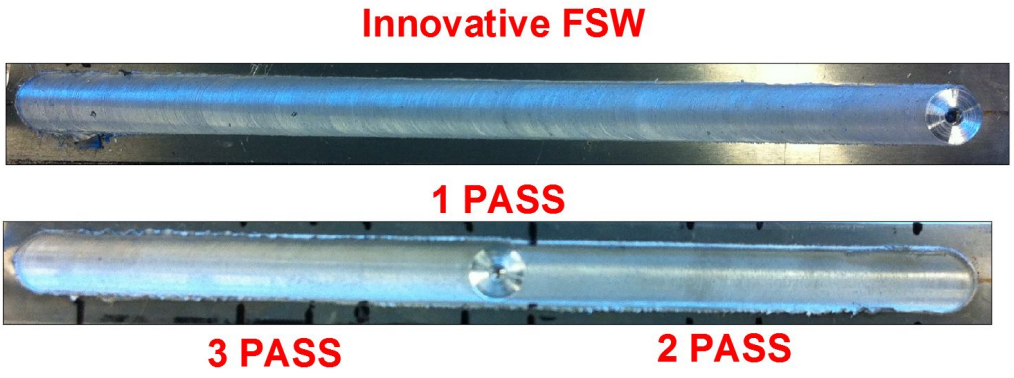

Figure 4.39: Superficial condition of multi-pass welds (2 and 3 passes) which were carried out as same welding parameters as weld 2'.

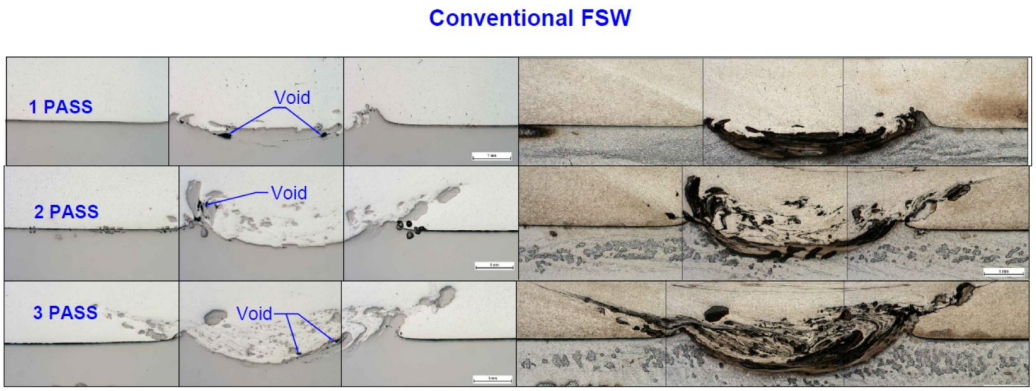

Figure 4.40: Optical macrographs of multi-pass welds with conventional faying surface which were carried out as same welding parameters as weld 3.

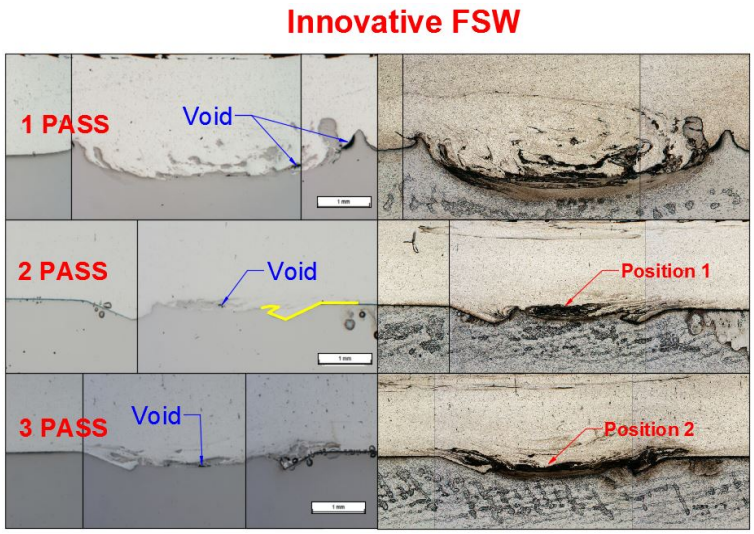

Figure 4.41: Optical macrographs of multi-pass welds with innovative faying surface which were carried out as same welding parameters as weld 3.

distance of the mixture layers of multi-pass welds are evidently less than that of single pass welds. This is because the heat input from the multi-pass welds is larger than single pass welds; therefore, a great amount of steel is stirred and distributed into the processing zone of aluminium alloy sheet. Furthermore, Figure 4.43 shows the microscopic images of position 1 and 2 in Figure 4.41. A few Fe particles accumulate on the weld interface of innovative lap joints with 2 passes and 3 passes, which may result in an unsound bond.

Figure 4.44 shows the effective thickness of aluminium alloy sheet of conventional lap joint with single pass welding and its multi-pass welds. The conventional lap joints with two passes welding has the best effective thickness value which is 1.72 mm. However, big Fe fragments are observed near to the hook. These Fe fragments likely serve as a stress riser which causes crack formation and thus reduce the weld strength. The conventional lap joint with three passes welding has only 1 mm thickness value which is the worst result. This thin thickness aluminium alloy sheet may results in an inferior weld quality. Figure 4.45 show the effective thickness of aluminium alloy sheet of innovative lap joint with single pass welding and its multi-pass welds. The innovative lap joint with two passes welding has the same effective thickness as the innovative lap joint with three passes welding. The yellow curve in Figure 4.41 highlights the hook shape of the innovative lap joint with two passes welding which shows an interlocking feature between the hook and the edge of the groove. Nonetheless, the interlocking feature does not show on the innovative lap joint with three passes welding as a result of the rotating probe shattered the hook during the third welding process.

4.5.3 Mechanical tests

Figure 4.46 shows the result of the tensile shear test. The conventional lap joint with single pass welding (weld 3) has 249 N/mm tensile shear strength. Under the same welding parameters as conventional weld 3, conventional lap joint with two passes welding has 259 N/mm tensile shear strength and conventional lap joint with three passes welding has 158 N/mm tensile shear strength. Fracture in both conventional lap joint with single pass welding and multi-pass welds happened at the aluminium alloy sheet (mode 2). Consequently, the strength of the weld is dependent on the effective thickness of aluminium alloy sheet. As shown in Figure 4.44, the conventional lap joint with two passes welding has relative large effective thickness; therefore, this weld has the best strength. The conventional lap joint with three passes welding has only 1 mm effective thickness. Thus the strength of this weld is lower.

Fracture for innovative lap joint with single pass welding happened at the

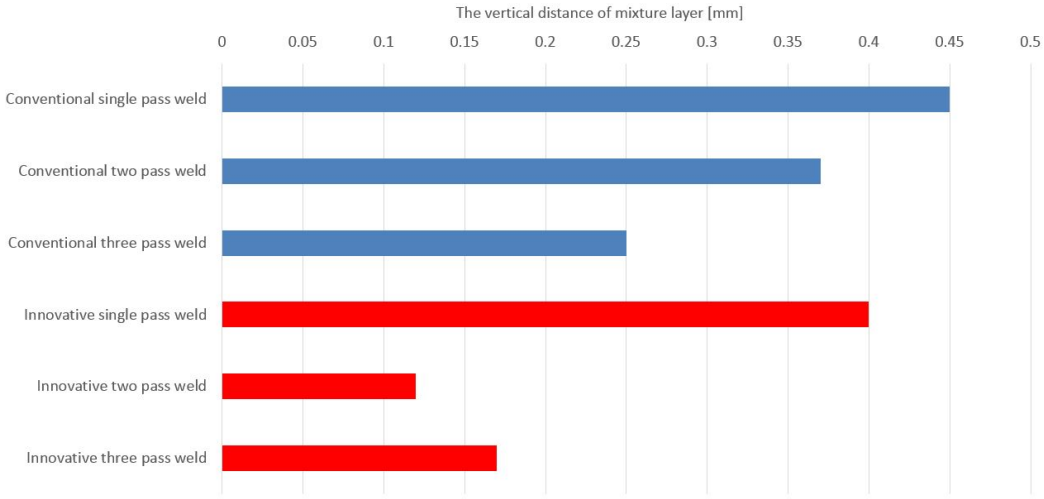

Figure 4.42: The vertical distance of mixture layer for both conventional lap joint with 1 to 3 pass welding and innovative lap joint with 1 to 3 pass welding.

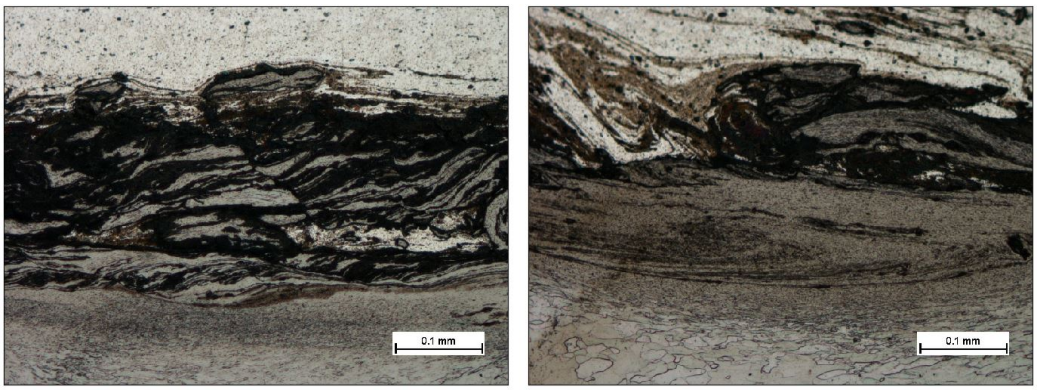

Figure 4.43: Micrographs on the weld shown in Figure 4.41 from position 1-2, (1) weld center of innovative lap joint with 2 passes welding, (2) weld center of innovative lap joint with 3 passes welding.

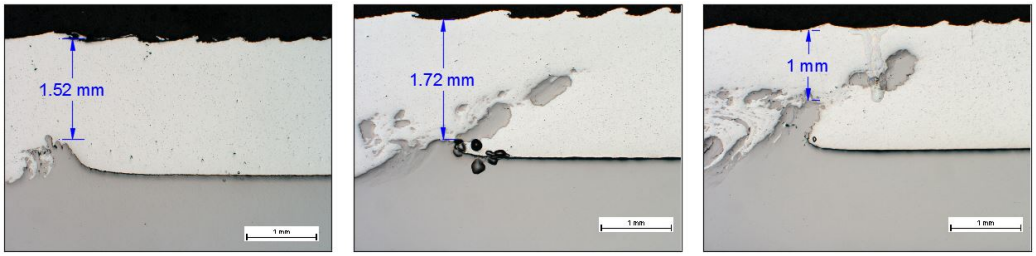

Figure 4.44: The effective thickness of aluminium alloy sheet of weld 3 and its multi-pass welds.

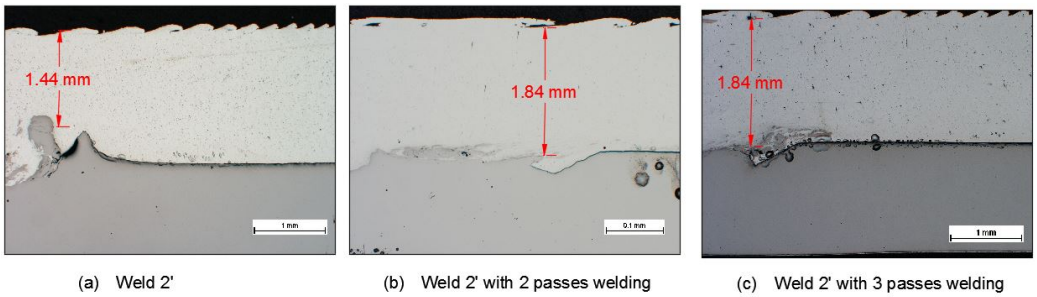

Figure 4.45: The effective thickness of aluminium alloy sheet of weld 2' and its multi-pass welds.

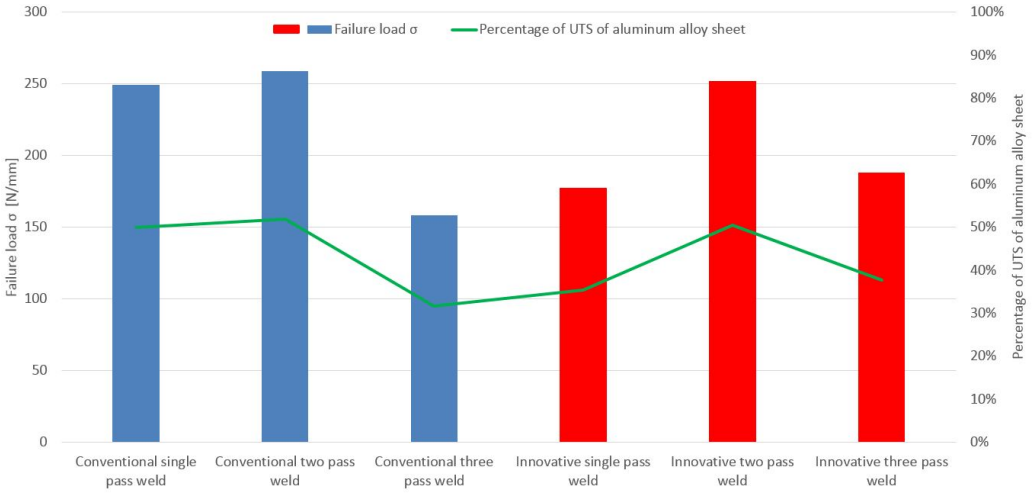

Figure 4.46: The tensile shear test result for both conventional lap joint with 1 to 3 pass welding and innovative lap joint with 1 to 3 pass welding.

aluminium alloy sheet (mode 2). However, fracture in innovative lap joint with 2 and 3 passes welding happened at the weld interface (mode 1). According to previous microstructure observation, a few Fe particles accumulated on the weld interface of both the two passes weld and the three passes weld, which may result in an unsound bond. Figure 4.46 shows that the innovative single weld 2' has 177 N/mm tensile shear strength, the innovative lap joint with two pass welding has 252 N/mm shear strength and the innovative lap joint with three passes welding has 188 N/mm. It is worth noting that the innovative lap joint with two passes welding has a higher strength value (252 N/mm) which is close to the best result (259 N/mm) from the conventional two passes weld. As per prior microstructure observation, the additional interlocking feature formed in the grooves of the innovative lap joint with two passes welding. However, this feature was not found in the innovative lap joint with three passes welding, which showed an inferior result (188 N/mm). Consequently, the formation of interlocking feature may provide additional mechanical bonding which lead to a high shear strength.

4.6 Summary

Two types of fracture modes were found in the tests. Mode 1 fracture was throughout the nugget while mode 2 was fracture at aluminium alloy sheet. All specimens from the weld 1 and the weld 1' broke in mode 1. This is

mainly because of excessive heat input. Therefore, a huge amount of IMCs and fine Fe fragments were formed on the weld interface which resulted in unsound welds. Two specimens from weld 3' also broke in this mode due to a number of voids formed in stir zone. Opposite to mode 1, mode 2 showed that aluminium alloy and steel were sufficiently bonded; thus all the tensile loads concentrated on the hook, which ultimately caused fracture at the aluminium alloy sheet. Consequently, the effective thickness of aluminium alloy sheet was a critical factor that affected the mechanical resistance. Big hook, high penetration of the shoulder into the top surface of aluminium alloy sheet and Fe inclusions could be the causes that reduced the mechanical resistance of aluminium alloy sheet. According to the results from mechanical tests, the mechanical resistance of innovative lap joints were inferior than that of conventional lap joints. The is because of the localized plastic deformation that happened at the innovative faying interface, which provided addition heat input. The extra heat input accelerated the upward material flow of the steel. Thus a big hook formed in the innovative faying surface, which decreased the effective thickness of the aluminium alloy sheet. Additionally, the interlocking feature in the weld 3' was not helpful to a better mechanical performance. This is because the failure did not occur by pure shear. Rather, it was due to the separation of the plates by bending. However, the innovative lap joint with two pass welding showed a favourable mechanical performance. This is likely due to the formation of interlocking feature in the weld zone, which takes on loads during the tensile shear test.

Chapter 5

Final Remarks

5.1 Conclusions

A new lap joint concept was tested and compared with conventional lap joint for FSW of aluminium alloy AA5754-H22 to steel DX54. The main conclusions from the research are the following:

- The results of the innovative lap joint concept implemented exhibited less or equal mechanical resistance than the conventional overlap joint concept.
- The method applied to produce the pre-weld deformation shape of the steel at the faying interface with the aluminium did not result in the originally planned geometry and this fact compromised the full exploration of the potential of the innovative concept but present results provide important information for future innovations.
- Both conventional and innovative lap joint concepts have shown the best properties with lower travel pitch ratios (rotation speed versus travel speed). At the lower travel pitch ratios, the mechanical resistance of the welds was mainly affected by effective thickness of aluminium alloy sheets.
- Multi-pass welds with 2 passes presented the best mechanical properties when compared with single pass or 3 passes welds.
- The superficial inspection of the aluminium layer processed by the shoulder presented sound and regular surface finishing emphasizing the stability of the selected parameters and welding procedures. Exception are the start zone showing some flash formation due to excessive penetration during the dwell period. Also, due to aluminium adhesion to

the shoulder some instability is evident in one weld with lower travel speed.

- Voids were found at the Al-Fe interface, which can be observed in the optical macrographs. The intermediate travel speed conditions presented the lower level of void formation in size and quantity. Multi-pass welding accelerated the material flow within the processing zone, which was helpful to eliminate voids. The layered structure of IMCs and steel was dependent on the axial forging force. Higher axial forcing force generated larger layered structure and larger downward pressure which facilitated the consolidation of both innovative and conventional lap joints. Moreover, the layered structure provided extra joinining mechanism which increased the mechanical resistance of the welds.

- The optical micrographs showed that fine Fe fragments and thick IMCs were preferentially formed at higher travel pitch ratio as a result of higher heat input. The higher travel pitch ratios resulted in a more evident swirl-like pattern in the weld. This pattern was the outcome of the thermo-mechanical history and it declined when decreasing the travel pitch ratio. Furthermore, the extra plastic deformation from the innovative lap joint contributed for additional heat input, which promoted the formation of swirl-like pattern.

- In the innovative lap joints, the steel flowed into the aluminium alloy sheet forming a larger hook compared to the hook in the conventional lap joints. The larger hook reduced the effective thickness of aluminium sheet which considerably influenced the mechanical resistance of the welds. In addition, the presence of Fe fragments near to the hook could decrease the mechanical resistance of the welds as well. Multi-pass welding promoted additional material flow within the processing zone, which increased the size of the hooks considerably.

- As per EDX analysis, the thickness of IMCs in the innovative lap joint produced by intermediate travel speed was thinner than the conventional lap joint produced by high travel speed. The aluminium content of IMCs in the innovative lap joint produced by intermediate travel speed was lower than the conventional lap joint produced by high travel speed. The formation of thin IMCs with low aluminium content may improve the mechanical resistance of the weld.

- The microhardness test showed that the innovative lap joint produced by intermediate travel speed has higher microhardness values on the

steel-stir zone compared to the conventional lap joint produced by high travel speed.

- According to the results of the peel tests, the welds with low travel speed show lower maximum force. In these welds, the fracture propagated along the weld interface. For the welds with higher travel speed, the maximum peeling force was higher and dropped immediately after reaching the maximum loads. This is because the fracture happened in the aluminium alloy base material zone.

5.2 Future developments

The innovative lap joint concept can be further implemented in the future investigation. Figure 5.1 shows the schematic of a new lap joint concept. Figure 5.1 (a) shows an anvil with protrusion is placed under the steel sheet while a roller with particular surface acts on the top surface of the steel. The anvil is helpful to form a protrusion above the top surface of the steel. Next, the steel sheet is clamped with aluminium alloy sheet. Another roller with flat surface acts on the top surface of aluminium alloy sheet, the protrusion of steel penetrates into the aluminum alloy sheet and the downward force from the roller destroy the tip of the protrusion resulting in the formation of a chemically active surface, as shown in Figure 5.1 (b). During the FSW process, the aluminium alloy will fill into the grooves and forming an interlocking between aluminium alloy and steel after solidification. Based on the optical macroscopic observation of former innovative lap joint design, the interlocking feature was not evident in the joint region. Consequently, it is highly recommend to make deeper grooves in the further studies.

The galvanized steel (DX54) were chosen as one of the materials for the experiment. The zinc coating was not totally removed by disc grinder before the welding process. Furthermore, the surface finishing of steel is not favorable. Thus steels with and without coating should be used in further investigation.

Welding parameters, such as rotational speed and welding speed, have a considerably large effect on weld quality. In this study, only three welding parameters were investigated for the experiment. Therefore, more welding parameters should be investigated to optimize the joint quality in future studies.

Probe design is also a very important factor which affects the mechanical resistance of the welds. The three dimensional movement of material caused by the probe may remove the oxide on the joining line and minimize or even

eliminate void defects in the weld nugget. In this study, a probe with a low thread depth was used so that the vertical material flow was insufficient.

Moreover, the fracture happened at the aluminium sheet indicated that the effective thickness of aluminium alloy sheet is a critical factor affecting the joint mechanical performance. Therefore, minimizing the hook size should be carefully taken into consideration in future investigation.

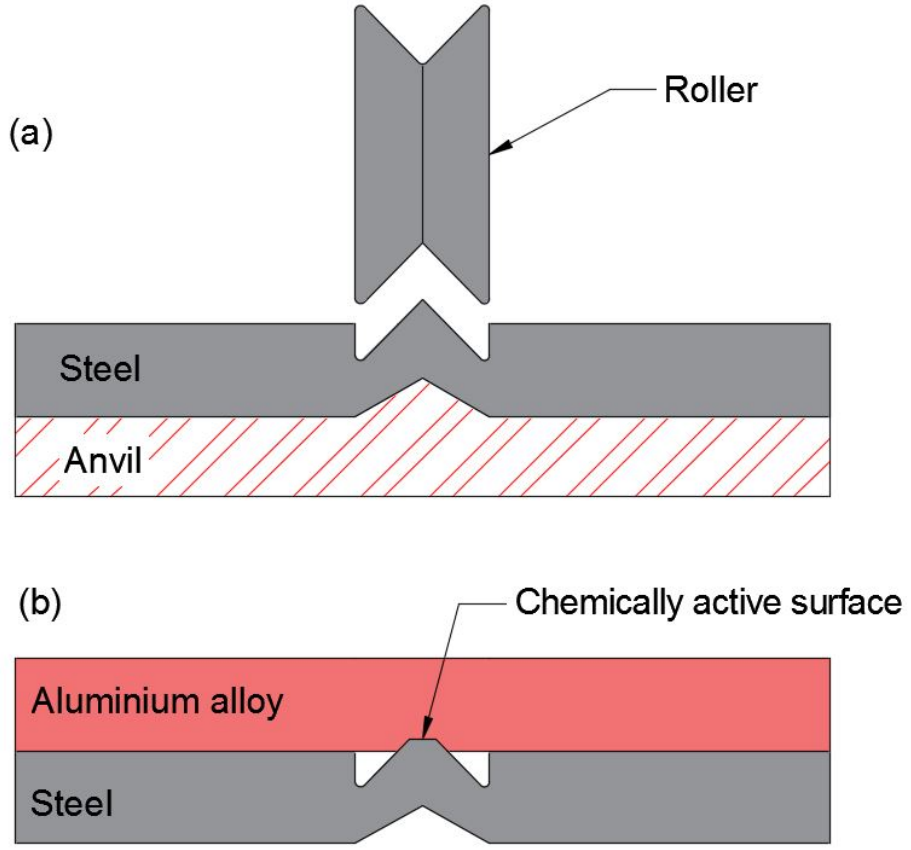

Figure 5.1: New lap joint concept for future development: (a) new geometry on steel sheet, (b) new lap joint concept.

Bibliography

[1] X Liu, S Lan, and J Ni. Analysis of process parameters effects on friction stir welding of dissimilar aluminum alloy to advanced high strength steel. *Materials & Design*, 59:50–62, 2014.

[2] H Uzun, C Dalle Donne, A Argagnotto, T Ghidini, and C Gambaro. Friction stir welding of dissimilar al 6013-t4 to x5crni18-10 stainless steel. *Materials & design*, 26(1):41–46, 2005.

[3] X Yong-qing. Aluminum alloy-the optimum material for modern light weight automobile [j]. *Aluminum Fabrication*, 5:013, 2005.

[4] MS Kenevisi and SM Mousavi Khoie. A study on the effect of bonding time on the properties of al7075 to ti–6al–4v diffusion bonded joint. *Materials Letters*, 76:144–146, 2012.

[5] M Dehghani, A Amadeh, and SAA Akbari Mousavi. Investigations on the effects of friction stir welding parameters on intermetallic and defect formation in joining aluminum alloy to mild steel. *Materials & Design*, 49:433–441, 2013.

[6] K Kimapong and T Watanabe. Friction stir welding of aluminum alloy to steel. *Welding journal*, 83(10):277, 2004.

[7] MJ Torkamany, S Tahamtan, and J Sabbaghzadeh. Dissimilar welding of carbon steel to 5754 aluminum alloy by nd: Yag pulsed laser. *Materials & Design*, 31(1):458–465, 2010.

[8] CG Rhodes, MW Mahoney, WH Bingel, RA Spurling, and CC Bampton. Effects of friction stir welding on microstructure of 7075 aluminum. *Scripta materialia*, 36(1):69–75, 1997.

[9] R Coelho, A Kostka, S Sheikhi, J dos Santos, and A Pyzalla. Microstructure and mechanical properties of an aa6181-t4 aluminium alloy

to hc340la high strength steel friction stir overlap weld. *Advanced Engineering Materials*, 10(10):961–972, 2008.

[10] H Bang, H Bang, G Jeon, I Oh, and C Ro. Gas tungsten arc welding assisted hybrid friction stir welding of dissimilar materials al6061-t6 aluminum alloy and sts304 stainless steel. *Materials & Design*, 37:48–55, 2012.

[11] B Bartczak, J Mucha, and T Trzepieciński. Stress distribution in adhesively-bonded joints and the loading capacity of hybrid joints of car body steels for the automotive industry. *International Journal of Adhesion and Adhesives*, 45:42–52, 2013.

[12] P Groche, S Wohletz, M Brenneis, C Pabst, and F Resch. Joining by formingâa review on joint mechanisms, applications and future trends. *Journal of Materials Processing Technology*, 214(10):1972–1994, 2014.

[13] CJ Lee, JY Kim, SK Lee, DC Ko, and BM Kim. Parametric study on mechanical clinching process for joining aluminum alloy and high-strength steel sheets. *Journal of Mechanical Science and Technology*, 24 (1):123–126, 2010.

[14] Y Abe, K Mori, and T Kato. Joining of high strength steel and aluminium alloy sheets by mechanical clinching with dies for control of metal flow. *Journal of materials processing technology*, 212(4):884–889, 2012.

[15] K Mori, T Kato, Y Abe, and Y Ravshanbek. Plastic joining of ultra high strength steel and aluminium alloy sheets by self piercing rivet. *CIRP Annals-Manufacturing Technology*, 55(1):283–286, 2006.

[16] G Meschut, V Janzen, and T Olfermann. Innovative and highly productive joining technologies for multi-material lightweight car body structures. *Journal of materials engineering and performance*, 23(5):1515–1523, 2014.

[17] F Haddadi. Rapid intermetallic growth under high strain rate deformation during high power ultrasonic spot welding of aluminium to steel. *Materials & Design*, 66:459–472, 2015.

[18] WJ Cheng and CJ Wang. Microstructural evolution of intermetallic layer in hot-dipped aluminide mild steel with silicon addition. *Surface and Coatings Technology*, 205(19):4726–4731, 2011.

[19] PB Prangnell and D Bakavos. Novel approaches to friction spot welding thin aluminium automotive sheet. In *Materials Science Forum*, volume 638, pages 1237–1242. Trans Tech Publ, 2010.

[20] A Gerlich, P Su, M Yamamoto, and TH North. Effect of welding parameters on the strain rate and microstructure of friction stir spot welded 2024 aluminum alloy. *Journal of materials science*, 42(14):5589–5601, 2007.

[21] M Watanabe, K Feng, Y Nakamura, and S Kumai. Growth manner of intermetallic compound layer produced at welding interface of friction stir spot welded aluminum/steel lap joint. *Materials transactions*, 52 (5):953–959, 2011.

[22] W Yuan, RS Mishra, B Carlson, R Verma, and RK Mishra. Material flow and microstructural evolution during friction stir spot welding of az31 magnesium alloy. *Materials Science and Engineering: A*, 543:200–209, 2012.

[23] S Bozzi, AL Helbert-Etter, T Baudin, B Criqui, and JG Kerbiguet. Intermetallic compounds in al 6016/if-steel friction stir spot welds. *Materials Science and Engineering: A*, 527(16):4505–4509, 2010.

[24] R Qiu, H Shi, K Zhang, Y Tu, C Iwamoto, and S Satonaka. Interfacial characterization of joint between mild steel and aluminum alloy welded by resistance spot welding. *Materials characterization*, 61(7):684–688, 2010.

[25] Z Feng, ML Santella, SA David, RJ Steel, SM Packer, T Pan, M Kuo, and RS Bhatnagar. Friction stir spot welding of advanced high-strength steels-a feasibility study. Technical report, SAE Technical Paper, 2005.

[26] C Leitao, RM Leal, DM Rodrigues, A Loureiro, and P Vilaça. Mechanical behaviour of similar and dissimilar aa5182-h111 and aa6016-t4 thin friction stir welds. *Materials & Design*, 30(1):101–108, 2009.

[27] X Liu, S Lan, and J Ni. Electrically assisted friction stir welding for joining al 6061 to trip 780 steel. *Journal of Materials Processing Technology*, 219:112–123, 2015.

[28] M Haghshenas, A Abdel-Gwad, AM Omran, B Gökçe, S Sahraeinejad, and AP Gerlich. Friction stir weld assisted diffusion bonding of 5754 aluminum alloy to coated high strength steels. *Materials & Design*, 55: 442–449, 2014.

[29] H Fujii, L Cui, M Maeda, and K Nogi. Effect of tool shape on mechanical properties and microstructure of friction stir welded aluminum alloys. *Materials Science and Engineering: A*, 419(1):25–31, 2006.

[30] HK Mohanty, MM Mahapatra, P Kumar, P Biswas, and NR Mandal. Effect of tool shoulder and pin probe profiles on friction stirred aluminum weldsâa comparative study. *Journal of Marine Science and Application*, 11(2):200–207, 2012.

[31] YC Lin, JJ Liu, and JN Chen. Material flow tracking for various tool geometries during the friction stir spot welding process. *Journal of materials engineering and performance*, 22(12):3674–3683, 2013.

[32] K Reshad Seighalani, MK Besharati Givi, AM Nasiri, and P Bahemmat. Investigations on the effects of the tool material, geometry, and tilt angle on friction stir welding of pure titanium. *Journal of materials engineering and performance*, 19(7):955–962, 2010.

[33] T Tanaka, T Morishige, and T Hirata. Comprehensive analysis of joint strength for dissimilar friction stir welds of mild steel to aluminum alloys. *Scripta Materialia*, 61(7):756–759, 2009.

[34] TA Barnes and IR Pashby. Joining techniques for aluminium spaceframes used in automobiles: Part iâsolid and liquid phase welding. *Journal of Materials Processing Technology*, 99(1):62–71, 2000.

[35] J Sarkar, TRG Kutty, KT Conlon, DS Wilkinson, JD Embury, and DJ Lloyd. Tensile and bending properties of aa5754 aluminum alloys. *Materials Science and Engineering: A*, 316(1):52–59, 2001.

[36] ZW Chen, S Yazdanian, and G Littlefair. The role of joint interface on tensile-shear fracture strength of friction stir lap diffusion al-to-steel welds. 2012.

[37] K Kimapong and T Watanabe. Lap joint of a5083 aluminum alloy and ss400 steel by friction stir welding. *Materials transactions*, 46(4):835–841, 2005.

[38] M Zhou, SJ Hu, and H Zhang. Critical specimen sizes for tensile-shear testing of steel sheets. *WELDING JOURNAL-NEW YORK-*, 78:305–s, 1999.

[39] S Yazdanian, ZW Chen, and G Littlefair. Effects of friction stir lap welding parameters on weld features on advancing side and fracture

strength of aa6060-t5 welds. *Journal of materials science*, 47(3):1251–1261, 2012.

[40] A Elrefaey, M Gouda, M Takahashi, and K Ikeuchi. Characterization of aluminum/steel lap joint by friction stir welding. *Journal of Materials Engineering and Performance*, 14(1):10–17, 2005.

[41] GMD Cantin, SA David, WM Thomas, E Lara-Curzio, and SS Babu. Friction skew-stir welding of lap joints in 5083–0 aluminium. *Science and Technology of Welding & Joining*, 10(3):268–280, 2005.

[42] A Elrefaey, M Takahashi, and K Ikeuchi. Friction-stir-welded lap joint of aluminum to zinc-coated steel. *quarterly journal of the Japan Welding Society*, 23(2):186–193, 2005.

Appendix A

Engineering drawing of the FSW tool components

A.1 FSW tool's shoulder

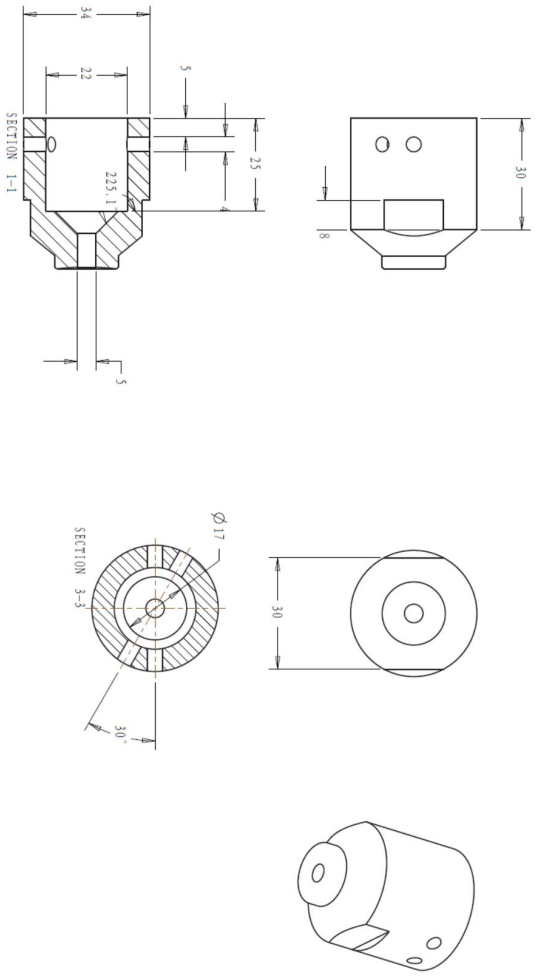

Figure A.1: The engineering drawing of FSW tool's shoulder. All dimensions are in mm.

A.2 FSW tool's probe

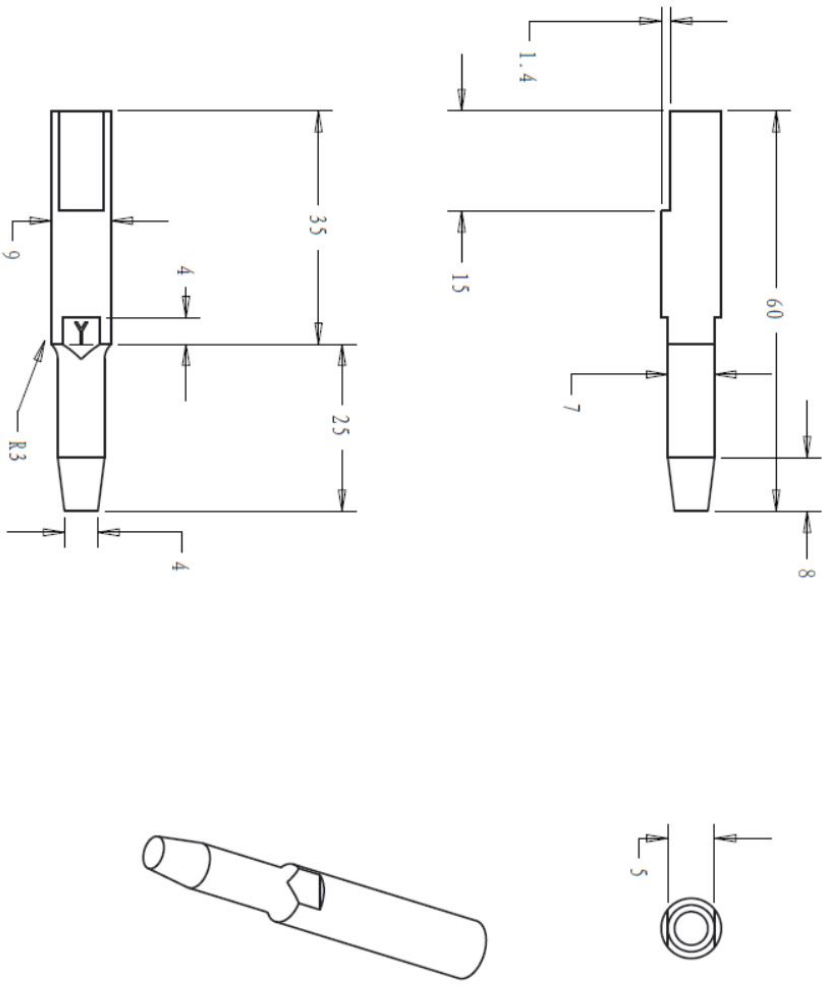

Figure A.2: The engineering drawing of FSW tool's probe. All dimensions are in mm.